Lack of NFATc1 SUMOylation prevents autoimmunity and alloreactivity

Fehlende NFATc1-SUMOylierung verhindert Autoimmunität und Alloreaktivität

Doctoral Thesis for a doctoral degree at the
Graduate School of Life Sciences,
Julius-Maximilians-Universität Würzburg
Section Infection and Immunity

submitted by

Yin Xiao

from Jiang Su, China

Würzburg 2022

Submitted on: ……

Office stamp

Members of the Thesis Committee

Chairperson: Prof. Dr. med. Georg Gasteiger

Primary Supervisor: PD Dr. Friederike Berberich-Siebelt

Supervisor (Second): Prof. Dr. Andreas Rosenwald

Supervisor (Third): Prof Dr. Wolfgang Kastenmüller

Supervisor (Fourth): Dr. Florian Groeber-Becker

Date of Public Defence: ……

Date of Receipt of Certificates: ……

Acknowledgments

At this very moment, I would like to thank all my colleagues, collaborators, friends, and families, who supported me to finish my doctoral thesis and life here, especially for the difficult time during the COVID-19 pandemic.

Firstly, I would like to express my sincere gratitude to my first supervisor and the leader of our lab, PD Dr. Friederike Berberich-Siebelt for giving me a chance to work in her lovely group, and for helping me with my Ph.D. study and related research during these years, for her patience, motivation, and immense knowledge to guide me. Moreover, many thanks for being so kind and being concerned about me personally.

Besides my advisor, I would also like to thank the rest of my thesis committee, Prof. Dr. Andreas Rosenwald, Prof Dr. Wolfgang Kastenmüller, and Dr. Florian Groeber-Becker, for their insightful comments and intensive discussion during the annual meetings. In particular, a special mention and thanks to Dr. Florian Groeber-Becker for deeply discussing results and suggestions, even inviting Dr. Gudrun Dandekar to help with follicular lymphoma organoid culture. Furthermore, I would like to express my gratitude to Prof. Dr. Andreas Rosenwald for always supporting research materials during these years.

I would also like to thank my former and current colleagues, especially when I could not go back to China during the COVID-19 pandemic situation, they became my friends to give me love to go through the tough time. Also, thanks for the nice discussions and the help on my experimental work. Without the support of Prof. Dr. Edgar Serfling, Dr. Martin Vaeth, Dr. Raghu Erapaneedi, Dr. Stefan-Klein Hessling, Anika König, Benjamin Lunz, Musga Qureischi, Lena Dietz, Cristina Chiarolla, Nadine Hundhausen, Snigdha Majumder, Rishav Seal, Sabrina Giampaolo, Muhammad Azeem, and Salvador Sampere, this work would not have been the same. I am very glad to have them in my life.

Thanks to all my Chinese friends here, for making my off-work time colourful and helping me go through the hard time when I am sad and homesick.

I would like to thank the Graduate School of Life Sciences (GSLS) for awarding me with a fellowship from the German Academic Exchange Service (DAAD) and for supporting me with another 6 months of work. Furthermore, I would like to thank especially China Scholarship Council (CSC), which supports my life here and allows me to finish my work.

Finally, a special thanks goes to my parents and my family for always supporting me and allowing me to go far away to realize my dreams.

Table of Contents

1 Affidavit/Declaration

I hereby confirm that my thesis entitled “Lack of NFATc1 SUMOylation prevents autoimmunity and alloreactivity” is the result of my own work. I did not receive any help or support from commercial consultants.
All sources and/or materials applied are listed and specified in the thesis.

Furthermore, I confirm that this thesis has not yet been submitted as part of another examination process neither in identical nor in similar form.

Place, Date Signature

Eidesstattliche Erklärung

Hiermit erkläre ich an Eides statt, die Dissertation „Fehlende NFATc1-SUMOylierung verhindert Autoimmunität und Alloreaktivität, d.h. insbesondere selbständig und ohne Hilfe eines kommerziellen Promotionsberaters, angefertigt und keine anderen als die von mir angegebenen Quellen und Hilfsmittel verwendet zu haben.

Ich erkläre außerdem, dass die Dissertation weder in gleicher noch in ähnlicher Form bereits in einem anderen Prüfungsverfahren vorgelegen hat.

Ort, Datum Unterschrift

2 List of Figures

3 Summary

SUMOylation, as a post-translational modification, plays a crucial role in several biological processes. *Small ubiquitin-like modifier* (SUMO) proteins can be reversibly linked to the lysine residues located within specific motifs on numerous target proteins, leading to the change of stability, localization, activity of target proteins, mostly by promoting or interfering with the interaction with other molecules. Consequently, it can regulate gene transcription, migration, cell cycle progression, cellular responses to stress, and tumorigenesis.

NFATc1 belongs to the *Nuclear Factor of Activated T-cells* (NFAT) transcription factor family, which is dephosphorylated and translocates to the nucleus upon cell stimulation, which provokes Ca^{2+} signalling. NFAT plays a crucial role in the development and function of the immune system. NFATc1 has three SUMOylation sites at the position of aa 349, 702, and 914. In our previous study, we demonstrated that point mutations performed on the SUMOylation sites on all three or only at the lysine residues K702 and K914 lead to enhanced expression of IL-2 *in vitro*. To evaluate the function of SUMOylation of NFATc1 on T cell-mediated immunity *in vivo*, we not only generated a transgenic mouse strain (NFATc1/ΔS^+ mouse) by point mutations from Lysine to Arginine on the two SUMOylation sites within exon 10 of *Nfatc1* to prevent their SUMOylation, but in combination created another mouse strain (NFATc1/ΔBC^+ mouse) that is completely *Nfatc1* exon 10-ablated by using the LoxP/Cre system. In NFATc1/ΔS^+ T cells, we observed enhanced IL-2 production and less IL-17A and IFN-γ expression. In line with exon 10 bearing the relevant SUMO sites, NFATc1/ΔBC^+ $CD4^+$ T cells behaved similarly as NFATc1/ΔS^+ ones. The mechanism is that elevated IL-2 secretion can counteract the expression of IL-17A and IFN-γ via STAT5 and Blimp-1 induction. Afterwards, Blimp-1 suppressed IL-2 itself as well as Bcl2A1. Next, we performed two disease models with our NFATc1/ΔS^+ mice. In a major mismatch model for acute graft-versus-host disease, we found that the mice transplanted with NFATc1/ΔS^+ $CD3^+$ T cells developed less severe disease, and T cells proliferated less due to increased Tregs. Moreover, when transferring 2D2.NFATc1/ΔS^+ Th1 plus Th17 cells to *Rag1*$^{-/-}$ mice to induce experimental autoimmune encephalitis, we also observed ameliorated disease compared to animals with transferred WT T cells as well as increased Tregs.

Taking all data together, the deficiency in SUMOylation of NFATc1 leads to an elevated IL-2 secretion in T cells and subsequent activation of STAT5, which competes with STAT3 to inhibit IL-17A production and promotes Treg expansion, as well as to an enforcement of Blimp-1 expression, which suppresses IFN-γ and IL-2 expression. Consequently and despite a short phase of enhanced IL-2 secretion, the deficiency of SUMOylation on NFATc1 can protect from autoreactive and alloreactive diseases.

Moreover, to further understand the function of SUMOylation of NFATc1 in humans, we started by establishing an *in vitro* 3D culture system for tonsil organoids, which was successful in the presence of feeder cells, along with IL-4 and IL-7 cytokines. To confirm that our 3D tonsil organoids can respond to real antigens, we used CMV peptides and peptides of spike proteins from Covid-19 as real antigens, and co-cultured with tonsil organoids, which indeed can generate memory cells and plasmablasts. In the end, we also compared 3D to 2D cultures. Although the total numbers of all B cell subsets were much less in 3D culture than that in 2D culture, still, it indicates that this *in-vitro* culture system has its limitation, while being usable to produce the similar results as 2D did. Therefore, this 3D culture system can be used as a platform to investigate NFATc1/ΔS^{+} or NFATc1/ΔBC^{+} T_{FH} and T_{FR} cells in the dynamic of human GC responses.

4 Zusammenfassung

SUMOylierung als posttranslationale Modifikation spielt bei mehreren biologischen Prozessen eine entscheidende Rolle. *Small Ubiquitin-like Modifier* (SUMO) Proteine können reversibel mit den Lysinresten innerhalb spezifischer Motive auf zahlreichen Zielproteinen verknüpft werden, was zu einer Veränderung der Stabilität, Lokalisation und Aktivität von Zielproteinen führt, insbesondere durch Interaktionsveränderungen mit anderen Molekülen. Folglich kann es die Gentranskription, Migration, das Fortschreiten des Zellzyklus, zelluläre Reaktionen auf Stress sowie die Tumorentstehung regulieren.

NFATc1 ist ein Mitglied der Transkriptionsfaktorfamilie *Nuclear Factor of Activated T-Cells* (NFAT), welches in Folge von Zellstimulation und einer intrazellulären Konzentrationserhöhung von Ca^{2+} dephosphoryliert wird, was wiederum die Translokation in den Zellkern ermöglicht. Grundsätzlich spielt NFAT eine entscheidende Rolle bei der Entwicklung und Funktion des Immunsystems. NFATc1 hat drei SUMOylierungsstellen an den Positionen aa 349, 702 und 914. In unserer vorherigen Studie hatten wir gezeigt, dass Punktmutationen innerhalb aller SUMOylierungsstellen, aber auch nur an den Lysinresten K702 und K914 *in vitro* zu einer verstärkten Expression von IL-2 führten. Um die Funktion der SUMOylierung von NFATc1 auf die T-zellvermittelte Immunität *in vivo* zu untersuchen, haben wir nicht nur einen transgenen Mausstamm (NFATc1/ΔS-Maus) durch (Lysin zu Arginin) Punktmutationen an den zwei SUMOylierungsstellen auf dem Exon 10 von NFATc1 erzeugt, sondern auch einen zweiten Mausstamm (NFATc1/ΔBC-Maus), bei welchem das Exon 10 unter Verwendung des LoxP/Cre-Systems vollständig ausschaltet wurde. In den NFATc1/ΔS^+ T-Zellen beobachteten wir eine erhöhte IL-2-Produktion und eine geringere IL-17A- und IFN-γ-Expression.–NFATc1/ΔBC-Mäuse verhielten sich ähnlich zu NFATc1/ΔS-Mäusen. In den $CD4^+$ T-Zellen mit diesen Genotypen wirkte die erhöhte IL-2 Sekretion der Expression von IL-17A und IFN-γ über Stat5- bzw. Blimp-1-Induktion entgegen. Desweiteren unterdrückte Blimp-1 auch IL-2 und reprimierte die Expression von Bcl2A1. Als nächstes evaluierten wir die NFATc1/ΔS Mäuse in zwei verschiedenen Krankheitsmodellen, der akuten Transplantat-gegen-Wirt-Reaktion (*graft-versus-host disease*; GvHD) und der Experimentellen autoimmunen Enzephalomyelitis (EAE). Wir stellten fest, dass bei der Induktion einer aGvHD durch Transplantation von Knochenmarkzellen zusammen mit NFATc1/ΔS^+ $CD3^+$ T-Zellen die Empfängertiere geschützter waren als in Anwesenheit von WT T-Zellen. Auch aufgrund einer erhöhten Anzahl von NFATc1/ΔS^+ Tregs proliferierten die NFATc1/ΔS^+ T Zellen weniger. Desgleichen war unter Verwendung von 2D2.NFATc1/ΔS^+ T-Helfer 1 und 17 war eine Transfer-EAE in Rag Mäusen wesentlich schwächer induziert als bei der Verwendung von WT T-Zellen. Auch in diesem Modell konnten wie einen schützenden Effekt u.a. in Folge einer erhöhten Anzahl an Tregs feststellen.

Zusammenfassend konnte gezeigt werden, dass die Vermeidung einer NFATc1-SUMOylierung zu einer erhöhten IL-2 Sekretion in T-Zellen führt und somit STAT5 aktiviert. STAT5 kompetiert mit STAT3 und hemmt so die IL-17A Produktion. STAT5 beeinflusste auch die Höhe der Blimp-1-Expression, wodurch IFN-γ sowie auf Dauer IL-2 supprimiert wurde. Darüber hinaus fördert IL-2 die Differenzierung und Expansion von Tregs. So kann trotz einer nur kurzen Phase an erhöhter IL-2-Sekretion eine fehlende NFATc1-SUMOylierung vor autoreaktiven und alloreaktiven Krankheiten schützen.

Um die Funktion der SUMOylierung von NFATc1 beim Menschen zu verstehen, haben wir zunächst ein *In vitro*-3D-Kultursystem entwickelt. Unter der Verwendung von Organoiden aus Tonsillen, in Gegenwart von *Feeder*-Zellen, IL-4 und IL-7. Um zu bestätigen, dass 3D-Tonsillen-Organoide auf echte Antigene reagieren, wurden CMV-Peptide und Peptide von Covid-19 Spike-Proteinen verwendet. Wir konnten zeigen, dass wir durch die Co-Kultivierung der Peptide mit den Organoiden tatsächlich in der Lage sind, Gedächtniszellen und Plasmablasten zu generieren. Schließlich wurden die 3D und 2D Kulturen miteinander verglichen. Trotz der limitierten Gesamtzahl an B-Zellen in der 3D-Kultur, verglichen zur 2D-Kultur, konnten wir äquivalente Tendenzen der Erzeugung von Plasmablasten und Gedächtniszellen feststellen. Dies deutet darauf hin, dass die Verwendung dieses 3D-Kultursystems ein geeignetes *in vitro*-model darstellt, um NFATc1/ΔS^{+} oder NFATc1/ΔBC^{+} T_{FH}- und T_{FR}-Zellen in der Dynamik menschlicher GC-Antworten zu untersuchen.

5 Introduction

5.1 Immune system

The immune system plays a crucial and indispensable role for the health of human beings. It is a complex system involving different types of molecules, cells, tissues, and organs throughout the whole body. Its primary functions are to distinguish foreign substances from self-antigens and to protect the human body from infections as well as other diseases. The foreign substances can be germs such as bacteria and viruses, and other materials such as chemicals and toxins. Under some circumstances, the dead and faulty cells of the body themselves will also be treated as foreign substances. The protective immunity against microbes is mediated by the earlier responses of innate immunity and the later responses of adaptive immunity. The innate immunity provides the first protecting line to defend against microbes by physical, chemical barriers and by phagocytes such as neutrophils and macrophages, natural killer (NK) cells, as well as by some proteins and cytokines in the blood. The innate immune system usually acts very quickly and is general effective [1]. If the foreign substances persist, the adaptive system will be further recruited as the second protecting line. Similar to the innate immune system, the adaptive immune system consists of humoral immunity components and cell-mediated immunity components. However, there lies a significant difference between them: the innate immune system responds only pattern-specifically to common broad categories of the pathogen while the adaptive immune system is highly specific to recognize each particular pathogen. Besides, due to the formation of memory cells during the primary infection, the adaptive immune system will respond more fiercely and quickly once encountering the same antigen again. Basically, two main kinds of immune cells are involved in the adaptive immune system, i.e., the T lymphocytes and B lymphocytes. They express highly diverse and specific antigen receptors and are responsible for the specificity and memory of the adaptive immune system. Nevertheless, their functions and recognition of antigens are quite different, which will be described in detail in the following parts.

5.1.1 T lymphocytes (T cells)

T cells are derived from the common lymphoid progenitor, which are differentiated from hematopoietic stem cells in the bone marrow (BM). Lymphoid progenitor cells migrate to the thymus and undergo differentiation and selection, ultimately, maturate into functional T cells. T cells can recognize antigens by the T-cell receptor (TCR). Most T cells express TCR containing two glycoprotein chains, i.e., an α (alpha) chain and a β (beta) TCR chain, whereas there is a minor population of T cells called gamma-delta (γδ) T cells with unique features of a TCR with one γ (gamma) chain and one δ (delta) chain. Conventional αβ T cells can only recognize and bind to the antigen as peptides presented by major histocompatibility complex

(MHC) molecules. There are two types of MHC molecules, MHC I and MHC II. The MHC I are expressed on all nucleated cells, whereas MHC II are expressed mainly on antigen-presenting cells (APCs) such as dendritic cells, macrophages, B cells, and a few other cell types including endothelial and epithelial cells [2]. Due to the TCR itself lacking an intracellular domain, it is unable to initiate downstream signaling. Instead, it is noncovalently associated with the CD3 molecules to form a TCR/CD3 complex to process the downstream signaling [3]. The CD3 molecule is a multimeric protein complex, which consists of three pairs of dimers (CD3εγ, CD3εδ, and CD3ζζ). The CD3γ/δ/ε chains each contain one immunoreceptor tyrosine-based activation motif (ITAM), whereas CD3ζ has three ITAMs. ITAMs are required for initiation of the signaling cascade upon T-cells activation [4]. According to their restriction on TCRs, T cells can divide into $CD4^+$ T cells (recognizing MHC II) and $CD8^+$ T cells (recognizing MHC I). In strong contrast to αβ T cells, γδ T cells can directly recognize antigens independent of an MHC complex [5], some γδ T cells even can serve as APCs, and prime $CD4^+$ T cells and $CD8^+$ T cells [6].

Upon TCR engagement, naïve $CD4^+$ T cells can differentiate into different T helper (Th) lineages, such as Th1, Th2, Th9, Th17, follicular T helper cells (T_{FH}), and regulatory T cells (Treg) (Figure 1). The differentiation of Th cells is determined by the cytokines in the environment during encounters with APCs. The naïve $CD4^+$ T cells are activated by two signals. The first one is via the interaction of TCRs expressed on T cells with the MHC-peptide complex. The second signal, also known as co-stimulatory signal, is via the binding of CD28 expressed on T cells with its ligands CD80 (B7-1) or CD86 (B7-2) expressed on APCs. As a third signal, cytokines promote the differentiation of T cells [7, 8]. The Th cell subset is distinguished predominantly by the cytokines it produces. Specifically, Th1 cells mainly secrete interferon-γ (IFN-γ), and lymphotoxin, while Th2 cells mainly produce IL-4, IL-5, and IL-13. Moreover, Th17 cells and Th9 cells are characterized by the production of IL-17 and IL-9, respectively. Each Th-cell subset exhibits a different effector function, which is mediated by the production of chemokines and cytokines [9-11]. For example, during virus infections, the differentiation of Th1 cells is promoted by interleukin-12 (IL-12), which activates signal transducer and activator of transcription 4 (STAT4). The subsequent cooperation with IFN-γ-activated STAT1 leads to the expression of T-box transcription factor T-bet and the expression of Th1-related genes [12]. Th1 cells can produce a high amount of IFN-γ, which activates macrophages to clean up pathogens [13]. The development of Th2 cells is involved in extracellular immunity to control parasites and in allergic immune responses and asthma. The Th2 polarization is driven by IL-4 via STAT6, followed by the induction of the transcription factor GATA3. Both Th1 and Th2 cells play a crucial role in regulating proliferation and immunoglobulin class switching of B cells. For instance, the immunoglobulin G2a (IgG2a) production is regulated by IFN-γ, while IL-4 promotes IgG1/IgE class switching [14]. The IL-21 and IL-4 secreting T_{FH} cells support

germinal center (GC) B cells to differentiate into plasma cells and memory cells, which are extensively involved in humoral immunity [15].

Tregs are a unique subpopulation of T cells that can suppress the immune response by inhibiting different cell types, therefore maintaining homeostasis and self-tolerance [16, 17]. Fork-head box P3 (Foxp3) is the master transcription factor for Tregs, and it cooperates with many other transcription factors to maintain the suppressive function and the stability of Tregs. Tregs might fully differentiate within the thymus and are then called thymic-derived natural Tregs (tTregs), but they can also stem from naive $CD4^+$ T cells and are – like Th cells – peripherally induced in response to the specific cytokine milieu. Lately, nomenclature discriminates such Tregs as pTregs, when skewing happens *in vivo* or iTregs, when they are differentiated in a culture dish.

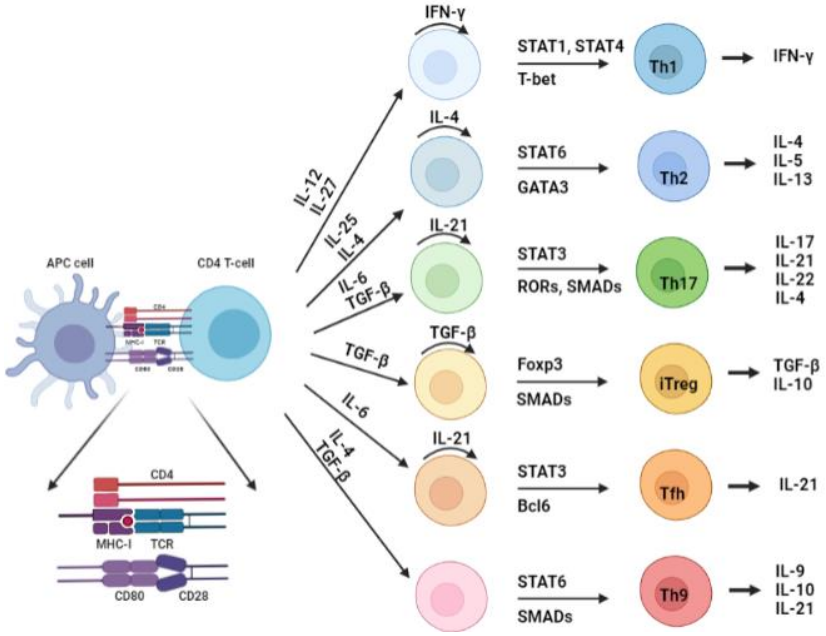

Figure 1: Differentiation of T helper cells.

A naïve T cell becomes activated through the interaction between the TCR and the MHCII-peptide complex and the co-stimulatory signaling via the binding of CD28 with CD80 or CD86. $CD4^+$ T cells differentiate into different T-helper lineages depending on the cytokines secreted by APC cells. Each T-helper cell subset is characterized by its specific cytokine and chemokine production, as well as the expression of unique transcription factors. The picture was created with Biorender.com and adapted from reference [18].

5.1.2 B lymphocytes (B cells)

Similar to T cells, B cells express a highly specific B-cell receptor (BCR). In the mature resting B cells, the IgM and/or IgD antibodies can be produced. Since those antibodies are inserted into the plasma membrane, they serve as BCRs. However, the cytoplasmic tail of IgM and IgD are too short for sufficient signaling. Thus, signal transduction of BCRs is mediated by two

other molecules, called Igα and Igβ. These two molecules are bisulfide-linked to each other and noncovalently associated with membrane Ig to form the BCR complex [19, 20].

Like T cells, B cells derive from the common lymphoid progenitors, which are differentiated from hematopoietic stem cells in the BM The development of B cells begins in the fetal liver and continues in the BM throughout humans' lives. Once B cells express a functional BCR, they will migrate into the periphery, and get activated by antigens in the secondary (or peripheral) lymphoid tissues such as the spleen, lymph nodes, and Peyer's patches (PPs). The B cells are activated once their BCR binds to either soluble or membrane-bound antigens. When antigen is detected by the BCR on naïve B cells, two different types of activation can occur, i.e., T cell-dependent or T cell-independent activation. The non-protein antigens, such as polysaccharides, membrane glycolipids, and nucleic acids that are multivalent can cross-link multiple BCRs, leading to a T cell-independent B-cell activation. However, protein antigens need to be internalized by the BCR and undergo enzymatic processing. Eventually, the peptides are loaded on MHC molecules by B cells and presented to T cells, giving rise to the activation of B cells in a T-cell-dependent manner [21]. Apart from BCRs, most complex antigens will engage other receptors on the B cell such as toll-like receptors (TLRs) or complement receptors (CR2), which results in amplification and modification of BCR signaling [22, 23].

5.1.3 Germinal center (GC)

Germinal center is a specialized microstructure that forms in B cell-rich follicles of secondary lymphoid organs (SLOs). GCs are the place where B cells undergo proliferation and selection for high affinity BCRs upon antigen stimulation, eventually differentiating into long-lived plasma cells and memory cells (Figure 2) [24]. The GC formation starts upon resting B cells interacting with antigen via their BCR. B cells can directly bind soluble antigens or antigens presented by follicular dendritic cells (FDCs), dendritic cells (DC), or macrophages [25]. Once B cells get activated through their BCR, they upregulate the chemokine receptor CCR7, and then migrate to the T cell-rich area (known as the T-cell zone) via CCR7 to interact with its ligands (CCL19 and CCL21) expressed in the T cell zone [26]. At the border between the B-cell follicle and the T-cell zone (T:B border), B cells interact with $CD4^+$ pre-T_{FH} cells through MHC II-presented antigen and receive the co-stimulatory signal via CD40-CD40L to become fully activated. The tumor necrosis factor (TNF)-receptor family member CD40 is expressed on B cells, and its ligand CD154 (also called CD40L) is induced on T cells upon activation and highly expressed by T_{FH} cells. Consequently, the activated B cells undergo proliferation and will either initiate the GC response or differentiate into short-lived extrafollicular plasma cells or memory B cells [27, 28]. Short-lived plasma cells can produce an initial wave of antibodies for early control of infection before the establishment of GC responses [29].

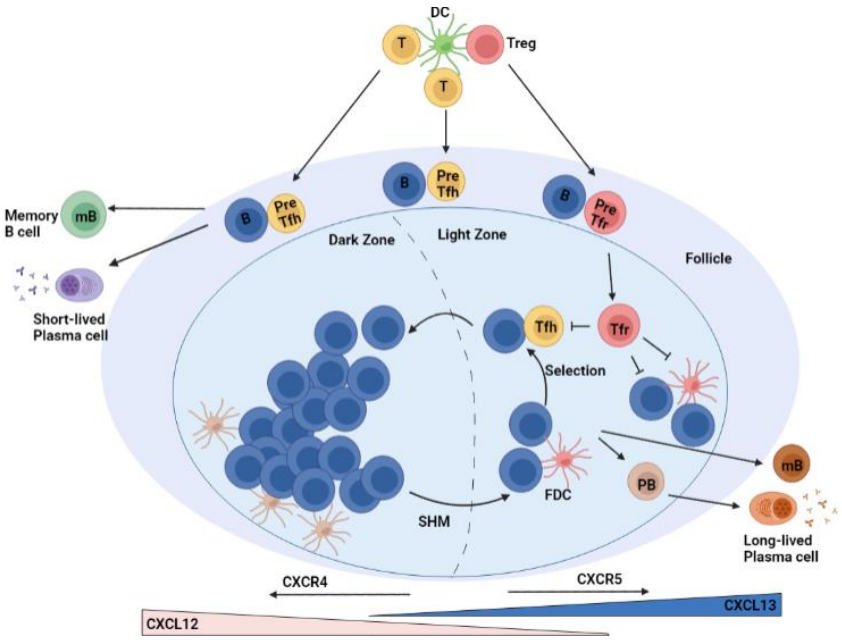

Figure 2: Overview of the GC reaction.

GC starts to form when B cells encounter antigen. The GC is divided into two compartments, LZ and DZ. Centroblasts undergo the SHM and clonal expansion to generate the diversity of BCRs of B cells in the DZ, then centroblasts differentiate into centrocytes and move to the LZ. With the help of T_{FH} and FDCs, centrocytes are selected in the LZ. Alternatively, a small subset of GC B cells can recycle back to the DZ for additional SHM and clonal expansion. Eventually, antigen-selected centrocytes differentiate into memory B cells or long-lived plasma cells. The picture was created with Biorender.com and adapted from reference [30].

After interaction with $CD4^+$ pre-T_{FH} cells, activated B cells will move to the primary follicle to initiate the GC response (Figure 2). Those GC-precursor B cells start to proliferate rapidly and undergo clonal expansion and then become GC-B cells. Later on, the GC divides into two distinct compartments, the dark zone (DZ) and the light zone (LZ). The DZ consists of rapidly proliferating B cells known as centroblasts. In the DZ, those centroblasts highly express the enzyme activation-induced deaminase (AID), which can induce somatic hypermutation (SHM) within the variable regions of the BCR leading to diversity of B cells with different affinities of BCR for antigens as well as class switch recombination (CSR). These centroblasts locate in the DZ by expressing the chemokine receptor CXCR4, which can bind with its ligand CXCL12 produced by stromal cells in the DZ. After GC-B cells undergo SHM in the DZ, they downregulate CXCR4 and upregulate CXCR5. Following the CXCL13 gradient, they migrate to the LZ and are known as centrocytes. The centrocytes with different affinities to antigens need to be selected in the LZ. Two antigen-based signals are available for B-cell selection in the LZ. The first signal is from the antigen itself. Only those B cells that can bind to the antigen presented by FDCs will survive. The second signal is available once B cells can deliver uptaken antigen to T_{FH} cells presented on MHC II. Around 10% of the selected B cells can recycle to

the DZ to undergo more SHM to increase the BCRs affinity for the antigen and migrate to the LZ for further selection [31]. Except for T_{FH} and FDCs, T_{FR} cells play a vital role in regulating the output of the GC response in the LZ in a concerted action of all cells within a GC, the selected B cells with higher affinity for antigen eventually differentiate into plasma cells and memory cells [32]. Those effector cells can provide antibodies to protect against infection and long lasting immunity for the host.

T_{FH} cells, defined by surface expression as $CD4^+$ $CXCR5^+$ $PD1^+$ $ICOS^+$ T cells, are essential for the development of GC responses and also a unique subset of $CD4^+$ T cells that specialize in helping B cells to produce antibodies. Without rescuing signals, isolated GC-B cells are prone to rapid apoptosis *in vitro*. They highly express the pro-apoptotic molecule CD95 (also known as Fas) and lack anti-apoptotic factors such as B-cell lymphoma 2 (Bcl-2) [33]. However, GC-B cells can receive survival signals from T_{FH} cells via the interaction between ICOS and its ligand ICOSL on B cells. Once the interaction happens, it will promote T_{FH} cells to upregulate CD40L, which, in turn, further upregulates ICOSL expression on B cells, resulting in enhanced interaction between T_{FH} and B cells [34]. Such feedback stimulates T_{FH} cells to produce the cytokines IL-4 and IL-21. These cytokines promote B-cell proliferation, CSR, and differentiation into plasma cells or GC-B cells. Specifically, IL-21 can promote the expression of the transcription factor Bcl6 in GC-B cells to regulate the GC response [35]. In addition, IL-21 can also support B cells to proliferate and differentiate into plasma cells [36]. IL-4 was first recognized as a cytokine that can induce the expression of the Bcl2 family member B-cell lymphoma-extra large (Bcl-xL) and enhance glucose metabolism through STAT6, therefore it can protect B cells from apoptosis [37, 38]. Except for its role in fostering the survival of B cells, IL-4 induces CSR and promotes isotype switching [39]. Another cytokine, called B cell-activating factor (BAFF), also plays a vital role in the survival of B cells. BAFF is produced by FDCs and follicular reticular cells (FRCs) in the LZ. BAFF enhances the CD40 expression on B cells [40], and activates several downstream pathways to promote the survival of B cells [41].

5.2 Hematopoietic stem cell transplantation (HCT)

Hematopoietic stem cell transplantation is a well-established and curative treatment for hematologic and lymphoid malignancies [42] and many inherited or acquired immune disorder diseases [43]. There are two main kinds of hematopoietic stem cell transplantation, i.e., autologous (auto-) HCT and allogeneic (allo-) HCT. Prior to HCT, patients are treated with conditioning therapy, which includes combinations of chemotherapy and/or radiotherapy. It can help to reduce the numbers of tumor cells and immunosuppressive ability to donor cells, as well as provide the space for the donor stem cells [44]. For allo-HCT, patients receive hematopoietic stem cells (HSCs) from another donor, and for auto-HCT, patients use their own stem cells. When transplanted stem cells are derived from the patient's own stem cells, they

do not cause graft-versus-host disease (GvHD). Consequently, autologous HCT is associated with less morbidity and mortality than allogeneic HCT. However, the most challenging problem is that autologous HCT does not exert a graft-versus-tumor (GvL) effect, which means residual cancer cells still can escape from the incoming as well as rebuilt immune system, resulting in a cancer relapse.

MHCs are the genetic loci involved in the rejection of the transplanted organs. In human bodies, the MHC, also called the human leukocyte antigens (HLA) system, is highly polymorphic. The genes *HLA-A*, *HLA-B,* and *HLA-C* encode MHC I molecules, and *HLA-DR*, *HLA-DQ,* and *HLA-DP* encode MHC II molecules. To date, the donor selection for transplantation depends on the matching of class I HLA-A, HLA-B, HLA-C, and class II HLA-DR. This is the minimum level of HLA match between donor and recipient (called 8/8 matches). The preferred choice for a donor is 10/10 HLA match (including HLA-DQ). The patients who do not find 8/8 matches will undergo haploidentical transplantation like parent to child, which increases the risk of GvHD [45]. In humans, BM or peripheral blood - enriched with G-CSF-mobilized BM cells - can be used to collect HSCs for transplantation. Once HSCs are transplanted intravenously, circulating hematopoietic stem and progenitor cells are arrested by stromal cell-derived factor-1 (SDF-1) that is expressed by BM endothelial cells [46]. The SDF-1 also activates integrin interaction between hematopoietic stem cells and extracellular matrix protein fibronectin, such as integrin very late activation antigen-5 (VLA)-5 and VLA-4 and their ligands VCAM-1 and ICAM-1 [47]. Therefore, the cells can extravasate through the endothelium into the hematopoietic compartments, where they differentiate into different immune cells to rebuild a new immune system to replace the eradicated hosts' immune system. The recovery of the immune system after HCT is a highly dynamic and a prolonged process. Generally, innate immunity, which includes NK cells, neutrophils and monocytes, starts to recover within a few weeks after HCT. Following the innate immunity, $CD8^+$ T cells and B cells often reach to normal level within 12 months. However, the functionality of B cells can be still affected by the degree of $CD4^+$ T cells. As $CD4^+$ T cells start to appear around three months after HCT but it takes up to 2 years to recover the T-cell compartment fully [48-50].

5.2.1 Graft-versus-host disease (GvHD)

GvHD is a major complication that can occur after allo-HCT. It is an immunological disorder mediated by donor T cells that leads to the damage of tissues and organs of recipients and causes a high risk of morbidity and mortality. GvHD also has a significant negative effect on the life quality of patients, especially in the chronic stage of GvHD. GvHD occurs in two phases: acute GvHD (aGvHD) and chronic GvHD (cGvHD). The aGvHD usually develops within 100 days after allo-HCT, whereas the cGvHD is defined to arise later (more than 100 days) and has some features of autoimmune diseases [51]. Generally, 40%-50% of patients will

experience aGvHD after HCT from a human leukocyte antigen (HLA)-matched sibling [52]. 60%-80% of patients can develop chronic GvHD [53] and more than 10% will die after HCT [54]. Except for HCT, solid organ transplantation also can lead to GvHD.

Thus, the most fatal risk factor for GvHD is an HLA mismatch. Additional risk factors include gender disparity between donor and recipient, myeloablative conditioning regimens, increased age and ineffective GvHD prophylaxis, the source of hematopoietic stem cells, and Cytomegalovirus or Epstein Barr virus seropositivity [55]. For example, Gratwohl *et al*. reported that female recipients are more protected from GvHD than male recipients, as - due to the mismatched minor histocompatibility antigens present on Y chromosome (H-Y) in male recipients - the risk of GvHD increases when male recipients receive stem cells from female donors [56].

5.2.1.1 Pathophysiology of acute GvHD

The aGvHD can cause the damage of tissues and organs, the main target organs are the skin, liver, and gastrointestinal (GI) tract. At the onset of GvHD, around 75% of patients have skin problems, about 30% of patients have GI dysfunction, and 8% of patients have liver disease [54]. Generally, the pathophysiology of aGvHD consists of three phases (Figure 3). In the first phase, patients are treated with a high dose of radiation therapy and /or chemotherapy before transplantation, which results in massive tissue damage, especially the damage of epithelial barriers. Upon damage, the cells release pathogen-associated molecular patterns (PAMPs), danger-associated molecular patterns (DAMPs) and pro-inflammatory cytokines, such as IL-1, IL-6, and TNF-α. PAMPs and DAMPs can be detected by pathogen recognition receptors on recipient APCs, such as TLRs, NOD-like receptors (NLRs), which leads to the activation of APCs. The extracellular adenosine triphosphate (ATP) can serve as a DAMP, which binds to P2X purinoreceptor 7 receptor ($P2X_7R$) on host APCs, enhancing the expression of costimulatory molecules, thus enhancing the antigen-presenting ability [57]. In the second phase, cotransplanted donor T cells are activated by recipient APCs, and then differentiate into Th1, Th2, Th17, and cytotoxic effector T cells, which causes the release of additional inflammatory cytokines, further recruiting additional effector cells including NK cells and neutrophils. In the final phase, pro-inflammatory cytokines and effector T cells further attack the epithelial cells of the skin, liver, lung, and gastrointestinal tract, resulting in further tissues damage.

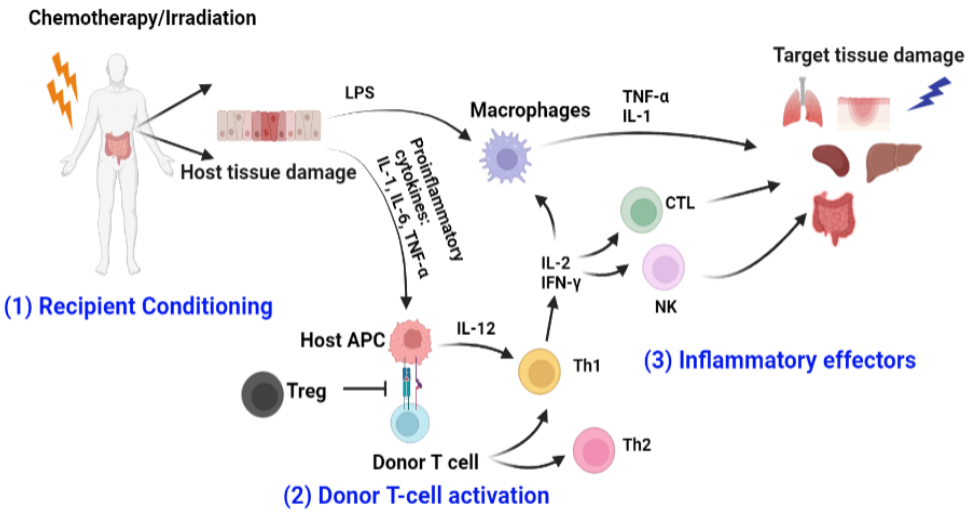

Figure 3: Overview of the GvHD pathogenesis.

(1) Before transplantation, recipients receive conditioning treatments (radiation and/or chemotherapy), causing tissue damage and resulting in the release of proinflammatory cytokines. (2) Transplanted donor T cells are activated by host APCs, leading to T-cell activation and differentiation. (3) Cytotoxic T cells and additional inflammatory cytokines further damage host tissues and organs. APC, antigen-presenting cell; CTL, cytotoxic T lymphocyte; IFN-γ, interferon-γ; IL, interleukin; LPS, lipopolysaccharide; NK, natural killer cell; TNF-α, tumor necrosis factor-α. The picture was created with Biorender.com and adapted from Reference [58].

5.3 Autoimmune disease

A healthy immune system is developed to protect hosts from diseases and infections. However, if tolerance mechanisms fail, the body cannot distinguish between harming foreign and self-antigens. This results in mistakenly attacking the body's own healthy cells, tissues, and organs, and unfortunately causing organ damage or dysfunction, which is called autoimmune disease. The etiology of autoimmune disease is multifactorial, i.e., linked to genetic, environmental, hormonal, and immunological factors [59]. However, the triggers for the onset of at least 50% of autoimmune diseases are still unknown. There are more than 100 autoimmune diseases, some of them are well known, such as type 1 diabetes, multiple sclerosis (MS), Systemic lupus erythematosus (SLE), and rheumatoid arthritis (RA), whereas others are rare diseases that are difficult to be diagnosed [60].

5.3.1 Multiple sclerosis (MS)

Multiple sclerosis is a chronic inflammatory disease of the central nervous system (CNS), which causes demyelination and neurodegeneration of the CNS in young adults. The MS is a complex autoimmune disease, which again is associated with multiple factors, including genetics and environment. The most well-established environmental factors are Epstein-Barr virus (EBV) infection, a lack of sun exposure (particularly exposure to ultraviolet-B radiation), low level of vitamin D, obesity, and tobacco exposure via active or passive smoking. Other

less-defined risk factors include night shift work, alcohol consumption, and caffeine consumption [61].

The MS is quite heterogeneous in clinical course and symptoms. Typically, it can be divided into four distinct clinical phenotypes (Figure 4): relapsing-remitting multiple sclerosis (RRMS), secondary-progressive multiple sclerosis (SPMS), primary progressive multiple sclerosis (PPMS), and progressive relapsing multiple sclerosis (PRMS) [62]. Generally, 85% of patients start with RRMS, which is characterized by an episode of neurological dysfunction and remission. During the relapse period, the inflammation and demyelination in the CNS can be detected by magnetic resonance imaging (MRI). As the disease progresses, around 80% of patients continue to develop SPMS within 1-2 decades after initial diagnosis. In SPMS patients, the occurence of inflammatory lesions is diminished. SPMS patients do not experience a period of relapse and recovery anymore, while the disability due to axonal loss increases [63].

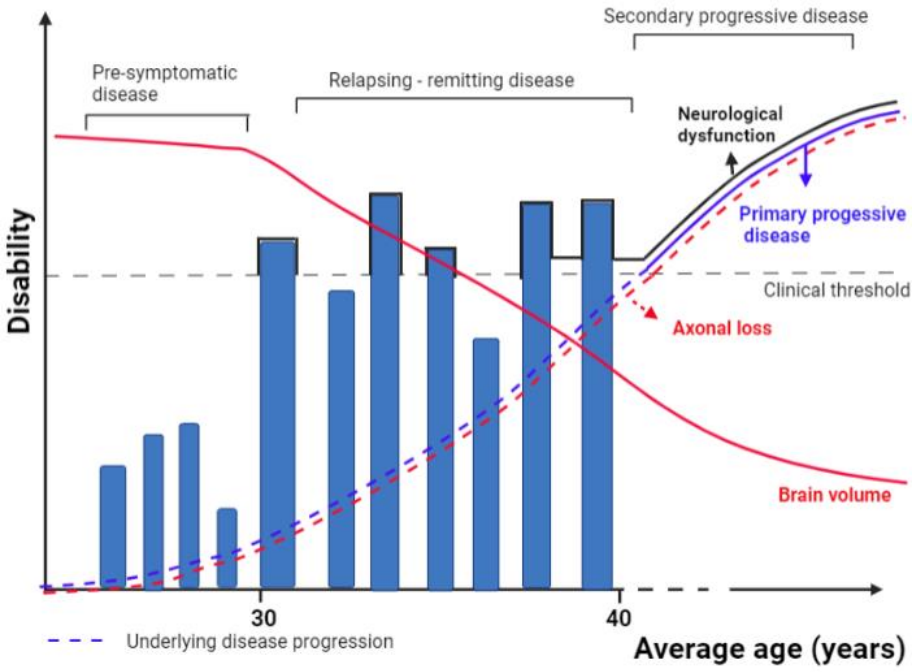

Figure 4: The clinical course of multiple sclerosis.

The US National Multiple Sclerosis Society (NMSS) Advisory Committee on clinical trials in multiple sclerosis defined four clinical courses of MS: relapsing-remitting MS (RRMS), secondary progressive MS (SPMS), primary progressive MS (PPMS), and progressive relapsing MS (PRMS) [62]. The picture was created with Biorender.com and adapted from reference [63].

Although two contradictory concepts have been employed to explain the etiology of MS, its exact cause is still unclear up to now. An inside-out concept indicates that MS starts with the release of myelin antigens from damaged or destabilized myelin, caused by an infection or neurodegeneration. Those myelin antigens are released to the periphery, leading to the

activation and expansion of autoreactive T cells. Once those autoreactive T cells migrate to the CNS and are reactivated by APCs there, they will release cytokines leading directly and indirectly to further myelin destruction. Moreover, naïve $CD4^+$ T cells can get activated through epitope spreading induced by T-cell responses, i.e., T cells respond to endogenous epitopes secondary to the release of self-antigens [64], causing further inflammation [65]. In the outside-in concept, T cells are activated by antigens expressed by some viruses or other microbes which have a mimic epitope of myelin peptide, a phenomenon referred to as 'molecular mimicry'. Those falsely myelin-specific and activated T cells then migrate into the CNS and lead to myelin destruction in the way similar to the inside-out concept. The latter is supported by the findings of the experimental autoimmune encephalomyelitis mouse model (EAE). Irrespective of the initial cause, activated $CD4^+$ T cells differentiate into Th1 and Th17 cells, then infiltrate into the CNS, subsequently reactivated by resident APCs such as DCs, microglia, and astrocytes. The cytokines IFN-γ and IL-17 produced by Th1 and Th17 cells increase the permeability of the blood-brain barrier (BBB) and recruit other immune cells to the CNS. Furthermore, microglia cells are activated in the CNS, which in turn produce pro-inflammatory cytokines, leading to the demyelination and the loss of axons [66].

5.3.1.1 The mechanism of multiple sclerosis (MS)

The mechanism of multiple sclerosis is different during different stages of diseases. In the earlier stage of the disease, many immune cells, such as T cells, B cells, monocytes, infiltrate into the CNS and together with resident microglia and astrocytes contribute to demyelination (Figure 5), whereas the infiltration of immune cells into the CNS is reduced in the later stage of the disease. But long-term inflammation and neurodegeneration are still ongoing due to the formation of tertiary lymphoid structures and the dysfunction of astrocytes and microglia. Tertiary lymphoid structures resemble GCs and often contain B cells, T cells, FDCs, and plasma cells, which provide the environment for supporting the activation and maturation of local B and T cells [67]. Microglia and astrocytes play a key role in regulating the inflammatory responses in the CNS. Microglia are the resident macrophages in the CNS, they can be pro-inflammatory or neuroprotective. For example, they can secret anti-inflammatory molecules or phagocyte the debris to promote remyelination. On the other hand, they can produce pro-inflammatory molecules to damage the myelin sheath and oligodendrocytes [68]. The activated microglia can also promote astrocytes to produce CCL2 and GM-CSF, which in turn recruits and activates more microglia to the site of demyelination. Astrocytes can indirectly inhibit remyelination by preventing the generation of mature oligodendrocytes [69]. The acute or chronic oxidative stresses produced by innate or adaptive immune cells are neurotoxic and finally cause continuous inflammation and neurodegeneration in the CNS (Figure 6) [63].

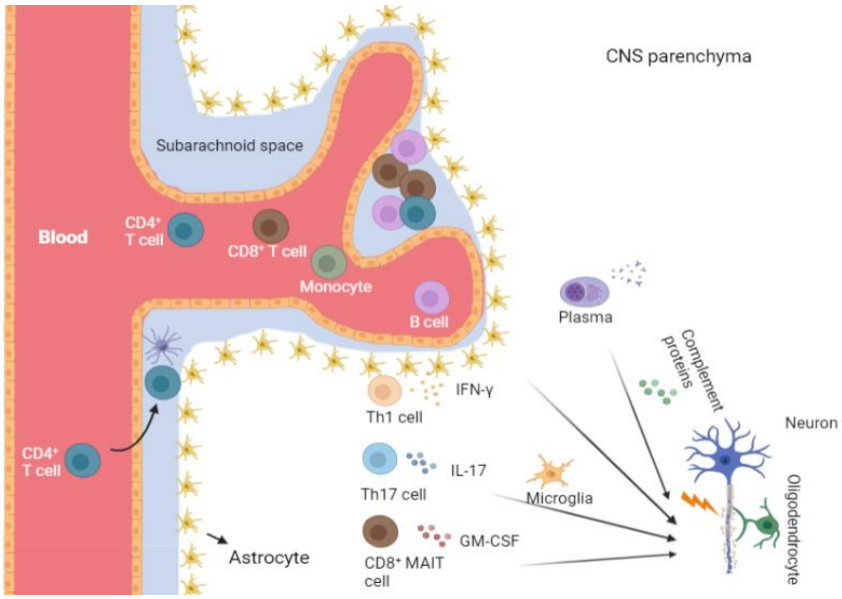

Figure 5: Dysregulation of the immune response in the CNS in the early stage of MS.

The infiltrated immune cells from the periphery are reactivated by APC cells in the CNS, causing the production of pro-inflammatory cytokines, which in turn enhances the infiltration of further immune cells. Those immune cells together with resident microglia cause demyelination and axonal loss. Autoantibodies produced by plasma cells cause further damage of myelin by antibody-dependent cellular cytotoxicity (ADCC) and complement-mediated cytotoxicity (CDC). The picture was created with Biorender.com and adapted from reference [70].

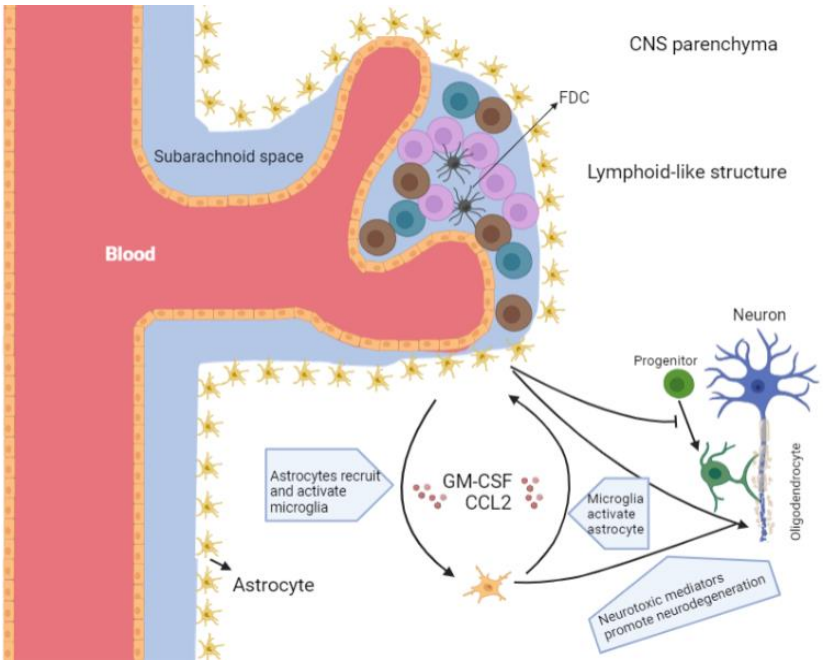

Figure 6: Immune cells are involved in the later stage of MS.

The infiltration of immune cells is diminished, due to the chronic exposure of antigens, leading to the exhaustion of immune cells. However, the chronic inflammation of the CNS is still ongoing. The Meningeal tertiary lymphoid-like structures and the dysfunction of astrocytes and microglia contribute to late-stage inflammation in patients. Activated microglia can promote astrocytes to produce CCL2 and GM-CSF, which in turn recruit and activate more microglia to the site of demyelination. Astrocytes promote demyelination. Those pro-inflammatory mediators contribute to continuous inflammation and neurodegeneration in the CNS. The picture was created with Biorender.com and adapted from reference [70].

Under normal conditions, the blood-brain barrier (BBB) is formed by endothelial cells in the interior of all blood vessels, which are extremely close to each other to form the endothelial tight junction (TJ) and to build a barrier between the circulating blood and the CNS. Those endothelial cells express several adhesion molecules such as intercellular and vascular cellular adhesion molecules (ICAM-1, VCAM-1), P- and E-selectins [71]. These adhesion molecules are necessary for cells to attach to the vessel wall. In the absence of neuroinflammation, the BBB allowed limited immune cells to migrate into the CNS during immune surveillance. However, in the neuroinflammation situation, e.g., EAE or MS, the permeability of the BBB is enhanced [72].

Both Th1 and Th17 cells can induce EAE via the cytokines IFN-γ and IL-17. The IFN-γ exacerbates EAE during disease induction by disrupting tight junction through VE-cadherin and tight junction molecules. Moreover, IFN-γ induces adhesion molecule ICAM-1 and MHC II expression on the surface of endothelial cells of BBB, which promotes the transendothelial migration of antigen-specific $CD4^+$ T cells [73]. In addition, IFN-γ affects CNS cells. It can induce chemokine expression by astrocytes, such as CCL2, CXCL10, enhancing the recruitment of myeloid cells and increasing the expression of MHC I and II [74]. Like IFN-γ, IL-17 can disrupt the BBB by recruiting neutrophils. Besides, the IL-17 enhances the activation of matrix metalloproteinase-3 (MMP-3) and attracts neutrophils to the site of inflammation. MMPs, together with other proteases, and gelatinases can be activated by neutrophils, resulting in BBB impairment [75, 76]. IL-17 can also increase inflammation by inducing chemokine production and enhancing the transmigration of T cells and monocytes to the CNS [77]. Both Th1 and Th17 can produce GM-CSF, which is considered to be essential for disease development, especially in the effector phase of disease since the treatment of anti-GM-CSF antibodies at disease onset can ameliorate disease [78].

However, IFN-γ has both anti-inflammatory and pro-inflammatory effects in the CNS, which reflects different outcomes of treatment with IFN-γ at different stages of the disease. Treatment with IFN-γ on mice during the inductive phase of EAE (d 1 - d 9) exacerbates EAE, while treatment at the effector phase (d 10 - d 19) reduces the severity of EAE [79]. The reason for the opposing activities of IFN-γ exerted in MS and different models of EAE remain unclear, as IFN-γ exerts opposing effects on many immune cells, including innate and adaptive immune cells. For example, IFN-γ can induce Indoleamine-2,3-dioxygenase (IDO) expression in microglia via STAT-1 and phosphatidylinositol 3-kinase (PI3K) signaling pathways. The IDO can reduce extracellular tryptophan and increase the production of kynurenine which suppresses the proliferation of myelin-specific T cells and inhibits the production of Th1 cytokines [80]. IFN-γ can promote the infiltration of macrophages and neutrophils into the CNS, and the differentiation of Th1 cells [81]. Apart from $CD4^+$ T cells, $CD8^+$ T cells are also involved

in MS pathogenesis. In the body of MS patients, the level of IL-8 in the serum is significantly increased [82], which can activate $CD8^+$ mucosa-associated invariant T (MAIT) cells and enhance their ability to infiltrate the CNS, which also produce IL-17 cytokine [83]. Another lymphoid subpopulation, i.e., Tregs, play a very important protective role in MS. Tregs can suppress autoimmune responses and inhibit inflammatory cells. However, the expression of the key transcription factor Foxp3 is significantly reduced, and consequently the suppressive function of Tregs is dramatically diminished in MS patients [84], which causes disease exacerbation and progression.

5.3.2 Experimental autoimmune encephalomyelitis (EAE)

EAE is the most common rodent model, which has been widely used for investigating aspects of human MS. Several antigens have been identified as target antigens to induce EAE, such as myelin oligodendrocyte glycoprotein (MOG), proteolipid protein (PLP), and myelin basic protein (MBP) [85]. Here, we focus on MOG only since it has become an important target in MS. MOG is a transmembrane protein, which is expressed on the surface of oligodendrocytes and the outer surface of myelin sheaths. MOG only accounts for 0.1% of total CNS myelin protein. However, autoreactive T cells specific for MOG are most likely more readily detected in MS patients than the T cells specific to PLP and MBP [86]. In EAE models, the disease is induced through actively immunizing with specific antigens, or passively transferring encephalitogenic T cells. During immunization, pertussis toxin (PT) further promotes the opening of the BBB [87]. For passive EAE, 2D2 mice were created by Bettelli *et al.* [88]. In these mice, more than 90% of T cells express transgenic TCR Vα and Vβ chains, which are specific for $MOG_{35–55}$.

5.4 Nuclear factor of activated T-cells (NFAT)

Nuclear factor of activated T-cells (NFAT) is a family of transcription factors that consists of five family members: NFATc1 (NFAT2 or NFATc), NFATc2 (NFAT1 or NFATp), NFATc3 (NFAT4 or NFATx), NFATc4 (NFAT3), and NFAT5 (TonEBP) [89, 90]. NFAT5 is regulated by osmotic stress [91], and the remaining four NFAT proteins (referred to NFATs in the following) are regulated by calcium signaling. NFATc1, NFATc2, and NFATc3 have two or more isoforms generated by alternative splicing and / or the use of different promoters. All the NFATs share a similar structure, which contains four domains, namely, N-terminal transactivation domain (TAD-N), regulatory domain, also known as NFAT-homology region (NHR), DNA-binding domain, also known as Rel-homology region (RHR), and second transactivation domain at the C-terminus (TAD-C). Regulatory domain and DNA-binding domain (around 68-73% sequence homology) are quite conserved among different NFATs. The regulatory domain has docking sites for calcineurin and NFAT kinases, which regulate the activation of NFATs by determining

the phosphorylation status of multiple serine and threonine residues. The regulatory domain also contains the nuclear localization signals (NLS) and nuclear export signals (NES), which determine the subcellular localization of NFATs (Figure 7).

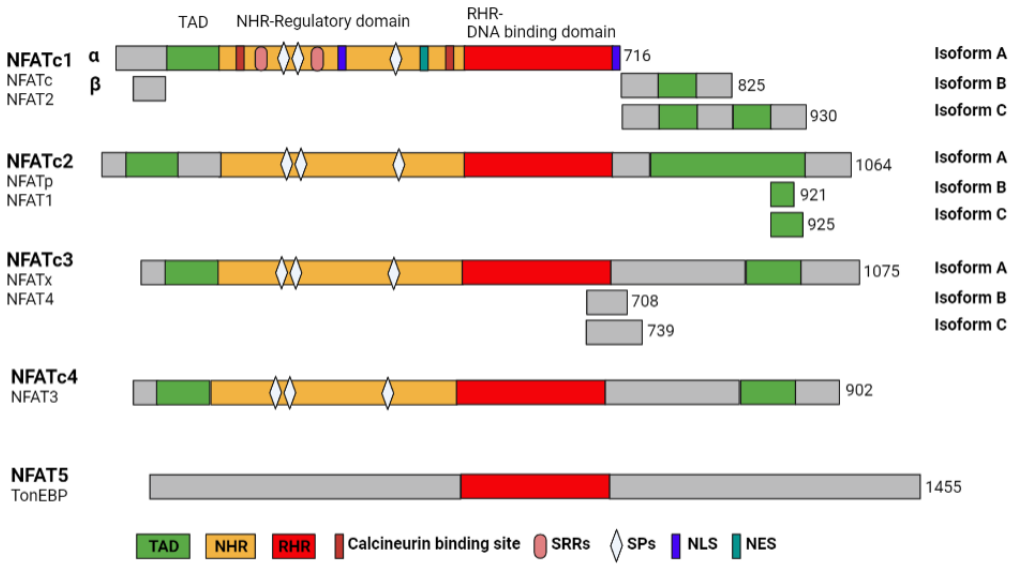

Figure 7: Schematic structure of all NFAT family members.

The structure of all five NFAT proteins is shown with their alternative names (on the left) and the amino acid length of each isoform (on the right). The picture was created with Biorender.com and adapted from reference [92].

The knock-out of individual NFAT genes in mice revealed a functional dichotomy between the three NFATs in lymphocytes. Here, let us focus on NFATc1. NFATc1 has six different isoforms as it is generated by the usage of two different promoters, alternative splicing and two poly-A sites. The two promoters consist of the inducible P1 and the constitutive P2. As shown in Figure 8, both P1 and P2 give rise to three different mature transcripts. P1 transcripts start at exon 1 and encode NFATc1 proteins with the N-terminal α peptide, while P2 transcripts start at exon 2 and code for proteins with the N-terminal β peptide [93, 94]. The 3'-encoded differences for the C-termini of these proteins result in either the short isoform A or the longer isoforms B and C. The B and C isoforms are caused by alternative splicing and additional poly-A site (pA2), whereas the short isoform A is terminated at the poly-A site pA1 [95]. In resting T cells, NFATc1 predominately exists as isoform B and C. However, following T-cells activation and nuclear translocation of pre-existing NFATs, those can induce the massive expression of NFATc1/αA, as NFATs transactivate P1, which drives the expression of NFATc1/αA, the so-called autoregulation of the P1 promoter [96].

NFATs have several SUMOylation sites. For example, within the long isoform NFATc1/C of NFATc1 three SUMO consensus sites were identified at the position of aa 349, 702, and 914, whereas the shortest isoforms of NFATc1/A (c1/A) only harbors the common SUMOylation site

at aa 349 [97]. As we know, NFATc2 has two homologous SUMOylation sites at the position of aa 684 and 897 [98]. Similarly, NFATc3 also has three SUMOylation sites at the position of aa 435, 704, and 1014 [99]. SUMOylation of NFATc1 and NFATc2 causes different functional outcomes. SUMOylation of the C termini of NFATc2 promotes nuclear localization [98], whereas SUMOylation of NFATc1 dampens the transcription of *Il2* by chromatin condensation [97].

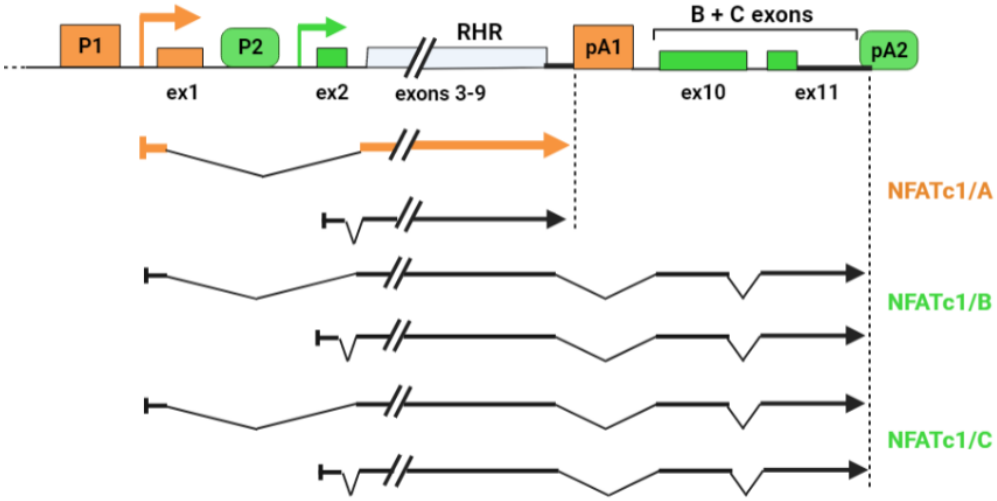

Figure 8: Schematic structure of NFATc1.

NFATc1 contains two promoters, P1 and P2, and the two poly-A addition sites, pA1 and pA2. P1 starts transcription from exon1, which splices to exon3. Transcription ends with pA1 to generate the short isoforms A (all NFATc1/αA-specific features are shown in orange). Green indicates the long isoforms B and C, which are controlled by promoter P2 and pA2. The picture was created with Biorender.com and adapted from reference [100].

5.5 SUMOylation

SUMOylation is a post-transcriptional modification that attaches the Small Ubiquitin-like Modifier (SUMO) proteins covalently to specific lysine residues in target proteins, resulting in functional change of proteins [101-103]. In line, SUMOylation is involved in several biological processes, including DNA damage repair, gene transcription, cell cycle progression, apoptosis and response to stress [104]. There are four mammalian members of the SUMO family that have already been identified, namely, SUMO-1, SUMO-2, SUMO-3, and SUMO-4. SUMO-2 is quite similar to SUMO3 (95% identical, consequently referred to as SUMO2/3), but both of them are only around 45% identical to SUMO-1. SUMO-1 mainly participates in normal cellular physiological processes, such as nuclear transportation, cell cycle progression, and oncogenesis, whereas SUMO-2 and SUMO-3 are mainly involved in the cell stress response [105]. SUMO-4, belonging to another SUMO protein family, has around 86% sequence identity with SUMO-2 and SUMO-3. However, its function remains enigmatic as it cannot be conjugated under normal conditions. Still, it is widely used for modification of proteins under stress conditions like starvation [106].

Similar to ubiquitin, all SUMO family members undergo a series of enzyme catalytic steps for protein modification (Figure 9). This includes maturation, activation, conjugation, and ligation [107]. Firstly, inactive SUMO precursor proteins are cleaved by a family of SENP (sentrin/SUMO-specific protease) enzymes at the C-terminus to produce a terminal diglycine GG motif [108]. In the second step, the mature SUMO is activated by the SUMO E1 enzymes in an ATP-dependent reaction with two steps. The SUMO E1 contains two SUMO-activating enzyme subunits 1 and 2 (SAE1/SAE2, also called activator of SUMO1 (Aos1)/ubiquitin-like modifier activating enzyme 2 (Uba2)), which can form a heterodimer. SAE1 (Aos1) promotes adenylation of the SUMO C-terminus to form the SUMO-adenosine monophosphate (AMP) intermediate, then transfer SUMO to the Cys residue on SAE2 (Uba2) via a thioester bond [109]. In the third step, SUMO is transferred from the SUMO E1 enzyme to the Cys residue on SUMO E2 via a thioester bond. The ubiquitin-conjugating enzyme 9 (Ubc9) is the only known SUMO E2 for the conjugating step for SUMOylation [110]. In the fourth step, Ubc9 can directly transfer SUMO to a Lys residue of some target proteins via an isopeptide bond. SUMOylation occurs mostly on the Lys within the consensus core motif Ψ-Lys-*X*-Glu (Ψ: a hydrophobic amino acid, *X*: any amino acids) [111]. Normally, Ubc9 works together with a SUMO E3 ligase, which can stimulate Ubc9 to release SUMO and enhance the efficiency of the conjugation between SUMO and substrate, providing substrate specificity. SUMOylation is a reversible process, which is readily annulled by SENPs.

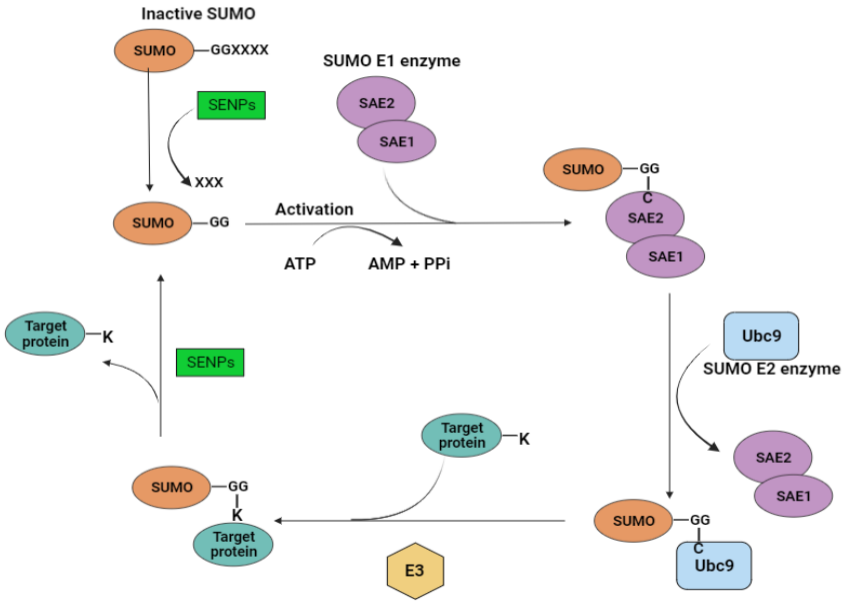

Figure 9: The mechanism of SUMOylation.

SUMOylation is an enzymatic cascade of E1, E2, and E3 enzymes' progress. Firstly, the sentrin-specific proteases (SENPs) cleave four amino acids from the C terminus of SUMO, upon which those expose the Gly-Gly motif for conjugation. The mature SUMO is activated by enzyme E1 (SAE1- SAE2), then SUMO is transferred from E1 to E2-Ubc9. Finally, Ubc9 can directly transfer SUMO to the target protein or in combination with SUMO E3 ligases. SUMOylated target proteins also can be reversed by SENPs. The picture was created with Biorender.com and adapted from reference [112].

The SUMOylation/deSUMOylation cycle (Figure 9) is highly dynamic and it drastically influences the functions of target proteins, including stability, localization, and activity. On the molecular level, SUMOylation changes the protein surface, resulting in three different consequences on the surface of the protein. After SUMOylation, it may mask certain binding sites. It also can expose existing binding sites by conformational change or create a new interface on the target protein that can recruit other binding partners in a SUMOylation-dependent manner [113]. Therefore, SUMOylation influences the interaction between target proteins with other molecules. As the result, SUMOylation can either promote or interfere with protein interactions.

Only a small proportion of most target proteins need to be SUMOylated at the steady stage to achieve a maximal effect. Multiple transcriptional factors (TFs) turn into transcriptional repressors upon SUMOylation, which is mainly achieved through two mechanisms (Figure 10). First, the SUMOylation of the TF can recruit repressive factors with chromatin-remodelling activity, such as the histone deacetylases (HDACs) or death-domain-associated protein (DAXX) [114, 115]. The SUMO-mediated HDAC recruitment causes the deacetylation of local histones, resulting in a condensed chromatin structure, in the end inhibiting transcription. Likewise, SUMOylation could recruit some repressor proteins, such as DAXX, formatting a repressor complex. Interestingly, this repressor complex remains stable even after deSUMOylation. Under both situations, SUMOylation can negatively regulate gene transcription.

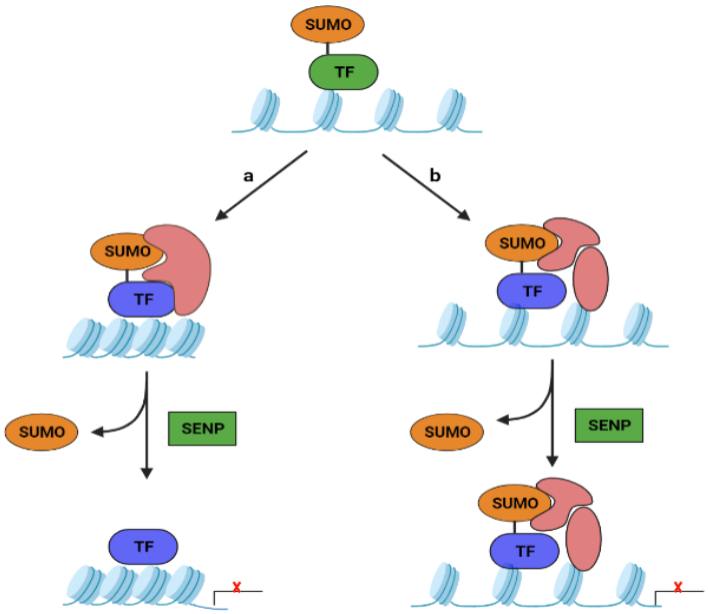

Figure 10: The SUMOylation of transcription factors can result in quantitative gene repression.

(a) SUMOylation of a TF can recruit downstream repressive effectors that can change the chromatin structure (such as HDAC), leading to the inhibition of transcription. (b) SUMOylation of a TF can recruit repressor proteins to form a repressor complex, resulting in the repression of transcription. The picture was created with Biorender.com and adapted from reference [116].

5.6 The role of NFAT in T cells

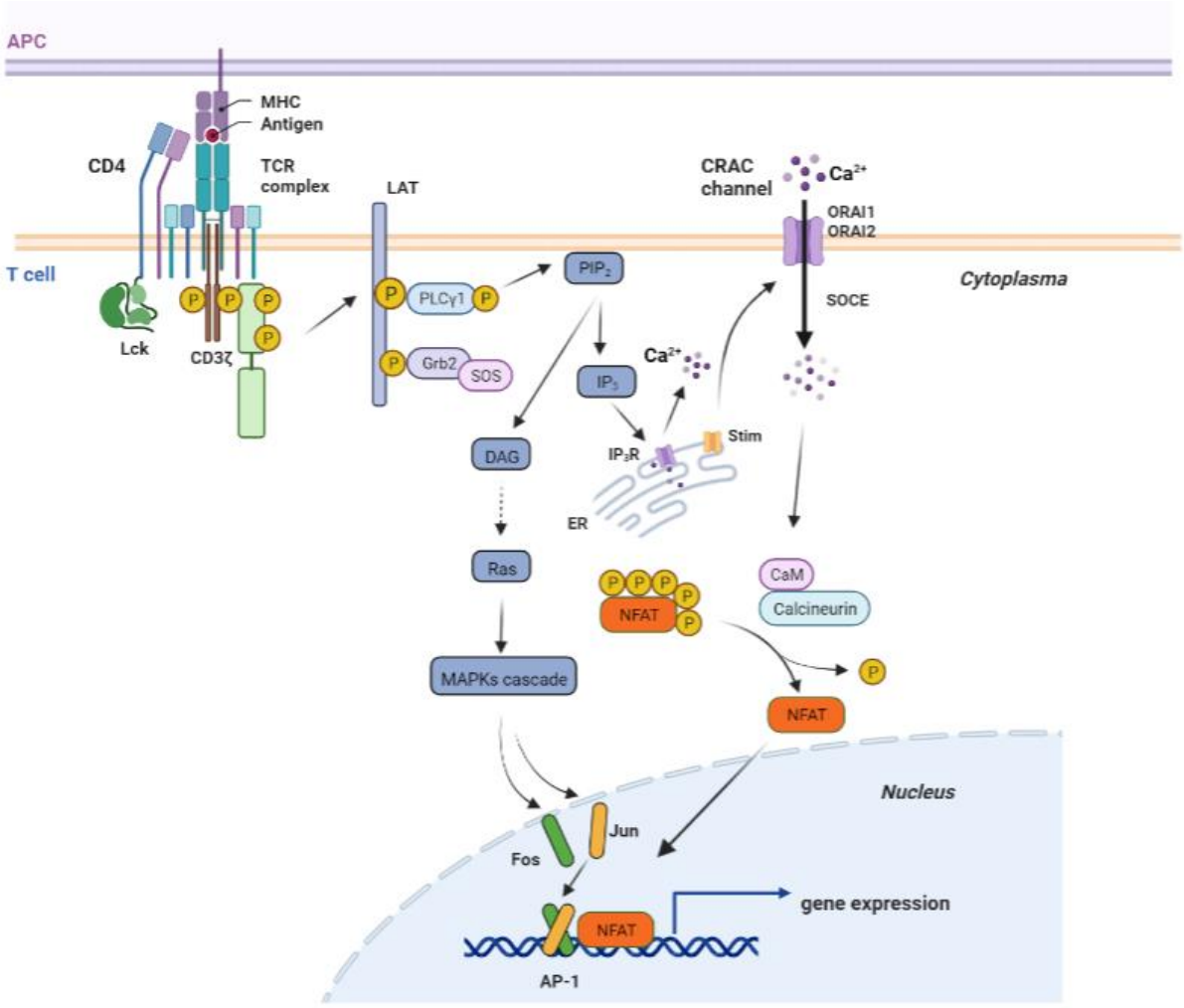

Figure 11: The NFAT signaling pathway.

Representation of NFAT activation and translocation to the nucleus. The engagement between TCR and MHC triggers the activation of tyrosine kinases that lead to the activation of PLC-γ, which promotes the hydrolysis of PIP2 to IP3. Then, IP3 binds to its IP3R receptors and releases the Ca^{2+} ions from the ER to the cytoplasm, which activates Stim proteins and results in conformational change. Consequently, Stim proteins bind to Orai to form the Ca^{2+} release-activated Ca^{2+} (CRAC) channel and SOCE, which leads to the activation of the phosphatase calcineurin. In the end, NFATs are dephosphorylated and translocated to the nucleus. In the nucleus, NFAT binds to DNA and regulates gene expression. PIP2: phosphatidylinositol-4,5-bisphosphate; IP3: inositol-1,4,5-trisphosphate; ER: endoplasmic reticulum. The picture was created with Biorender.com and adapted from reference [92].

NFATs are expressed in many different cell types and involved in many organs, including blood vessels, heart, kidney, central nervous system, bone, and hematopoietic stem cells [117, 118]. In lymphocytes, NFATc1, NFATc2, and NFATc3 are highly expressed. They control development, activation, and differentiation of T cells by regulating other genes' expression. The activation of NFAT is led by the engagement of receptors that are involved in the calcium-signaling pathway, such as the antigen receptors expressed on T and B cells, the Fcγ receptors

expressed on monocytes and natural killer cells, or the Fcε receptors expressed on mast cells. Here, we use the T cells as an example to describe how NFAT is activated in T cells (Figure 11). Upon TCR engagement with peptide-MHC presented by APC cells, the src family kinase Lck phosphorylates the tyrosine residues located in ITAM in CD3 molecules, resulting in the recruitment and phosphorylation of Zap70 kinase [119]. The activated Zap70 binds to and phosphorylates the transmembrane adaptor protein Lat. The phosphorylated Lat induces the recruitment of further adaptor proteins (Gads, Adap, Slp76, and Grb2) and signaling molecules (PLCγ1, Sos1, and Vav1). Afterwards, phospholipase C-γ1 (PLCγ1) hydrolyzes phosphatidylinositol-4,5-bisphosphate (PIP_2) into inositol-1,4,5-trisphosphate (IP_3) and diacylglycerol (DAG). IP_3 binds to the IP_3 receptors (IP_3R) expressed on the endoplasmic reticulum (ER), inducing the release of calcium ions (Ca^{2+}) from the ER. Stim proteins of the ER sense the Ca-emptiness and interact with Orai proteins at the plasma membrane. This leads to channel formation and store-operated Ca entry (SOCE). This highly elevated intracellular Ca^{2+} activates the phosphatase calcineurin. Afterwards, calcineurin dephosphorylates specific NFAT serine residues, which causes a conformational change of NFATs to expose the NLS and translocate to the nucleus. Finally, the NFATs bind to DNA alone or together with other nuclear proteins to regulate gene expression [92, 120, 121].

6 Objective of the work

In NFATc1, the long isoform NFATc1/C has three SUMO consensus sites at the position of aa 349, 702, and 914, whereas NFATc1/A (c1/A) only harbors the common SUMOylation site at aa 349. Previous studies of our group had shown that the SUMOylation site at aa 349 was an extremely weak SUMOylation site, i.e., when either the C-terminal or all three SUMOylation sites were mutated, the effect on NFATc1 was the same. In particular, SUMO1 posttranslationally modifies NFATc1/C within its C-terminus at the lysine residues K702 and K914 in EL-4 cells, causing less production of IL-2 [97]. The mechanism relies on the recruitment of HDACs to the *Il2* promoter by SUMOylation, resulting in a condensed structure of the chromatin at *Il2*. Eventually, this inhibits the transcription of IL-2. This raised three questions: The first one is how it will affect T cells *in vivo* once generating the corresponding mutations in the mouse genome; the second one is, as the SUMOylation sites are located in the exon 10-encoded C-terminus of NFATc1, whether knocking out the whole exon 10 can cause the same effects; the last one is the role of SUMOylation of NFATc1 in T cell-mediated diseases.

To solve these questions, we generated a transgenic mouse which carries point mutations at the two C-terminal SUMOylation sites of *Nfatc1*. Thereby, the lysines were exchange with arginine residues (K702R and K914R). The respective NFATc1 protein was named NFATc1/ΔS. Concomitantly, we inserted loxP sites in the intron preceding and following exon 10, thereby creating the possibility to completely ablate the SUMOylation site-containing exon 10. This artificial isoform was named NFATc1/ΔBC. The functions of NFATc1 SUMOylation on T cells were investigated in these two mice *ex vivo* and *in vivo*. For understanding the effects of SUMOylation of NFATc1 on T cell-mediated diseases, two different mouse disease models were used, i.e., the aGvHD and passive EAE mouse model.

Furthermore, our previous studies have demonstrated that T_{FH} and T_{FR} cells highly express NFATc1 [122, 123]. It is known that follicular T cells are critical for the development of GC-B cells and GC responses. Therefore, we also want to understand whether SUMOylation of NFATc1 has a special effect on T_{FH} cells and GC responses, including those in humans. For this purpose, an *in-vitro* culture system for the human GC reaction is needed. However, many *in-vitro* culture systems rely on isolated B cells or slices of tissues to prepare explant cultures. Unfortunately, these *in-vitro* culture systems either do not contain the entire cell composition or the cell components only can survive for 3 - 4 d. Therefore, we urgently need an optimal *in-vitro* culture system for tonsil organoids. Thus, it was the last aim to establish an *in-vitro* culture system for human tonsil organoids.

7 Materials and Methods

7.1 Materials

7.1.1 Chemicals and reagents

Chemical	Company
KCl	Roth
Na_2HPO_4	Roth
NaOH	Roth
$CaCl_2$	Roth
HCl	Roth
LiCl	Roth
NaCl	Roth
$MgCl_2$	Roth
NH_4Cl	Roth
$KHCO_3$	Roth
Acetic acid	Roth
Ethanol	Roth
Isopropanol	Roth
Agarose	AppliChem
Tris-HCl	Roth
$NaHCO_3$	Roth
Proteinase K	Thermo Fisher Scientific
6x DNA Loading Dye	Thermo Fisher Scientific
Midori Green	Nippon Genetics
DNA marker 1kb and 100bp	Thermo Fisher Scientific
NP-40	Roth
Dimethyl-sulfoxide (DMSO)	Gibco
Sodium Deoxycholate	Roth
β-Mercaptoethanol	Roth
Phenylmethylsulfonyl Fluoride (PMSF)	Roth
Sephadex G50	Sigma-Aldrich
Bradford Reagent	Bio Rad
Western Blotting Substrate	Thermo Fisher Scientific
Acrylamide	Roth

Tetramethylethylenediamine (TEMED)	Roth
TPA	Merck
Ionomycin	Sigma-Aldrich
Golgi-Stop	BD
Golgi-Plug	BD
DNase I	Roche
Collagenase D	Roche
Taq DNA polymerase	Thermo Fisher Scientific
PCR master mix	Thermo Fisher Scientific
Phenol/Chloroform/Isoamylalcohol	Roth
Sodium Lauryl Sulfate (SDS)	Roth
Glycine	Roth
Ponceau S	Sigma-Aldrich
Bromophenol Blue	Sigma-Aldrich
Agar	Roth
LB Medium	Roth
Ampicillin	Roth
Formaldehyde 37%	Roth
Triton-X 100	Roth
TurboFect TransfectionReagent™	Thermo Fisher Scientific
Bovine Serum Albumin (BSA)	Sigma-Aldrich
SYBR Green 2X	Thermo Fisher Scientific
Glycerol	Roth
3,3′-5,5′-Tetramethylbenzidine (TMB)	Bethyl
Acrylamid 30%	Roth
Ammonium Persulfate (APS)	Roth
Ethylenediaminetetraacetic acid (EDTA)	Roth
HEPES	Applichem
Trypan blue	Sigma-Aldrich
Collagen gel	Provided by Dr. Florian Groeber-Becker
FBS	Gibco
L-Glutamine	Gibco
Sodium pyruvate	Gibco
Penicillin/streptomycin	Gibco

β-mercaptoethanol	Gibco
DMEM	Gibco
RPMI1640	Gibco
Trypsin	Gibco
Insulin -transferrin-selenium 100 X	Gibco
Non-Essential Amino Acid (NEAA) 100 X	Gibco
HEPES for cell culture	Gibco
Puromycin	Sigma-Aldrich
Percoll	Sigma-Aldrich
10 x Permeabilization	Invitrogen
Diphtheria toxin	Sigma-Aldrich
D-luciferin	Biosynth
Ketamine hydrochloride	Pfizer
Xylazine	CP-pharma
Protein A/G beads	Thermo Fisher Scientific
Boric acid	Roth
Primocin	InvivoGen
GenJet™ Plus Transfection Reagent	SignaGen Laboratories
Polybrene	Sigma-Aldrich
CMV peptide pool	MabTech
Peptides from COVID-19 spike protein	Provided by Dr.Shiqiang Gao
E. coli DH5α	New England Biolabs
T4 Ligase	NEB
XbaII endonuclease	Thermo Fisher Scientific
SalI endonuclease	Thermo Fisher Scientific
Mitomycin C	Sigma-Aldrich

7.1.2 Consumables

Item	**Company**
Centrifuge tubes 15 ml and 50 ml	GBO
Reaction tubes 1,5 ml	Eppendorf
Safe-Lock centrifuge tube 1,5 ml	Eppendorf
Filtered pipette tips	Sarstedt
Pasteur glass pipettes	Scheller
PCR tubes and domed caps	Brand

Cuvettes (Quarz)	Hellma
Cell Strainer 70 µm Nylon filter	Falcon
Cell Strainer 70 µm Nylon filter	Falcon
Cryo tubes 2 ml	Greiner
Petri dishes 10 cm diameter	GBO
Serological pipettes 5 ml, 10 ml, 25 ml	GBO
Sterile filter (0,2 µm and 0,45 µm)	ROTH
Syringes (1 ml, 5 ml, 10 ml)	BD Pharmigen
Syringe needles 21Gx1 ½”	Neoject
Syringe needles 21GA2	BD
Cell culture dishes 6 cm	Greiner
Cell culture dishes 10 cm	Greiner
96-well-U plates (cell culture)	Greiner
96-well-F plates (cell culture)	Greiner
6-well plate (cell culture)	Greiner
96-well-V plates	Thermo Fisher Scientific
FACS small tubes	Starlab
LightCycler®v480 multiwell plate 96	Roche
Forceps and scissors	Hartenstein
ELISA plates half-area	Hartenstein Laborversand

7.1.3 Instruments

Machine	**Company**
Autoclave systec DX-45	Systec
Autoclave systec V-75	Systec
Blance PFB	Kern und Sohn
Ice machine Scotsmen AF100	Genheimer
BD FACSCANTO™ II	BD
Fusion SL	Vilbert Lourmat
Gel Doc™ XR+	BioRad
Electrophoresis chamber	PeqLab
Real-time PCR machine	Roche
Fridges 4°C	Liebherr, Privileg
Freezer -20°C	Liebherr, Privileg
Freezer -70°C	Siemens
Incubator	Heraeus

Centrifuge Eppendorf 5415C	Eppendorf
Centrifuge Eppendorf 5424	Eppendorf
Centrifuge Rotina 420R	Hettich Laborapparate
Microplate reader Fluostar Omega	BMG Labtech
Microliter pipettes	Brand
Vortexer Reamix 2789	Vortexer Reamix 2789
Orbital shaker KS10 DIGI	Edmund Bühler
Light microscope LEICA DMIL	Leica
Ph meter	WTW
GeneQuant pro	Amersham Biosciences
Photometer nanodrop	PeqLab
Sterile work bench	Heraeus
SimpliAmp thermocycler	Thermo Fisher Scientific
Waterbath	RM6 LAUDA
Vibra Cell	SONICS
Incubator shaker	Innova®43
Platform mixer	Ratek
Magnetic stirrer	Heidolph
PCR machine	Aviso

7.1.4 Buffers

Buffers	Components	Concentration/Quantity
TAE 50X	Tris HCl	242 g
	Acetic Acid	57,1 ml
	0,5 M EDTA pH 8,0	100 ml
	dH_2O	up to 1 L
MACS Buffer	NaCl pH 7,4	137 mM
	Na_2HPO_4	10 mM
	KCl	2,6 mM
	KH_2PO_4	1,8 mM
	BSA	0,5% (w/v)
	NaN_3	0,1% (w/v)
	EDTA	2 mM
FACS Buffer	NaCl pH 7,4	137 mM
	Na_2HPO_4	10 mM
	KCl	2,6 mM
	KH_2PO_4	1,8 mM

	BSA	0,1% (w/v)
	NaN_3	0,1% (w/v)
Phosphate buffered saline	NaCl (pH 7,4)	137 mM
(PBS)	Na_2HPO_4	10 mM
	KCl	2,6 mM
	KH_2PO_4	1,8 mM
Red blood cell lysis (RBC)	NH_4Cl	150 mM
buffer	$KHCO_3$	10 mM
	EDTA	1 mM

7.1.5 Kits

Item	**Company**
CD4 T cell negative selection kit	Biolegend
CD3 T cell negative selection kit	Biolegend
Intracellular Fixation & Permeabilization Buffer	Thermo Fisher Scientific
Foxp3/Transcription Factor Staining Buffer kit	Thermo Fisher Scientific
IL-2 ELISA KIt	BD
Superscript™ IV VILO	Thermo Fisher Scientific
Nuclear and Cytoplasmic Extraction kit	Thermo Fisher Scientific
Zombie NIR™ Fixable Viability Kit	Biolegend
Zombie Aqua™ Fixable Viability Kit	Biolegend
RNeasy Plus Mini Kit	QIAGEN

7.1.6 Oligonucleotides

7.1.6.1 Generation of point mutations

Name	**Primers**
PT1	5’-AACTTCGTACGTCCTCTTCGTATTAGAACCAGCTG-3’
PT2	5’-CCGTATAATTGGAACTGTGGAGAGGAAAG-3’
PT3	5’-TCCTCTCCACAGTTCCAATTATACGGACAGAACCCACGGACGACTTTGAG-3’
PT4	5’-ACAGCTACTGTTCAGATGTGGAC-3’
PT5	5’-TGAGTCCACATCTGAACAGTAGC-3’
PT6	5’-CCGGATCACTAC AGGAATAGGGGCCAAG-3’
PT7	5’-TGGCCCCTATTCCTGTAGTGATCCGGCAAGAGCCTGAGGAATTGGACC-3’
PT8	5’-ACAGTCGTACGACTGTCTGAGGTTGACATGG-3’

PT1-4 were used for engineering the first point mutation, and PT5-8 were used for engineering the second point mutation.

7.1.6.2 Genotyping

Mouse strain	Primers
Nfatc1^{deltaSUMO}	fw 5'-CCTGGTGGTTGAGATACC-3'
(NFATc1/ΔS)	rev 5'-GCTGGAGAGGTCGTGCTA-3'
Nfatc1^{deltaBC}	fw 5'-ACTGGCAGAACTTACCAGAGTC-3'
(NFATc1/ΔBC)	rev 5'-CCGTATAATTGGAACTGTGGAGAGGAAAG-3'

7.1.6.3 Real-Time PCR

Target	Primers
Ifng	fw 5'-CACAAACAAAGGCTCCCTGT-3'
	rev 5'-CCACCTGTGCCATTCTTGT-3'
Il17a	fw 5'-AATAGATTCTCAATGGTAGCC-3'
	rev 5'-GAAAATTCTTACTTTTGTAAACAG-3'
Il2	fw 5'-ATGGGGGTGTCACGATGTTTT-3'
	rev 5'-AACCCGACC AAGAGGGATTTC-3'
Actb	fw 5'-TGCAAGAAGCTTGCAAAGAAGCT-3'
	rev 5'-GCCGTTCCGAAAGTTGCCTT-3'
Stat5 (P4)	fw 5'-TCATCGGCTCCCACACAGA-3'
	rev 5'-GGCAGTACCGAAGCTGTTTCA-3'
No binding site Nb1	fw 5'-CACCAGCCAACCCAATTAAAA-3'
	rev 5'-CCTTCCTCATGTGATATGGCAAA-3'

7.1.6.4 For cell line generation

Target	Primers
Cd40lg	fw 5'-ACCGACTCTAGAATGATCGAAACATACAAC-3'
	rev 5'-TGATTGTCGACTCAGAGTTTGAGTAAGCC-3'
Baff	fw 5'-CCGACTCTAGAATGGATGACTCCACAGAAAG-3'
	rev 5'-TGATTGTCGACTCACAGCAGTTTCAATGC-3'

Restriction sites for *XbaII* and *SalI* were indicated in red.

7.1.7 Cell culture

7.1.7.1 Ligands and chemicals for cell stimulation and culture

Reagent	Company
12-O-Tetradecanoylphorbol-13-acetate (TPA)	Merck
ConA	Sigma
Ionomycin	Thermo Fisher Scientific

Golgi-Stop	BD ebioscience
Golgi-Plug	BD ebioscience
Anti-hamster IgG	Jackson immunoresearch
Hamster anti-mouse CD3	Bioxcell
Hamster anti-mouse CD28	Bioxcell
Anti-mouse IFN-γ	Bioxcell
Anti-mouse IL-4	Bioxcell
Anti-mouse IL-2	Bioxcell
IgG control antibody	Bioxcell
Recombinant murine IL-12	Peprotech
Recombinant human TGF-β	Peprotech
Recombinant murine IL-6	Peprotech
Recombinant murine IL-4	Peprotech
Recombinant murine IL-7	Peprotech
Recombinant murine IL-1β	Peprotech
Recombinant human IL-2	Peprotech
Recombinant human IL-4	Peprotech
Recombinant human IL-7	Peprotech

7.1.8 Antibodies and conjugates

7.1.8.1 Antibodies for ChIP

Reagent	Clone	Company
Anti-NFATc1	7A6	BD PharMingen
Anti-IgG	Polyclone	BD PharMingen
Rabbit anti-H3AC	30139	Active Motif
Rabbit anti-STAT5	AF2168	R&D system
Rabbit IgG	02-6102	Thermo Fisher Scientific

7.1.8.2 Antibodies for flow cytometry

Antibody-Conjugated	Clone	Supplier	Dilution
Anti-Ms CD16/CD32	93	Biolegend	1:200
Anti-Ms CD4	RM4-5	Biolegend	1:330
Anti-Ms CD8α	53-6.7	Biolegend	1:330
Anti-Ms CD90.1	OX-7	Biolegend	1:330
Anti-Ms CD25	PC61	Biolegend	1:330
Anti-Ms CD62L	MEL-14	Biolegend	1:330

Anti-Ms CD69	H1.2F3	Biolegend	1:330
Anti-Ms CD45	30-F11	Biolegend	1:330
Anti-Ms CD11b	M1/70	Biolegend	1:330
Anti-Ms PD1	J43	Biolegend	1:160
Anti-Ms CD27	LG.3A10	Biolegend	1:330
Anti-Ms TIGIT	Vstm3	Biolegend	1:330
Anti-Ms Foxp3	FJK-16s	eBioscience	1:250
Anti-Ms IL-2	JES6-5H4	Biolegend	1:250
Anti-Ms IFN-γ	XMG1.2	Biolegend	1:250
Anti-Ms IL-10	JES5-16E3	eBioscience	1:250
Anti-Ms IL-4	11B11	eBioscience	1:250
Anti-Ms IL-17A	eBio17B7	eBioscience	1:250
Anti-Ms GM-CSF	MP1-22E9	eBioscience	1:250
Anti-Ms TNF-α	MP6-XT22	eBioscience	1:250
Anti-Hu CD19	HIB19	BioLegend	1:200
Anti-Hu CD27	O323	BioLegend	1:330
Anti-Hu CD38	HIT2	BioLegend	1:200
Anti-Hu CD138	DL-101	BioLegend	1:200
Anti-Hu IgD	IA6-2	BioLegend	1:250
Anti-Hu IgM	MHM-88	BioLegend	1:250
Human Fc Blocking Solution		BioLegend	1:250
Anti-Hu CXCR5	RF8B2	eBioscience	1:250
Anti-Hu PD1	NAT105	BioLegend	1:250
Anti-Hu CD4	RPA-T4	BioLegend	1:330
Anti-Hu CD3	HIT3a	BioLegend	1:330
Anti-Hu Foxp3	PCH101	eBioscience	1:200
Anti-Hu CD40L	24-31	BioLegend	1:250

7.1.8.3 Primary and Secondary Antibodies for Western Blots

Antibody	**Clone**	**Supplier**
Rat anti-Bcl2A1		Kindly provided by Marco J. Herold
Mouse anti-NFATc1	7A6	BD PharMingen
Rabbit anti-NFATc2	IG-209	ImmunoGlobe
Goat anti-Blimp-1	C-21	Santa Cruz Biotechnology
Goat anti-lamin B	C-20	Santa Cruz Biotechnology
Mouse anti-β-actin	C-4	Santa Cruz Biotechnology

Anti-ERK	H-72	Santa Cruz Biotechnology
Goat anti-mouse IgG HRP	A2304	Invitrogen
Goat anti-rabbit IgG HRP	Polyclone	Invitrogen

7.1.8.4 Antibodies for EMSA

Antibody	**Clone**	**Supplier**
Anti-NFATc1	AB1-205	ImmunoGlobe
Anti-NFATc2	IG-209	ImmunoGlobe
Anti-Blimp-1	C-21	Santa Cruz Biotechnology
Anti-Flag	M2	Sigma-Aldrich

7.1.9 Mice

The mice used in the following were bred and kept in the “Zentrum fur Experimentelle Molekulare Medizin” (ZEMM) of the University of Würzburg in Würzburg following the guidelines of the German Animal Welfare Laws for Experimental Animals. The mice received water *ad libitum* and standard rodent chow. The mice were genotyped with biopsies from tail tips or the ear at the age of 4 weeks. The mice for the experiments should be more than 6 weeks. The following mice lines were used in the experiments:

Designated Line	**transgenic protein**	**Reference**
Nfatc1$^{\text{deltaSUMO}}$ knock in	NFATc1/ΔS	Generated in our lab
Nfatc1$^{\text{deltaBC}}$.*Cd4cre*	NFATc1/ΔBC: conditional deletion of the BC-terminus of NFATc1	Generated in our lab
2D2	MOG-specific transgenic TCR	Jackson Laboratory, Charles River [88]
Rag1-/-	Rag1 deletion	Jackson Laboratory, Charles River [124]
DEREG	BAC expressing a DTR-eGFP fusion protein under the control of the *foxp3* locus	Lahl, Loddenkemper *et al*. 2007 [125]

7.2 Methods

7.2.1 Cell culture

7.2.1.1 Cell culture medium

All cells were cultured in the cell incubator at 37°C with 5% CO_2. HEK 293T cells (abbreviated as 293T cells in the following), 293T-BAFF-CD40L, 293T-BAFF, 293T-CD40L were cultured

in DMEM, primary murine cells and human tonsil cells were cultured in RPMI1640 as indicated in the following:

DMEM supplemented with	10% FBS
	2 mM L-glutamine
	1 mM Sodium pyruvate
	100 U/ml Penicillin/streptomycin
	0,1 mM β-mercaptoethanol
RPMI1640 supplemented with	10% FBS
	2 mM L-glutamine
	1 mM Sodium pyruvate
	100 U/ml Penicillin/streptomycin
	0,1 mM β-mercaptoethanol
Culture medium for human tonsil cells	RPMI1640
	10% FBS
	2 mM L-glutamine
	1 mM Sodium pyruvate
	0,1 mM β-mercaptoethanol
	100 µg/ml Primocin (antimicrobial reagent)
	1 x Non-Essential Amino Acid (NEAA)
	1 x Insulin-transferrin-selenium 100 X

7.2.1.2 Cell counting

Trypan blue was used to stain dead cells, but leave live cells unstained since live cells have intact cell membranes. Different samples may require different dilutions. Here, we used 1:10 dilution as an example. Mixed 10 µl of cell suspension with 90 µl of trypan blue, then transferred 10 µl of mixture into a hemocytometer (Neubauer). Viable cells were counted in all 4 quadrants, cell numbers were calculated following the formula:

Cell concentration $A=\frac{B}{C} \times N \times 10^4$

A: concentration cell/ml, B: total cells in all quadrants, C: numbers of quadrants for counting cell, N: dilution factor

7.2.1.3 Generation of cell lines

Lentiviruses have been widely used as gene delivery vectors. Considering the safety of viruses, the components necessary for virus production are split into multiple plasmids. We used the 3rd generation for lentiviruses: packaging plasmid, envelop plasmid, and transfer plasmid.

(1) Preparation of lentiviral particles

Firstly, for the generation of lentivirus, 293T cells were seeded in a 10 cm-dish and grown until 90% confluent. One hour before transfection, the medium was changed with 6 ml of FBS-free medium. Then, 293T cells were co-transfected with the packing plasmid (psPAX2 plasmid), the envelope plasmid (pMD2.G plasmid), and a transfer plasmid containing the transgene (hCD40L or hBAFF). After 8 h, the transfection solution was replaced by 5 ml of DMEM with 10% FBS. The supernatants were collected after 24 h and 48 h and then passed through a 0.45 µm filter. Lentiviruses can be used immediately.

(2) Lentiviral transduction

To generate 293T-BAFF, 293T-CD40L cell lines, 5 ml of supernatants containing corresponding lentivirus particles were added separately to 293T cells (about 90% confluent) and incubated overnight. The transfer plasmid not only contained the transgene (hCD40L or hBAFF) but also a puromycin-resistant gene (puromycin-*N*-acetyltransferase gene), which is normally used as a selection marker. Once cells expressed BAFF and CD40L, they were also resistant to puromycin, thus those cells expressing BAFF or CD40L could be enriched by puromycin (1 µg/ml) selection. For 293T-BAFF-CD40L cell lines, 293T-CD40L cells were transfected with lentivirus containing BAFF again. Moreover, fluorescent activated cell sorting is a specialized type of flow cytometry, which is widely used as an important method to sort cells by staining interested cells with florescent dyes. According to the intensity of fluorescence of anti-CD40L and / or anti-BAFF staining, we could sort the cells of interest.

7.2.1.4 Stimulation of primary murine cells

For checking cytokine expression of murine cells, those were stimulated or restimulated with 12-O-tetradecanoylphorbol-13-acetate (TPA; 100 ng/ml) and ionomycin calcium salt (I; 100 ng/ml) in the presence of Golgi-Stop (1:1000) and Golgi-Plug (1:1000) while cultured with RPMI 1640 medium supplemented with 10% FBS in 96-well plate or 6-well plate for 5 h in the incubator.

7.2.1.5 *In vitro* differentiation of mouse $CD4^+$ T helper cells

Flat plates were used to be coated with anti-hamster IgG, and each well was coated with 60 µl of 12,5 µg/ml anti-hamster IgG (diluted in PBS) and incubated for overnight at 4°C or 37°C for

2 h. Afterwards, the anti-hamster IgG was discarded and the plate was washed twice with 100 µl of PBS, then the pre-coated plate was ready for use.

0,2 x 10^6 $CD4^+$ T cells resuspended in 100 µl of culture medium were seeded into the pre-coated plate and another 100 µl of antibodies and cytokines mixture added. The combination of antibodies and cytokines was prepared according to the following table. The plate was kept in the incubator for 2 days. On day 2, cells were transferred to another fresh plate, 100 µl of fresh medium was added and the cells were cultured for another day. The quality of differentiation can be checked by intracellular staining for specific cytokine expression.

Cell types	**Antibodies/cytokines**	**Final concentration**
Th1 cells	Anti-CD3	0,5 µg/ml
	Anti-CD28	1 µg/ml
	Anti-IL-4	2,5 µg/ml
	IL-12	10 ng/ml
Th2 cells	Anti-CD3	0,5 µg/ml
	Anti-CD28	1 µg/ml
	Anti-IFN-γ	2,5 µg/ml
	IL-4	50 ng/ml
Conventional Th17 cells	Anti-CD3	0,25 µg/ml
	Anti-CD28	1 µg/ml
	Anti-IFN-γ	2,5 µg/ml
	Anti-IL-4	2,5 µg/ml
	TGF-β	0,5 ng/ml
	IL-6	20 ng/ml
Pathogenic Th17 cells	Anti-CD3	0,25 µg/ml
	Anti-CD28	1 µg/ml
	Anti-IFN-γ	2,5 µg/ml
	Anti-IL-4	2,5 µg/ml
	IL-23	20 ng/ml
	IL-6	20 ng/ml
	IL-1β	20 ng/ml
iTregs	Anti-CD3	0,5 µg/ml
	Anti-CD28	1 µg/ml
	Anti-IFN-γ	2,5 µg/ml
	Anti-IL-4	2,5 µg/ml

TGF-β	5 ng/ml

7.2.2 Isolation of cells from mouse

7.2.2.1 Isolation of splenocytes of a naïve mouse

A 70 µm-cell strainer was placed on a 50 ml tube and pre-wet with 3 ml of BSS/BSA (provided by Institut für Virologie und Immunbiologie, Universität Würzburg), the spleen directly minced on the strainer and washed twice with 5 ml of BSS/BSA; then splenocytes were harvested after centrifugation with 400 x g for 5 min. The supernatant was discarded and the cells were resuspended with 2 ml of erythrocyte lysis buffer, after 1 min of cell lysis, 20 ml of PBS were added to stop the lysis. Splenocytes were again centrifuged with 400 x g for 5 min. The supernatant was discarded and the pellet resuspended with 2 ml of FACS buffer for counting. For isolation of T cells, splenocytes can be directly processed without erythrocyte lysis.

7.2.2.2 Isolation of $CD3^+$ and $CD4^+$ T cells from splenocytes

Splenocytes without erythrocyte lysis were used to isolate $CD3^+$ and $CD4^+$ T cells by applying a Mojosort $CD3^+$ and $CD4^+$ T cell negative selection kit according to the manufacturer's instructions, respectively. Briefly, 1 x 10^8 cells were resuspended with 1 ml of MACS buffer in a 15 ml tube, 50 µl of biotin-labeled antibody cocktail was added and incubated for 15 min on ice. After the incubation, 50 µl of streptavidin nanobeads were added and incubated for another 15 min. Afterwards, 5 ml of MACS buffer was added to each tube to be placed into a magnet for 5 min, the supernatant-containing cells were collected for further use.

7.2.2.3 Isolation of infiltrated lymphocytes in the CNS

After EAE, mice were killed with carbon dioxide, each mouse was perfused twice with 25 ml of PBS, then the spinal cord and brain were dissected and cut into small pieces. After transfer of all pieces into a 50 ml tube, RPMI1640 containing 20 U/ml DNaseI and 2 mg/ml collagenase D were added for digestion for 20 min at 37°C on a shaker.

Tubes were removed from the shaker and the tissues gently mashed through a 100 µm-cell strainer, the strainer washed with 20 ml of RPMI1640. Then cell pellets were obtained by centrifuging at 1200 rpm for 5 min at 4°C. Afterwards, the cells were loaded onto a 30%:37%:70% Percoll gradient in a 15 ml tube and density centrifuged at 1700 rpm for 20 min at 4°C. The enriched CNS infiltrates were harvested and used for flow cytometry to check the cytokine production and cell subpopulations.

7.2.2.4 Isolation of bone marrow cells

A 70 µm-cell strainer was placed on a 50 ml tube and pre-wetted with 3 ml of BSS/BSA. Then, bone marrow (BM) cells were collected by flushing femur and tibia bones from *Rag1*$^{-/-}$ mice with 3 ml of PBS containing 0.1% BSA and passed through the strainer, which was prepared before.

7.2.3 Flow cytometry

(1) Surface staining

The number of cells used for staining was determined by the percentage of the interested subpopulation. Here, we stained with 1 x 10^6 cells in a 96-well plate as an example. For distinguishing the live cells from dead cells, we apply live/dead staining with a Zombie staining kit at 1:1000 dilution in PBS. Each sample was stained with 100 µl of Zombie dye at RT for 15 min. Then 100 µl of PBS was added to each sample, and the plate was centrifuged at 400 x g for 5 min at 4°C.

Next, to reduce unspecific binding of antibodies, 90 µl of Fc block (anti-CD16/CD23 antibody) diluted in FACS buffer (1:250) was added into samples and incubated for 10 min at 4°C. Then, 10 µl of antibody mixture diluted in FACS buffer was added to each sample and incubated for another 15 min at RT in the dark. To remove unbound antibodies, 100 µl of FACS buffer was added to the plate, and the plate was centrifuged at 400 x g for 5 min at 4°C, the supernatant then was discarded. The cells were resuspended in 100 µl of FACS buffer, they can be measured immediately at the BD Canta II flow cytometry machine or can be fixed with 50 µl of 4% formaldehyde. Data were analyzed by FlowJo software.

(2) Intracellular staining for cytokines

For cytokines staining, the cells were stimulated or restimulated with 100 ng/ml TPA and Ionomycin for 5 h in the incubator in the presence of Golgi-Stop and Golgi-Plug with 1:1000 dilution. After stimulation, the cells were harvested and proceeded by surface staining as described above. The cells were fixed and permeabilized with 100 µl of IC Fix solution diluted with FACS buffer in the fridge. In the meanwhile, antibodies for cytokines were diluted in 1 x Perm buffer, which was diluted with water in 1:10 dilution. After 20 min, the cells were washed by adding 100 µl of 1 x Perm buffer and followed by centrifuging at 1800 rpm for 5 min at 4°C. The cell pellets were resuspended with 100 µl of prepared antibody mixture for overnight in the fridge or RT for 1 h. Next step, the cells were washed with 100 µl of 1 x Perm buffer and centrifuged for 5 min at 1800 rpm at 4°C. Afterwards, the cell pellets were resuspended with 100 µl of FACS buffer and ready for measuring.

(3) Nuclear staining

If needed, cells can be stained for surface markers as described above. Then, the cells were fixed and permeabilized with 100 µl of Fix/Perm buffer from Thermofisher in the fridge. In the meanwhile, nuclear antibodies were diluted in 1 x Perm buffer. After 20 min, the cells were washed by adding 100 µl of 1 x Perm buffer and followed by centrifuging at 1800 rpm for 5 min at 4°C. The cell pellets were resuspended with 100 µl of prepared antibody mixture for overnight in the fridge or RT for 1 h. Next step, the cells were washed with 100 µl of 1 x Perm buffer and centrifuged for 5 min at 1800 rpm at 4°C. Afterwards, the cell pellets were resuspended with 100 µl of FACS buffer and ready for measuring.

7.2.4 The depletion of Foxp3$^+$ Treg *in vivo*

To analyze the function of NFATc1/ΔS Tcon cells, we depleted Tregs completely by using DEREG mice. In DEREG mice, Foxp3$^+$ Tregs specifically express enhanced green fluorescence protein (eGFP) and the diphtheria toxin (DT) receptor, which allows to exclusively deplete Foxp3$^+$ Tregs by DT Mice were injected with 1 µg of DT intraperitoneally per mouse on day 1 and day 2. After 24 h, mice can be used for experiments.

7.2.5 Passive EAE model

For passive EAE, naïve CD4$^+$ T cells isolated from 2D2.WT and 2D2.NFAT/ΔS$^+$ mice were differentiated into Th1 and Th17 cells with or without 10 µg/ml anti-mouse IL-2 for 3 days *in vitro.* On day 2, the cells were transferred to another fresh uncoated plate. On day 3, cells were harvested and washed twice with sterile PBS, 5 x 10^6 cells mixed Th1 and Th17 cells in a 1:1 ratio were resuspended in 200 µl of PBS and transplanted to *Rag1*$^{-/-}$ mice retro-orbitally. Transplanted mice were injected intra-peritoneally with 200 µg of anti–mIL-2 or IgG control antibody in 200 µl on d 3 and 6. Clinical signs were assessed daily over the total of 20 days and scored in a single-blinded fashion as previously described [126]. The schematic diagram of the experiment was shown in Figure 12.

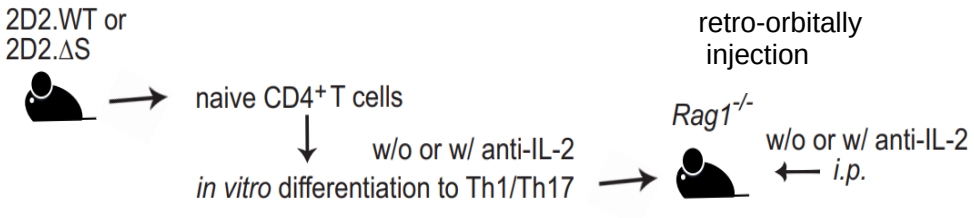

Figure 12: Passive EAE model by transfer of 2D2$^+$ Th1 and Th17 cells, differentiated *in vitro* for 3 d and combined for transferring into *Rag1*$^{-/-}$ mice.

5 × 10^6 Th1/Th17 cells in a 1:1 ratio were injected i.v. into *Rag1*$^{-/-}$ mice. Parallel cultures and transplanted mice were treated with anti–mIL-2.

7.2.6 Molecular methods

7.2.6.1 Polymerase Chain Reaction (PCR)

Polymerase chain reaction (PCR) is a powerful and widely used method that can amplify DNA sequences. The reaction system contains specific primers, template, DNA polymerase, and nucleotides. The *Taq* DNA polymerase, which can create two identical DNA duplexes from a single original DNA duplex, is essential for DNA replication. The PCR methods are mainly based on thermal cycling, starting with denaturation of DNA at 95°C, causing the separation of two double strands of DNA. Then the specific primers will hybridize with the template DNA at 55-65°C, which is called annealing. Afterwards, the *Taq* DNA polymerase synthesizes a new DNA strand complementary to the template strand by adding free dNTPs from the reaction mixture at 72°C. This step is called extension. It will be repeated for several cycles to make sure to generate enough DNA amplifications. Generally, the reaction mixture was as follows:

PCR mixture	2 x PCR master mix	10 µl
	Forward primer (10 µM)	0,25 µl
	Reverse primer (10 µM)	0,25 µl
	DNA template	1 µl
	H_2O	Up to 20 µl

7.2.6.2 Gel electrophoresis of DNA

Gel electrophoresis is a method used to separate DNA fragments according to their size and charge. Due to the same charge per mass of all DNA molecules, gel electrophoresis of DNA will separate only based on their size. Once DNA fragments are loaded into a gel, they will move to the positive pole as negatively charged. The smaller size of DNA fragments can move faster through the agarose gel than the large ones, therefore, the DNA fragments are separated according to their size. Moreover, it also can determine the size of DNA fragments by comparing with a standard DNA marker run in parallel.

7.2.6.3 Chromatin immunoprecipitation (ChIP)

For checking the histone acetylation on the promoter of *Il2* and *Il17* or the binding of STAT5 to the *Il17* promoter, $CD4^+$ T cells were differentiated into Th1 and Th17 cells for 3 days. Afterwards, 10^7 total cells were harvested and transferred into a new 15 ml tube for each ChIP assay, centrifuged at 400 x g for 5 min at 4°C, and then washed once with 5 ml of cold PBS. The cells were fixed with a final concentration of 1% of formaldehyde, shaking the 15 ml tube at RT for 5 min. Then 1,25 M glycine was used to quench the fixation reaction until the final concentration of glycine reached 125 mM, keeping the tubes in rotation at RT for 5 min.

Cells were washed twice with 10 ml of cold PBS and centrifuged at 400 x g for 5 min at 4°C. After discarding the supernatant, the cell pellets were resuspended with 1 ml of cold PBS, and then transferred into an Eppendorf tube, and centrifuged at 8000 rpm for 5 min at 4°C. Removing the supernatant, cell pellets either can be snap-frozen with liquid nitrogen and stored at -80°C or processed immediately.

The cell pellet was resuspended in 500 µl of lysis buffer containing serine protease inhibitor at 1:100 dilution. For homogenization, a 1 ml syringe with a 21GA2 needle was used to pass through the lysed cells 10 times, then the cells were kept on ice for 30 min. To obtain the length of chromosomal DNA fragments between 200-800 bp, sonication was performed at 35% amplitude alternating 30 sec of pulse and 30 sec of pause for 14 min, with a Vibra-Cell VCX 130 sonicator. Chromatin fragments were collected by centrifugation at 14000 rpm for 15 min at 4°C.

The amount of chromatin in each sample was measured by spectrometry at 260 nm and the chromatin concentration was adjusted in all samples to the equal value of OD260. 10% or 20% input DNA was taken aside from previously generated fragmented chromatin and stored at -20°C for subsequent analyses.

100 µl or 200 µl of fragmented chromatin (total around 50 µg of chromatin DNA) were transferred into a 1,5 ml Eppendorf tube and 900 µl or 800 µl of the IP buffer containing protein inhibitors added. Then 3 mg of control IgG and 100 ml of protein A/G beads were added into the tube and the tube placed on a roller shaker for 2 h at 4°C. The beads were harvested with a magnet and kept in 1 ml of the IP buffer. The supernatant was incubated with 3 µg antibodies (anti-H3AC or anti-STAT5), kept on the roller shaker, and incubated for overnight at 4°C. Afterwards, 100 µl of beads were added to the solution and incubated for another 2 h. The beads were magnetically harvested and resuspended with 1 ml of IP buffer, together with the beads obtained from control IgG. For washing the beads, first we placed the tube with the beads for rolling for 20 min at 4°C, then kept the tube on the magnet for 1 min to remove the IP buffer and repeated this step by adding 1 ml of IP buffer. Secondly, after removing the IP buffer, we added 1 ml of high salt buffer for rolling for 20 min at 4°C, then kept the tube on the magnet for 1 min to remove the high salt buffer, repeated one time more. Thirdly, after removing the high salt buffer, we added 1 ml of LiCl for rolling for 20 min at 4°C, then kept the tube on the magnet for 1 min to remove the buffer, and repeated once more. Lastly, we added 1 ml of TE buffer for rolling for 20 min at 4°C, then kept the tube on the magnet for 1 min to remove the buffer, and repeated once more. To elute the proteins and chromatin fragments from beads, two times 100 ml of elution buffer was added to the beads, kept at 65°C for 15 min. After keeping the beads on the magnet for 1 min, the supernatant was collected for further DNA extraction.

Lysis Buffer	Tris pH 7,9	50 mM
	EDTA pH 8,0	10 mM
	SDS	1%
IP Buffer	Tris pH 7,9	50 mM
	EDTA pH 8,0	10 mM
	NaCl	165 mM
	SDS	0,03%
	Sodiumdeoycholate	0,1%
High Salt Buffer	NaCl	500 mM
	Tris pH 7,9	50 mM
	EDTA pH 8,0	10 mM
	SDS	0,1%
	Sodiumdeoycholate	0,1%
LiCl Buffer	Tris pH 8,0	20 mM
	LiCl	250 mM
	EDTA pH 8,0	1 mM
	NP-40	0,5%
	Sodiumdeoycholate	0,5%
TE Buffer	EDTA pH 8,0	20 mM
	Tris pH 8,0	1 mM
	SDS	0,1%
Elution Buffer	Tris pH 8,0	50 mM
	EDTA pH 8,0	1 mM
	SDS	1%
	$NaHCO_3$	100 mM

7.2.6.4 DNA extraction

To purify the DNA fragment of the samples from the ChIP assay, first, 5 M NaCl was added into the supernatant collected in elution buffer until the final concentration of NaCl reached 200 mM and kept at 65°C for overnight to revert cross-linking between proteins and chromatin fragments. Afterwards, 2 µl of proteinase K (10 mg/ml) was added and kept at 56°C for 2 h. Then, the same volume (around 220 µl) of Phenol/Chloroform/Isoamyl alcohol (25/24/1 dilution) was added into each sample, ‘vortexed’ for 30 s, and centrifuged at 14000 rpm for 10 min at RT. 200 µl of the organic phase from the upper layer was transferred to a new 1,5 ml Eppendorf tube, then 200 µl of Chloroform/Isoamyl added, ‘vortexed’ thoroughly for 30 s, and centrifuged

at 14000 rpm for 10 min at RT. 180 µl of the upper layer were transferred to a new tube, then 20 µl of NaAC (3 M, pH 5,2), 2 µl of linear acrylamide (5 mg/ml) as a carrier and 500 µl of cold EtOH were added, mixed properly, and kept at -80°C at least for 3 h. To gather DNA, tubes were centrifuged at 14000 rpm for 30 min at 4°C, the supernatant discarded, and the pellet washed by adding 500 µl of 70% ethanol, centrifuged at 14000 rpm for 15 min at 4°C. Afterwards, all the supernatant was removed carefully, and the pellet dried shortly. The dried DNA pellets were resuspended with 20 µl of 10 mM Tris (pH 7,5). Then the DNA was ready to use or stored at -20°C.

7.2.6.5 RNA isolation and cDNA synthesis

RNA was extracted either from cultured T cells as described above or from freshly isolated splenocytes. T cells were transferred into an RNase-free plastic Eppendorf tube and washed once with 1 ml of PBS by centrifuging at 6000 rpm for 5 min at 4°C. The supernatant was removed, and cell pellets were lysed in 350 µl of RLT buffer containing 10 µl/ml β-mercaptoethanol by using the RNeasy Plus Mini Kit (QIAGEN). For homogenization, the 21G/A needle was used to pass through the solution 8 times, then the lysis solution either could be frozen at -70°C or processed immediately. Further steps were performed according to the manufacturer's protocol. In the end, the RNA was eluted with 20 µl of RNase-free water.

The concentration of RNA was measured by a Nanodrop spectrophotometer. Afterwards, an RNA amount between 100 ng and 500 ng was used as a template to generate cDNA. The Superscript™ IV VILO kit was used to generate complementary DNA, the reaction system for each sample was prepared according to the manufacturer's protocol. Briefly, it contained 4 µl of superscript master mixture, a specific amount of template RNA, and filled up with water up to 20 µl of total volume. The program for cDNA synthesis was as follows:

- 25°C for 10 min
- 50°C for 10 min
- 85°C for 5 min

The generated cDNA could be used immediately for real-time PCR or was stored at -20°C.

7.2.6.6 Real-Time PCR (qRT-PCR)

Real-time PCR is a reliable technique to quantify gene expression and detect gene expression differences. In the experiments, we used a non-specific detection method. Briefly, we used a non-specific fluorescent dye, SYBR Green, which can intercalate into any double-stranded DNA, upon which the dye fluoresces. The reaction mixture for one sample was prepared as follows:

SYBR Green 2X	10 µl
Forward Primers (10 µM)	0,4 µl
Reverse Primers (10 µM)	0,4 µl
H_2O	Up to 18,5 µl

Afterwards, 18,5 µl of prepared reaction mixture was added into the LightCycler® Multiwell Plate 96, then 1,5 µl cDNA was added into each well. The real-time PCR reaction was monitored in the real-time PCR machine. The program for qRT-PCR was as follows:

Steps	**Temperature**	**Time**
Pre-incubation	95°C	5 min
amplification	95°C	10 sec
	72°C	30 sec
Melting-curve	95°C	5 sec
	65°C	1 min
	97°C	continuous
Cooling	40°C	10 sec

The $2^{-\Delta\Delta CT}$ method is the method of relative quantification that is most frequently used for the analysis of qPCR experiments [127, 128]. The threshold cycle (CT) is the cycle at which the fluorescence level reaches a certain amount (the threshold). This method uses the CT value generated from a qPCR system to calculate the relative gene expression, which means the value shows the expressed target gene normalized against the reference gene. Here is an example to explain the calculation [129].

	Reference sample	Target sample
Reference gene	A	B
Target gene	C	D

$\Delta\Delta CT = \Delta CT$ (a target sample) – ΔCT (a reference sample) = $(CT_D - CT_B) - (CT_C - CT_A)$.

7.2.6.7 Enzyme-linked immunosorbent assay (ELISA)

The secretion of cytokines was detected by ELISA, according to the manufacturer's guidelines. Briefly, 50 µl of 4 mg/ml capture antibody diluted in PBS was added into a 96-well-coating plate at 4°C overnight. To remove unbound antibodies, supernatants were discarded, and plates were washed three times with 100 µl of washing buffer (PBS containing 0,05% Tween-20). Afterwards, 100 µl of 5 µg/ml skim milk was added to block unspecific binding at 37°C for 2 h. After being washed three times with 100 µl of washing buffer, cell culture supernatants were diluted with 1% BSA/PBS and 50 µl pipetted into each well. In addition, a standard cytokine was diluted serial (1:2 dilution) and 50 µl of each concentration was added into the plate, which

was placed at 37°C for 1 h. During the incubation, the cytokines bound to the capture antibodies.

After 1h incubation, supernatants and standard cytokines were discarded and the plate was washed three times as before. 50 µl of biotinylated detection antibody was employed to bind with cytokines and incubated for 1 h at 37°C. After repeating the washing step, 50 µl of streptavidin-HRP was added and incubated for 30 min at RT. The plate was washed as before to remove unbound antibody-enzyme conjugates. 50 µl of TMB substrate solution was added into the plate and incubated for 5-10 min, the colour changed to blue due to the peroxidase activity. The chemical reaction was stopped by adding 50 µl of 1 M HCl. The colour change can be detected with an ELISA reader.

7.2.6.8 Plasmid construction

According to the nucleotide sequence of the hBAFF and hCD40L gene, two pairs of primers were designed to clone both genes, and *XbaII* and *SalI* restriction sites were included. The amplified DNA fragments were ligated into the T vector for sequencing. After confirming the sequence, the recombinant plasmids were digested with *XbaII* and *SalI* endonucleases. Then, the digested DNA fragments were inserted into the transfer plasmid, which was also digested with *XbaII* and *SalI* endonucleases. The reconstructed plasmids were transformed into *E. coli* DH5α for plasmid purification.

7.2.7 RNA sequencing assays

Th1, Th2, and Th17 cells which were differentiated *in vitro* were collected on days 2.5 and 3.5 and resuspended in RNA lysis buffer. The Qubit 2.0 was used to assess the quantity of total RNA and RNA 6000 Pico chip was applied to check the quality of RNA on Agilent's bioanalyzer. Afterwards, 700 ng total RNA was used to prepare barcoded mRNA sequencing libraries by a NEBNext Poly(A) mRNA Magnetic Isolation Module and NEBNext Ultra II RNA Library Prep Kit for Illumina according to the manufacturer's guidelines. Barcoded RNA sequencing libraries were onboard clustered using HiSeq Rapid SR Cluster Kit v2 with 8 pM, and 59 nucleotides were sequenced on the Illumina HiSeq2500 using HiSeq Rapid SBS Kit v2 (59 cycles). The raw data were pre-processed according to the Illumina standard protocol. Analysis of raw sequencing data and calculation of RPKM (reads per kilobase of transcript per million mapped reads) was performed using the CLC Genomics Workbench v7.5 (Qiagen) with CLC's default settings for RNA sequencing analysis. Quality control was accessed using FASTQC, and low-quality ends and leftover adapter sequences were trimmed. The reads were aligned to the GRCm38 genome.

7.2.8 Tonsil organoid preparation

(1) Preparation of tonsil cells

Fresh tonsil tissue was obtained from surgery and kept in a 10 cm-dish with RPMI medium on ice to remove fatty or blood clots. Then the tissue was dissected into small pieces (around 5 mm) and mashed through a 100 µm-cell strainer with a syringe plunger. The strainer was washed with RPMI until the medium reach 20 ml in a 50 ml tube. Next step, lymphocytes were enriched by Ficoll density gradient separation. Briefly, 15 ml of Ficoll was added in a 50 ml tube, carefully overlayed with the cell suspension, centrifuged at 1750 rpm for 20 min without brake at RT. The white layer with lymphocytes was collected into a new 50 ml tube and washed twice with 10 ml cold PBS at 1500 rpm for 5 min. Cell were counted and frozen into aliquots in 90% FBS + 10% DMSO. Frozen cells were stored in liquid nitrogen.

Tonsil cells were thawed in a water bath at 37°C, transferred into a 15 ml tube containing 10 ml of RPMI1640 supplemented with 10% FBS and 100 µg/ml DNase I, then centrifuged at 1500 rpm for 5 min. Afterwards, cell pellets were resuspended with 10 ml of complete medium and transferred into a 10 cm-dish for 4 h.

(2) Preparation of cell lines

For the preparation of 293T cell lines or other cell lines, all medium from the cell culture dishes were removed, 5 ml of PBS was added slowly to wash the cells. After removing the PBS, 3 ml of trypsin was added slowly into the dishes and the dishes kept in the incubator for 3 min. When cells were separated from each other and detached from the plate, 5 ml of complete culture medium was put in to stop the digestion. Afterwards, the cell suspension was transferred into a 15 ml tube and centrifuged at 1500 rpm for 5 min. 1 x 10^7 cells per well (6-well plate), filled with medium to 4 ml, were treated with Mitomycin C to the finial concentration of 25 µg/ml. After 2 h, cells were washed 3 times with 10 ml of PBS, then resuspended in complete medium and counted for use.

(3) Preparation of collagen gel and tonsil organoid

For the preparation of collagen gel, 4 mg/ml of collagen gel was diluted with 0,1% acetic acid to the desired concentration. Here, we used 2 mg/ml collagen gel as an example. All reagents should be kept on ice, especially, after adding neutralization buffer, collagen solidifies very fast. Collagen gel was prepared as follows:

Reagent	Percentage	Volume
2 mg/ml collagen gel	70%	700 µl
FBS	15%	150 µl
10X medium	10%	100 µl

Neutralization buffer	5%	50 µl
		Up to 1 ml
Neutralization buffer	NaOH	0,2 g
	HEPES	5,2 g
	$NaHCO_3$	2,2 g
		Up to 100 ml

After preparing the collagen gel, the pH test strips were used to check whether the pH of collagen gel reached to around 7,4. 20 µl of prepared collagen gel was used to resuspend feeder and tonsil cells, the cell numbers were changed according to specific experiments, and transferred into the bottom of a 96-well-U plate. The plate was placed in the incubator for 15 min to solidify the collagen. Subsequently, 200 µl of complete medium was added to each well and the plate was kept in the incubator.

7.2.9 Statistical analysis

All the results are shown as median ± SEM or median ± SD. The statistical significance between the groups was determined by a Mann-Whitney test or unpaired student's t-tests. The results were analyzed with GraphPad 5 (Prism) software. Significant differences between data were indicated by p-values: $p \leq 0.05$ (*), $p \leq 0.01$ (**), $p \leq 0.001$ (***), $p \leq 0.0001$ (****).

8 Results

8.1 Part I

8.1.1 Generation and Phenotyping of *Nfatc1*^{deltaSUMO} mice

To better understand the function of SUMOylation of NFATc1 in T cell-mediated immune responses *in vivo*, we generated an *Nfatc1* mutant mouse strain, in which NFATc1 cannot be SUMOylated, termed *Nfatc1*^{deltaSUMO} encoding NFATc1/ΔS. We introduced point mutations on the two SUMOylation sites on exon 10 and thereby changed the codes from AAG for lysine K702 and K914 to CGG for Arginine (Figure 13 A). To confirm the correct positions of mutation, we extracted DNA from WT and *Nfatc1*^{deltaSUMO} tails to perform sequencing. It showed the correct site-specific mutations and successfully created K-to-R mutations on the two decisive SUMOylation sites in NFATc1/ΔS^{+} mice (Figure 13 B) [130].

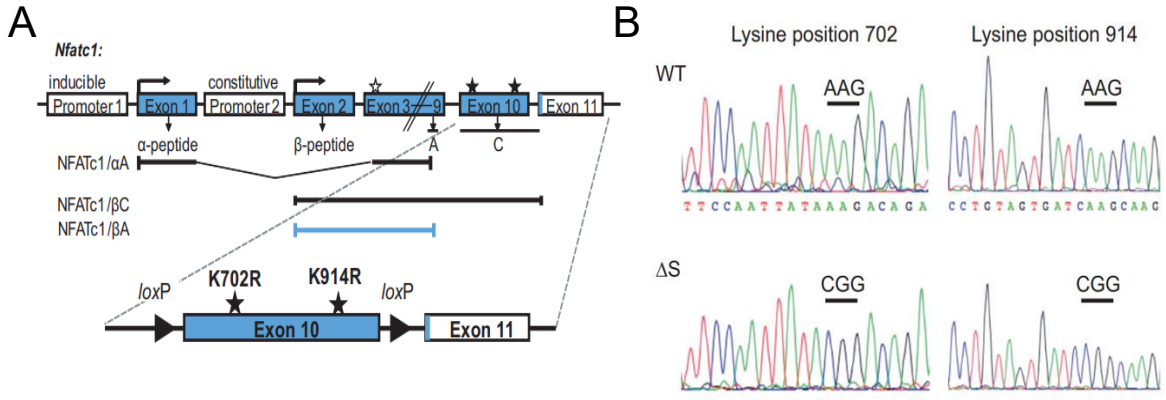

Figure 13: Point mutation on two SUMOylation sites or the C-terminal deletion of NFATc1.

(A) Strategy for creating a mouse strain that was unable to be SUMOylated on NFATc1 in conjunction with the possibility for losing long isoforms B and C through loxP sites. (B) Representative sequencing results of *Nfatc1* from mouse tail DNA demonstrated point mutations of lysine to arginine exchanges at amino acid positions 702 and 914 in *Nfatc1*^{deltaSUMO} mice (n = 3) [sequencing was performed by Lena Dietz].

Since we had introduced the point mutations on the SUMOylation sites of NFATc1, it was interesting for us to ask whether the mutations would affect the protein expression level. To answer this question, we performed a western blot of lymphocytes stimulated with TPA and Ionomycin for 6 h from spleen and LNs either from WT or *Nfatc1*^{deltaSUMO} mice. The distribution pattern of isoforms of NFATc1 in NFATc1/ΔS^{+} mice is similar to WT (Figure 14 A). For comparing the expression of NFATc1 after longer stimulation, CD4^{+} T cells from WT and NFATc1/ΔS^{+} mice were stimulated with anti-CD3/CD28 in the presence of IL-2 for 48 h and 72 h. Afterwards, whole protein extracts were used for western blot analysis. From Figure 14 B, we noticed that the expression level of NFATc1/ΔS as well as the distribution of isoforms was similar to that in WT mice.

Moreover, to figure out whether the time point or condition of stimulation would change the appearance of nuclear versus cytoplasmic NFATc1, we extracted nuclear and cytoplasmic proteins from CD4$^+$ T cells from spleen and LN and performed western blots. Before extraction, the cells were stimulated with Concanavalin A (ConA) for 1 or 4 d, the latter in parallel restimulated for 6 h with TPA and Ionomycin. As shown in Figure 14 C, the expression level and pattern of nuclear and cytoplasmic NFATc1/ΔS indeed showed no alterations at different time points or under different stimulation conditions.

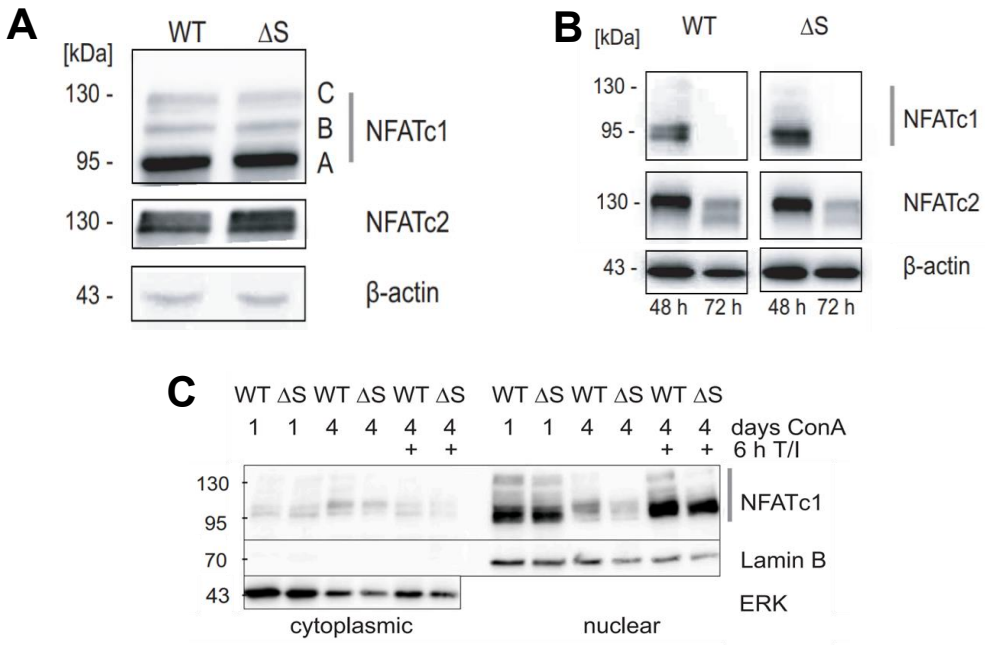

Figure 14: The protein expression level of NFATc1 in NFATc1/ΔS$^+$ mice is similar to WT.

(A and B) Western blot analysis of whole-cell extracts from spleen and LNs of WT and NFATc1/ΔS$^+$ mice, detecting expression of NFATc1 isoforms and NFATc2 in comparison to β-actin; total lymphocytes stimulated for 6 h by T/I (A) or CD4$^+$ T cells stimulated by anti-CD3/CD28 plus IL-2 for 48 and 72 h (B). (C) Western blot analysis of nuclear and cytoplasmic protein expression of WT NFATc1 and NFATc1/ΔS. CD4$^+$ T cells from the spleen and LNs were stimulated with ConA for 1 or 4 d and restimulated for 6 h with T/I as indicated [Figure 14 was performed by Lena Dietz].

To check whether SUMOylation of NFATc1 will influence the lymphoid cell subpopulations, we analyzed the distribution of lymphocytes in different organs in WT and NFATc1/ΔS$^+$ mice. We observed that NFATc1/ΔS$^+$ mice had a similar percentage of B cells and T cells in the spleen and LNs as WT mice (Figure 15 A). To further examine the distribution of different T cells subsets, flow cytometric analysis was performed to check the frequency of CD4$^+$ and CD8$^+$ T cells in the thymus, spleen, and LNs from WT and NFATc1/ΔS$^+$ mice. It revealed that NFATc1/ΔS$^+$ mice had a similar frequency of CD4$^+$ and CD8$^+$ T cell as WT mice (Figure 15 B). As Tregs are crucial for regulating immunity, we also needed to check their frequency. The FACS analysis of CD4$^+$ CD25$^+$ Foxp3$^+$ Tregs was performed accordingly. The frequency of Tregs was quite similar between the two genotypes (Figure 15 C and D). Besides, we also

counted total cell numbers in the thymus, spleen, and LNs in the two genotypes. It also revealed a similar total number of cells between the two genotypes. Hence, under steady-state conditions, the NFATc1/ΔS$^+$ mice appeared healthy and exhibited similar lymphoid compartments when compared to WT.

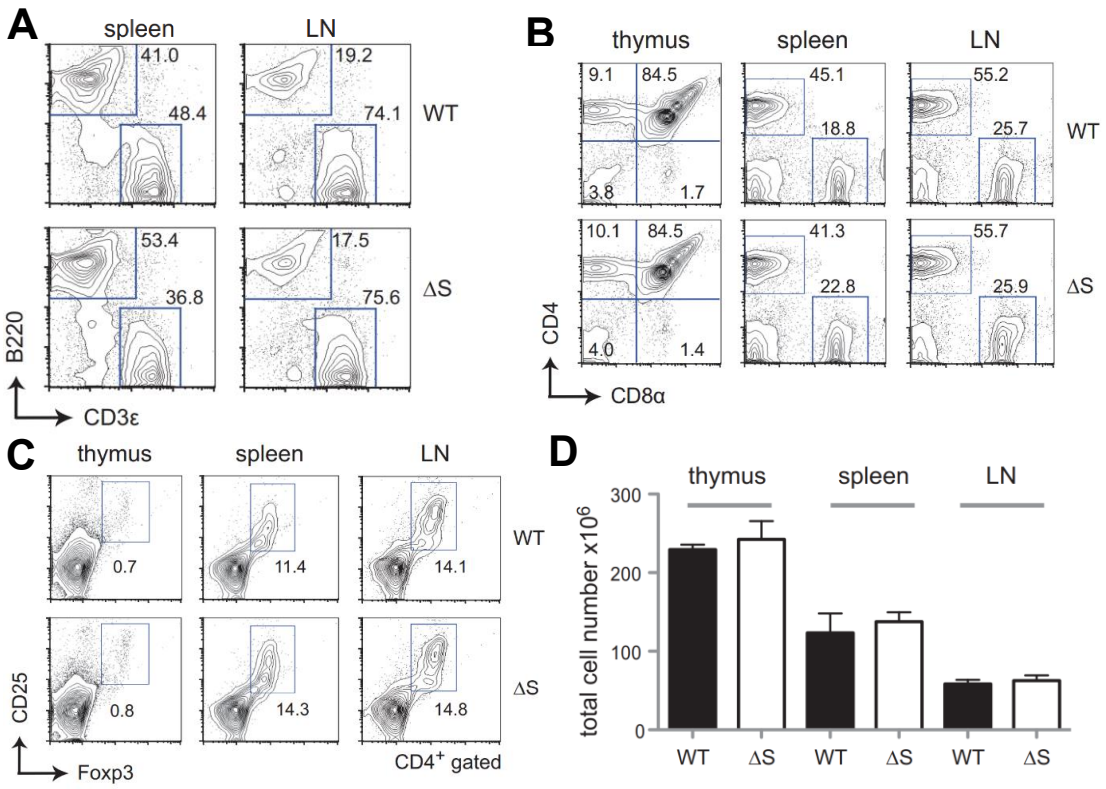

Figure 15: NFATc1/ΔS$^+$ mice showed unaltered lymphocyte subpopulations in the steady state.

(A) Flow cytometry analysis of the frequency of B and T cells in spleen and LN in WT and NFATc1/ΔS$^+$ mice. (B) The frequency of CD4$^+$ and CD8$^+$ T cells in thymus, spleen, and LNs of WT versus NFATc1/ΔS$^+$ mice was analyzed by flow cytometry. (C) Flow cytometric analysis of the frequency of CD25$^+$ Foxp3$^+$ Treg cells within the CD4$^+$ T cells in thymus, spleen, and LNs from WT and NFATc1/ΔS$^+$ mice. (D) Total cell number in thymus, spleen, and LNs in WT and NFATc1/ΔS$^+$ mice (mean ± SD, n > 3) [Figure 15 was performed by Lena Dietz].

8.1.2 Deficiency of NFATc1 SUMOylation dysregulates cytokine expression

Previously, Nayak *et al*. had demonstrated that NFATc1 SUMOylation inhibits IL-2 expression by using T-cell lines [97]. However, whether primary NFATc1/ΔS$^+$ CD4$^+$ T cells behaved similarly needed to be investigated. For this reason, naive CD4$^+$ T cells isolated from WT and NFATc1/ΔS$^+$ mice were stimulated for 6 h with TPA and Ionomycin in the presence of Golgi-Stop and Golgi-Plug. Then, the expression of IL-2 was measured by flow cytometry. As shown in Figure 16 A, the percentage of IL-2$^+$ cells was much higher in primary NFATc1/ΔS$^+$ CD4$^+$ T cells when compared to WT and statistically significant differences were observed with multiple *ex vivo* experiments (Figure 16 A).

To comprehensively understand cytokine expression by T-helper (Th) cells, we isolated naïve $CD4^+$ T cells from WT and NFATc1/ΔS^+ mice and skewed them towards Th1 and Th17 *in vitro* for 3 days. On day 3, cells were restimulated as mentioned above and stained for cytokines expression. The percentage of IL-2^+ cells was significantly increased in both NFATc1/ΔS^+ Th1 and Th17-skewed cells. However, the percentage of IFN-γ^+ cells was notably reduced in NFATc1/ΔS^+ Th1-skewed cells, and the percentage of IL-$17A^+$ cells was significantly decreased in NFATc1/ΔS^+ Th17-skewed cells (Figure 16 B).

Histone acetylation is a vital epigenetic modification, which changes chromatin architecture, known to be closely associated with gene activation. Accordingly, our group had published before that SUMOylated NFATc1 recruits HDAC1, 2 and 4 to the *Il2* promoter [130]. To assess whether the up-regulation of IL-2 in Th1 and Th17-skewed cells is associated with enhanced histone acetylation, we examined the histone acetylation level of *Il2* in Th1 and Th17-skewed cells by ChIP-qPCR assays. As shown in Figure 16 C, no difference in the enrichment of histone acetylation on the β-actin promoter in Th1 and Th17 cells was observed, which was used as a negative control. On the contrary, the histone acetylation level of *the Il2* promoter was significantly increased in both NFATc1/ΔS^+ Th1 and Th17-skewed cells (Figure 16 C), which is consistent with its increased level of IL-2 expression (Figure 16 B).

In summary, the lack of SUMOylation in NFATc1/ΔS^+ mice triggers $CD4^+$ T cells to produce more IL-2 but fewer IFN-γ as well as IL-17A. Moreover, elevated IL-2 is caused by the enhanced histone acetylation level of the *Il2* promoter.

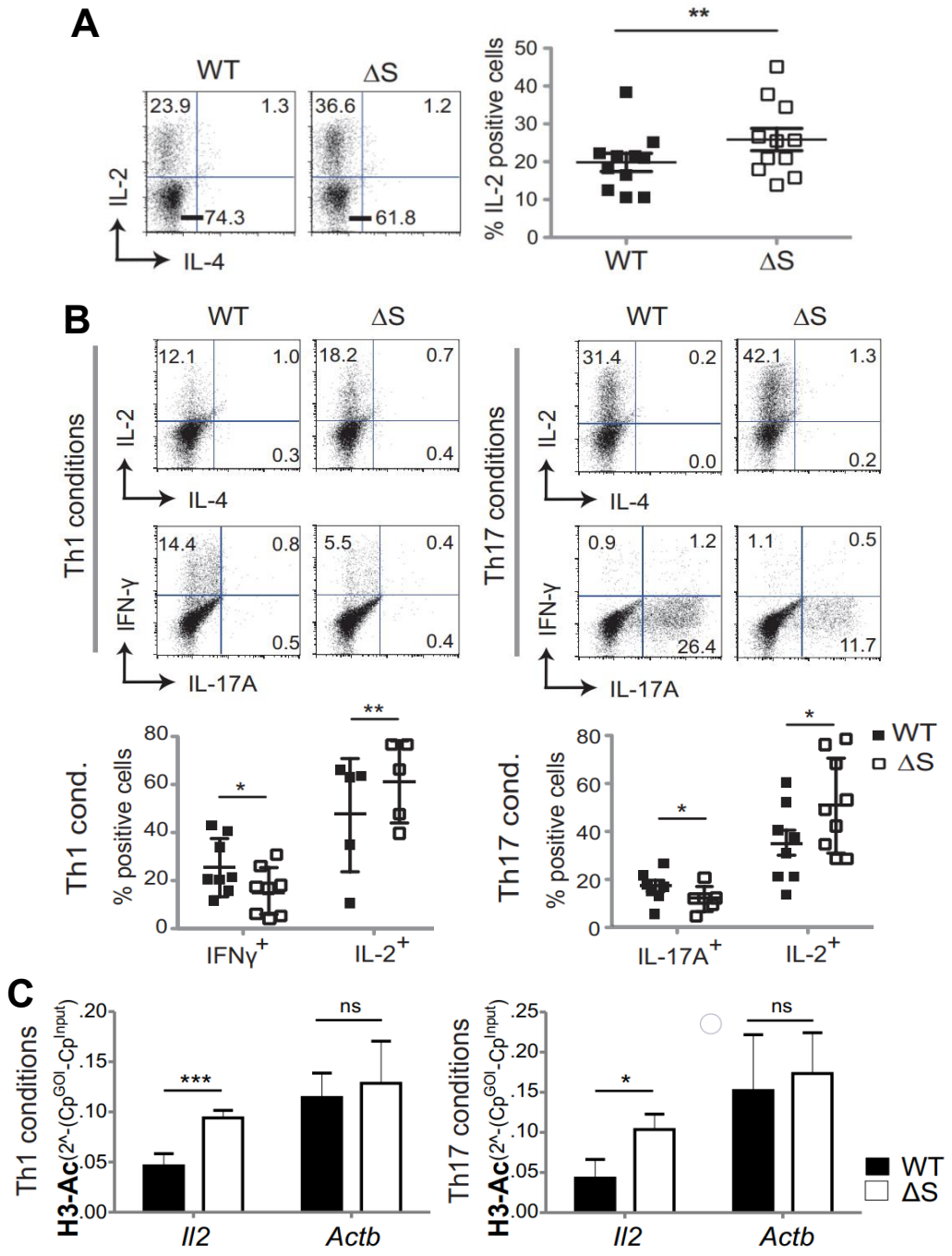

Figure 16: SUMOylation deficiency of NFATc1 triggers CD4⁺ T cells to produce more IL-2 and less IL-17A.

(A) Flow cytometric analysis of the expression of IL-2 in WT and NFATc1/ΔS⁺ CD4⁺ T cells stimulated for 6 h with T/I in the presence of Golgi-Stop and Golgi-Plug. Representative flow cytometry plots and multiple experiment comparison (n=11); statistical analysis by Student's t-test ± SEM (**, $p < 0.005$). (B) Flow cytometric analysis of IL-2 and IL-4 or IL-17A and IFN-γ in Th1 and Th17-skewed cells. Naïve CD4⁺ T cells isolated from WT and NFATc1/ΔS⁺ mice were differentiated *in vitro* for 3 days. On day 3, CD4⁺ T cells were restimulated as mentioned above followed by intracellular cytokine staining. Representative flow cytometry plots and comparison of WT versus NFATc1/ΔS⁺ CD4⁺ T cells (Statistical analysis was performed by Student's t-test (*, $p < 0.05$; **, $p < 0.005$; ***, $p < 0.001$); mean ± SEM; n = 10) [Figure A and B was performed by Lena Dietz]. (C) ChIP-qPCR analysis of histone acetylation on the *Il2* promoter. The chromatin of Th1 and Th17, prepared as for B, was precipitated by anti–H3-Ac. Isolated genomic DNA was subjected to PCR with primers specific for the *Il2* and *Actb* promoters. Statistical analysis was performed by Student's two-tailed t-test (*, $p < 0.05$; **, $p < 0.005$; ***, $p < 0.001$); mean ± SD; n > 3.

In the previous paragraph, we have shown that the frequency of IL-2$^+$ cells was increased and the frequency of IL-17A$^+$ cells was reduced in NFATc1/ΔS$^+$ Th17-skewed cells. Laurence *et al.* have reported that IL-2-mediated activation of STAT5 can inhibit *Il17a* transcription [131]. To evaluate again, whether IL-2 could directly affect the frequency of IL-17A$^+$ cells during Th17 differentiation, we skewed isolated naive CD4$^+$ T cells from WT mice towards Th17 with IL-6, TGF-β, anti–IL-4, and anti–IFN-γ *in vitro* for 3 days along with either hIL-2 or anti–mIL-2 or in combination. On day 3, the supernatant was used for detecting secreted IL-17A by ELISA. The remaining cells were restimulated by T/I to check intracellular cytokine expression by flow cytometry. As expected, additional hIL-2 could reduce the percentage of IL-17A$^+$ cells, whilst anti–mIL-2 increased IL-17A expression even completely restoring the expression of IL-17A in the presence of hIL-2 (Figure 17 A). Accordingly, when NFATc1/ΔS$^+$ naive CD4$^+$ T cells were differentiated towards Th17 without exogenous hIL-2, which led to more IL-2-producing but fewer IL-17A-producing cells compared to WT$^+$ Th17 cells, the addition of anti–mIL-2 totally restored IL-17A production, even enlarged the percentage of IL-17A$^+$ cells (Figure 17 B). In addition to the elevated IL-17A$^+$ cells, the total amount of IL-17A in the supernatant was also rescued by added anti–mIL2, equalizing the secreted amount of IL-17A of NFATc1/ΔS$^+$ versus WT$^+$ T cells upon higher concentration of anti–mIL-2 (Figure 17 C).

The binding of IL-6 / IL-21-activated STAT3 to the *Il17a* promoter is necessary for the expression of IL-17A. However, except for STAT3, STAT5 also can bind to the same region of the *Il17a* promoter, thus, it will repress IL17A expression by competing with the binding of STAT3 to the *Il17a* promoter [132]. To figure out whether less IL-17A production in mice with SUMOylation-deficient NFATc1 was caused by enhanced binding of STAT5 to *Il17a* promoter, we examined the binding level of STAT5 at the *Il17a* promoter in Th17-skewed cells by ChIP-qPCR assays. A pair of primers for the STAT5-binding site within the *Il17a* promoter (site 4) and a pair of primers for a non-binding site (Nb1) as negative control were used for qPCR. As shown in Figure 17 D, STAT5 enriched at the *Il17a* promoter in NFATc1/ΔS$^+$ T cells compared to WT. These results revealed that elevated IL-2 produced by NFATc1/ΔS$^+$ T cells could enhance the phosphorylation of STAT5, competing with STAT3 at the *Il17a* promoter, in the end, inhibiting the expression of IL-17A.

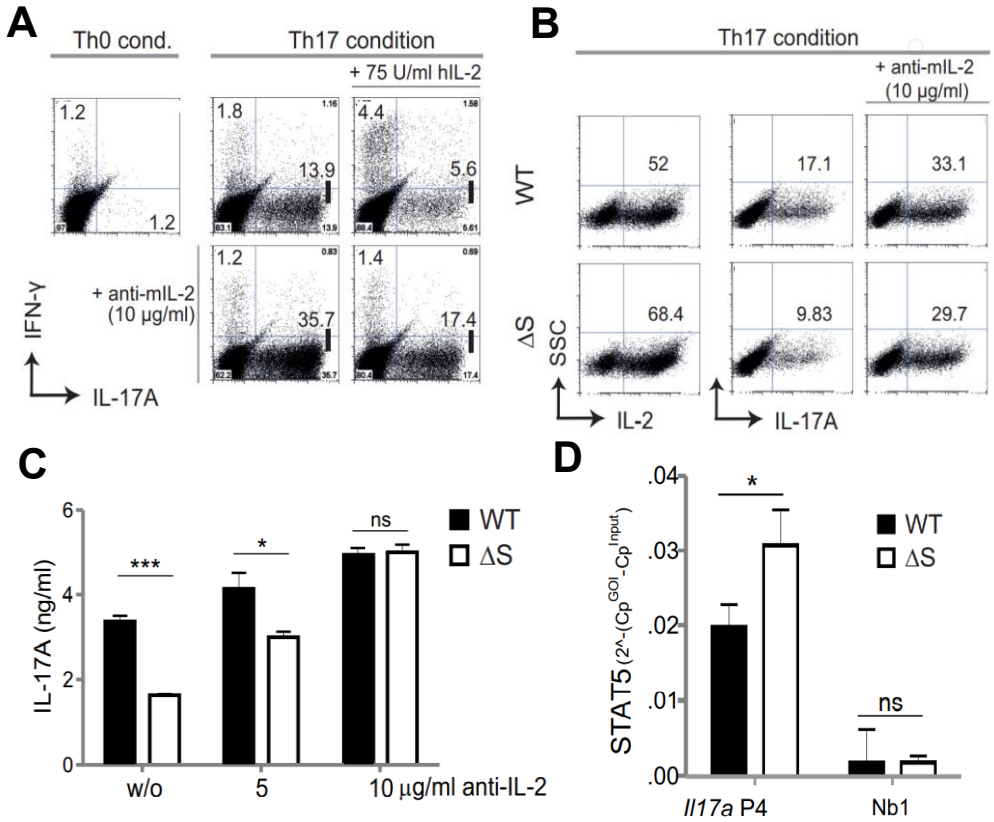

Figure 17: NFATc1/ΔS-induced surplus in IL-2 expression counteracts IL-17A expression.

(A) Representative flow cytometry plots of IFN-γ and IL-17A expression of Th17-skewed cells from WT mice with the addition of hIL-2 (75 U/ml) and/or anti–mIL-2 antibodies (10 µg/ml). (B) Representative flow cytometry plots of IL-2 and IL-17A expression of Th17-skewed cells from WT and NFATc1/ΔS$^+$ mice under normal and anti–mIL-2 conditions as performed for A [Figure A and B was performed by Lena Dietz]. (C) Amount of secreted IL-17 in the supernatants of Th17-skewed cells (n = 6) with increasing concentrations of anti–mIL-2 was measured by ELISA. (D) ChIP-qPCR assay of Th17-skewed cells for STAT5 bound to *Il17a* promoter (P4) and a non-binding site (n = 4). Statistical analysis for C and D was performed by Student's t-test, two-tailed (*, $p < 0.05$; ***, $p < 0.001$); mean ± SD.

To obtain a broader picture of differential gene expression in Th1 and Th17-skewed cells, we performed a bulk RNA sequencing to determine the transcriptome of Th1, Th2 and Th17-skewed cells at two different time points. As usual, Th1, Th17, and Th2 cells were differentiated from naïve CD4$^+$ T cells *in vitro* for 3 days, but we collected cells on day 2.5 and day 3.5, respectively. Before harvesting cells, part of them was restimulated as mentioned before and checked for cytokine expression by flow cytometry, which ensured enhanced IL-2 production and reduced effector cytokine production (Figure S1). Generally, transcriptional changes were mild without restimulation, and the difference in gene expression between the two genotypes was more obvious on day 2.5 compared to day 3.5. Interestingly, the most distinct differences were found in Th1-skewed cells (Figure S2). When we compared WT$^+$ Th1, Th2, and Th17 cells with the ones from NFATc1/ΔS$^+$ mice for both time points, we found a total of 38 genes which significantly differed between the two genotypes (Figure 18). The *Il2* RNA was notably increased in NFATc1/ΔS$^+$ Th1, Th2, and Th17 cells on day 2.5, yet it was not increased

anymore on day 3.5. In Th17-skewed cells, *Il17a* and *Il17f were* constantly reduced in NFATc1/ΔS$^+$ Th17 cells, which was consistent with our protein expression data. Surprisingly, *Ifng* was augmented at an earlier time point in NFATc1/ΔS$^+$ Th1 cells. We also observed a clear reduction of *Il5* and *Il13* in NFATc1/ΔS$^+$ Th2 cells, which was also consistent with our previous data on the mRNA expression of *Il13* with retrovirally infected EL-4 cells [97]. However, when we checked the frequency of IL-13$^+$ cells under Th2 differentiation condition, it did not significantly decrease (Figure S3). Some molecules related to effector function were significantly reduced in NFATc1/ΔS$^+$ T cells, such as *Gzma* and *Ctla4*. Another interesting marker, i.e., CD24 (also called heat-stable antigen), can provide CD28-independent co-stimulation for clonal expansion and functional differentiation of T cells [133-135]. Bai *et al.* claimed that the mutation of CD24 can abrogate the development of EAE, although it did not influence the induction of autoimmune T cells [136]. Here, CD24 was less expressed in NFATc1/ΔS$^+$ T cells, which indicates that NFATc1/ΔS might protect from induced EAE.

All in all, the histone acetylation on the *Il2* promoter is enhanced in NFATc1/ΔS$^+$ T cells, which causes a heightened IL-2 production. IL-2, in turn, activates the phosphorylation of STAT5, which will compete with STAT3 at the *Il17a* promoter, resulting in the inhibition of IL-17A production. Moreover, NFATc1/ΔS$^+$ T cells also can produce less IFN-γ cytokine.

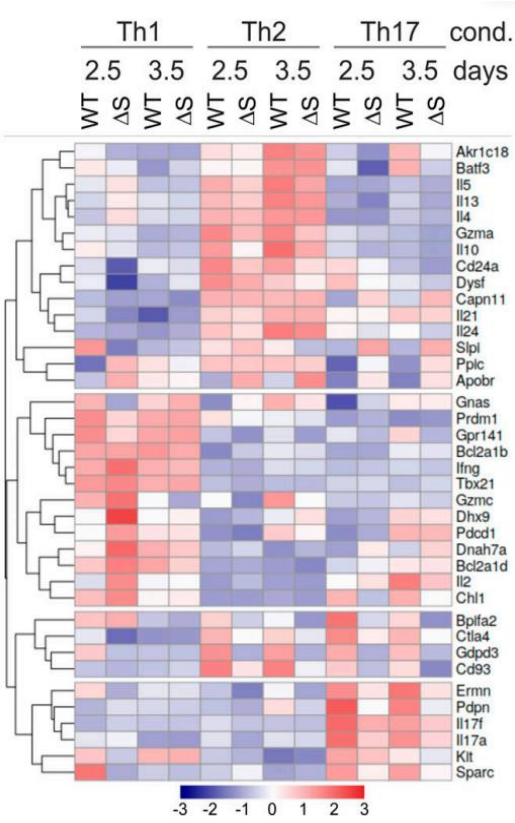

Figure 18: The heatmap of differentially expressed genes of Th1, Th2, and Th17-skewed cells between two genotypes at two different time points.

CD4$^+$ T cells isolated from LN and spleen were differentiated for Th1, Th2, and Th17 *in vitro*. On d 2.5 and 3.5, cells were extracted for RNA, then RNA was subjected to NGS. The heatmap shows 38 differentially expressed genes within all WT versus NFATc1/ ΔS$^+$ T cells of both days determined using the edgeR's glm model.

8.1.3 Elevated IL-2 production of NFATc1/ΔS$^+$ T cells enhances Foxp3 expression

IL-2 plays a critical role in the survival, proliferation, differentiation, and stability of Treg cells [137, 138]. Especially in Tregs, IL-2 via high-affinity IL-2R signaling, activates the transcription factor STAT5 by phosphorylation. The phosphorylated STAT5 can bind to the non-coding sequence 2 (CNS2) of the *Foxp3* enhancer, to maintain heritable transcription of *Foxp3*. To assess whether the increased IL-2 in NFATc1/ΔS$^+$ mice can enhance the Foxp3 expression in T-conventional (Tcon) cells, we checked the Foxp3 expression in Th17-skewed cells with or without exogenous IL-2. Our flow cytometric data showed that the percentage of Foxp3$^+$ T cells was dramatically increased in NFATc1/ΔS$^+$ Tcon, which reached around 8-fold compared to WT as long as exogenous IL-2 was avoided (Figure 19 A). To further study the effect of IL-2 on induced Tregs (iTregs), we performed iTreg induction in the presence of TGF-β for 3 days with or without additional anti–mIL-2. Foxp3 expression of CD4$^+$ Tcon cells was measured by flow cytometry. Without TGF-β, the percentage of iTregs was relatively low in both WT and NFATc1/ΔS$^+$ T cells after 3 days, but still two times higher in NFATc1/ΔS$^+$ T cells. On the contrary, with TGF-β, more than 60% of Tcon cells were skewed to iTregs, and the percentage of iTregs was still higher in NFATc1/ΔS$^+$ T cells. However, after blocked with anti–mIL-2, not only the total percentage of Foxp3$^+$ cells was reduced in both WT and NFATc1/ΔS$^+$ T-cell population, but also almost no difference in the frequency of Tregs between WT and *Nfatc1*$^{\text{deltaSUMO}}$ genotype was observed (Figure 19 B). A statistically significant increase of iTregs with NFATc1/ΔS$^+$ over WT$^+$ T cells was noted by analysing multiple experiments (Figure 19 C). These data indicated that enhanced IL-2 production by NFATc1/ΔS$^+$ CD4$^+$ T cells can increase the induction of Foxp3, thus supporting iTreg differentiation.

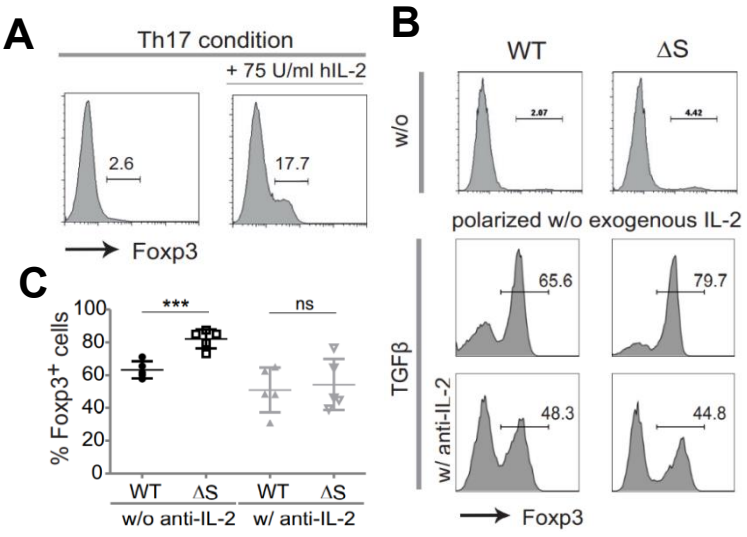

Figure 19: Elevated IL-2 by NFATc1/ΔS$^+$ T cells induces Foxp3 expression.

(A) Foxp3$^+$ expression was evaluated in WT CD4$^+$ T cells under Th17-inducing conditions on day 3, with or without additional IL-2 (75 U/ml rhIL-2). (B) The histogram of Foxp3 expression. Naive CD4$^+$ T cells from WT and NFATc1/ΔS$^+$ mice were polarized to iTregs with TGF-β, but without exogenous IL-2; parallel cultures were in the presence of 10 µg/ml anti–mIL-2. On day 3, cells were collected to measure the percentage of Foxp3 by flow cytometry. (C) Data are shown as representative flow cytometric plots for Foxp3$^+$ cells (n=5). Statistical analysis was performed by Student's t-test, two-tailed (*, $p < 0.05$; ***, $p < 0.001$); mean ± SD.

8.1.4 NFATc1/ΔBC mice behave similarly to NFATc1/ΔS mice

The two decisive SUMOylation sites, K702 and K914, are encoded in exon 10 of NFATc1, and they might be responsible for the special function of the long isoforms NFATc1/B and NFATc1/C. To evaluate a possible functional difference between long and short isoforms, which could depend on the C-terminal SUMOylation of NFATc1, we also framed exon 10 with two loxP sites. Thus, by crossing with a CD4 Cre-deleter mouse, we could specifically erase NFATc1 exon 10 in all T cells. In the end, the $CD4^+$ T cells in this mouse should only be able to express the short isoforms NFATc1/αA and NFATc1/βA. To indicate the loss of the long isoforms B and C, we termed this newly generated strain *Nfatc1*^{deltaBC} and the protein NFATc1/ΔBC (Figure 13 A).

We first evaluated whether the deletion of exon 10 was specific to T cells. For this purpose, we performed a qRT-PCR assay. Two pairs of primers were designed: one pair of primer was specific for exon 9 + 11 (Δexon10) and another primer was for exon 9 + 10 (WT). Only a small cDNA fragment could be observed in $CD3^+$ T cells, which amplified with the primer pairs for Δexon10 irrespective of stimulation. The result indicated that the exon 10 of NFATc1 was successfully deleted in T cells (Figure 20 A), and the deletion only specifically happened in T cells, not in other $CD3^-$ leukocytes. Accordingly, to examine the expression level of NFATc1 proteins, we extracted whole proteins of $CD4^+$ T cells from WT and NFATc1/ΔBC^+ with or without stimulation with T/I for 6 h. As expected, six isoforms could be observed in WT mice without stimulation, however, only the concentrated expression of the short isoforms NFATc1/αA and -βA could be detected in NFATc1/ΔBC^+ cells (Figure 20 B). Furthermore, the NFATc1 proteins run faster after stimulation, which implies dephosphorylation and activation (Figure 20 B). In conclusion, using LoxP and CD4 cre mice to specifically knock out NFATc1 exon 10, resulted in the deletion of the long isoforms NFATc1/B and NFATc1/C, while overall preserving NFAT expression under endogenous control.

Next step, to investigate whether $CD4^+$ T cells from NFATc1/ΔBC^+ mice behaved similarly to the ones from NFATc1/ΔS^+ mice, we also measured cytokine expression of Th1-skewed or Th17-skewed cells by flow cytometry. As shown in Figure 20 C, the percentage of IL-2^+ cells was increased, whereas the percentage of IFN-γ^+ cells was reduced in the NFATc1/ΔBC^+ Th1-skewed cells. Under Th17 differentiation, the percentage of IL-2^+ cells was also elevated, but the percentage of IL-$17A^+$ cells was condensed compared to Th17-skewed cells from WT mice, very much reflecting the NFATc1/ΔS phenotype.

To compare T cells expressing NFATc1/ΔBC or NFATc1/ΔS directly, we cultured $CD4^+$ T cells from both NFATc1 mutants and WT in the presence of anti-CD3 with or without anti-CD28 for 48 h. The amount of IL-2 in the supernatant was measured by ELISA. T cells stimulated only with anti-CD3 showed very less secretion of IL-2. Whereas, after stimulation with anti-CD3 and

anti-CD28, T cells produced an overall robust amount of IL-2 (Figure 20 D). Notably, not only the T cells from NFATc1/ΔS$^+$ mice but also those from NFATc1/ΔBC$^+$ mice produced more IL-2 compared to WT$^+$ T cells, and the total amount of secreted IL-2 was almost similar from NFATc1/ΔBC$^+$ and NFATc1/ΔS$^+$ T cells (Figure 20 D). This suggests that the function of NFATc1 long isoforms regulates cytokines expression through SUMOylation.

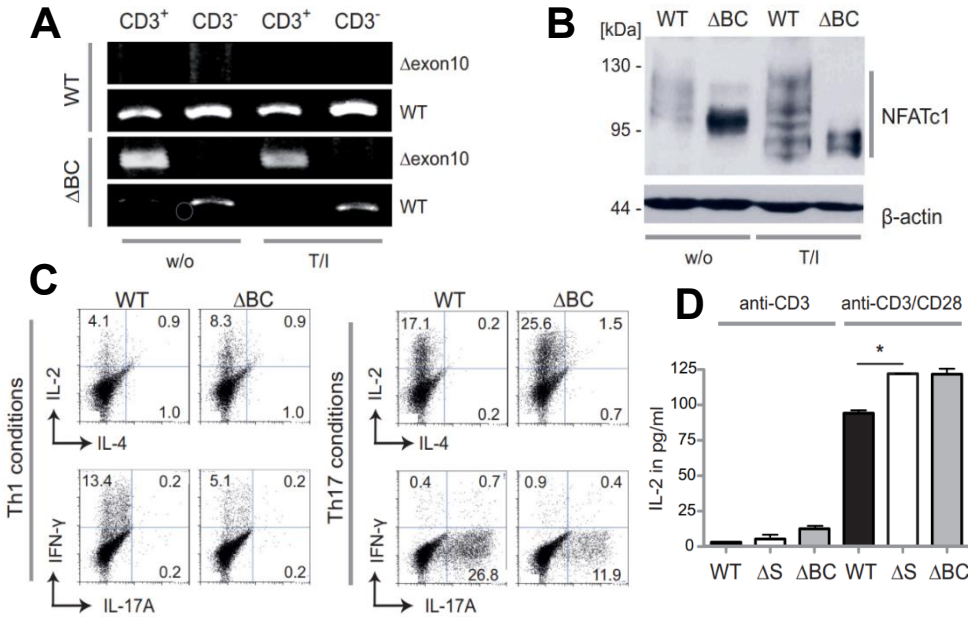

Figure 20: NFATc1/ΔBC$^+$ CD4$^+$ T cells express more IL-2 but less IFN-γ and IL-17A.

(A) RT-PCR with primers specific for exon 9 + 11 (Δexon10) showed deletion of the C-terminus in *Nfatc1* mRNA in CD3$^+$ T cells of NFATc1/ΔBC$^+$ but not in CD3$^-$ cells nor in WT cells. Primers binding to exon 9 + 10 detected WT *Nfatc1* mRNA; n > 3. (B) Western blot analysis of NFATc1 from unstimulated (w/o) and 6 h stimulated (T/I) CD4$^+$ T cells from WT and NFATc1/ΔBC$^+$ mice; n > 3. (C) Representative flow cytometric plots of IL-2, IL-4, IL-17A and IFN-γ expression in Th1-skewed and Th17-skewed cells *in vitro* from WT and NFATc1/ΔBC$^+$ mice. (D) ELISA of IL-2 in the supernatant of CD4$^+$ T cells stimulated by anti-CD3 or anti-CD3 / CD28 for 48 h from WT, NFATc1/ΔS$^+$, and NFATc1/ΔBC$^+$ mice. Statistical analysis was performed by Student's t test (*, $p < 0.05$; **, $p < 0.005$); n = 3 [Figure 20 was performed by Lena Dietz].

8.1.5 Transplanted NFATc1/ΔS$^+$ T cells shows less severe in aGvHD

To study the role of NFATc1 SUMOylation in pathogenic T-cell responses, we used a major histocompatibility complex (MHC) mismatch mouse model. Briefly, B6 T cells (H-2^b CD90.1$^+$ luc$^+$) were transplanted together with B6 BM cells (H-2^b CD90.2$^+$) into irradiated BALB/c recipient mice (H-2^d CD90.2$^+$). As shown in Figure 21 A and B, recipient mice transplanted with NFATc1/ΔS$^+$ T cells showed better survival and had a less severe GvHD score than WT$^+$ T cells. It was found that 50% of recipient mice that received NFATc1/ΔS$^+$ T cells survived until d 40 after allo-HCT. However, all mice that received WT$^+$ T cells were dead after d 20 already

(Figure 21 A). The difference in GvHD clinical score between WT and NFATc1/ΔS recipients became significant over time (Figure 21 B).

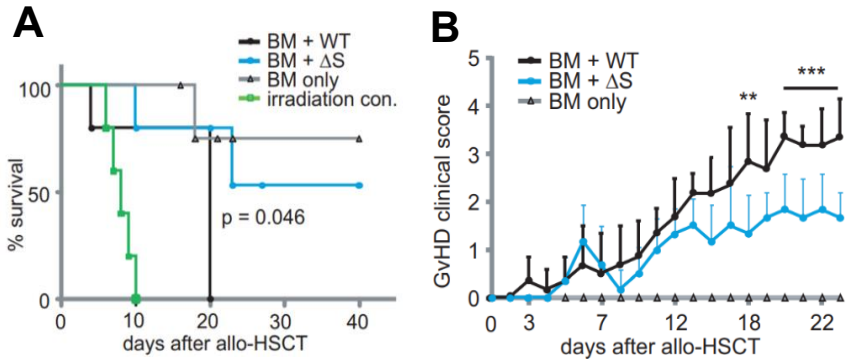

Figure 21: Survival and GvHD clinical score of WT⁺ and NFATc1/ΔS⁺ T cell-receiving mice after allogeneic HCT.

BALB/c recipient mice were irradiated with 8 Gy and injected i.v. with 1,2 x 10^6 T cells from WT and NFATc1/ΔS⁺ donors together with 5 x 10^6 BM cells from the WT or *Rag1*$^{-/-}$ B6 mice. Some BALB/c mice only received 5 x 10^6 BM cells as experimental BM control or were even only irradiated as irradiation control (A) Cumulative survival of the individual groups. p = 0.046 between WT and ΔS (log-rank test). (B) Clinical GvHD scoring of the recipient mice listed under A. statistical analysis was performed by Mann–Whitney U test; *, p < 0.05. [Figure 21 was performed by Musga Qureischi].

The proliferation of T cells *in vivo* after allo-HCT was monitored by *in vivo* bioluminescence imaging (BLI). Organs were harvested on day 6 after allo-HCT for *ex vivo* BLI to better monitor infiltration of T cells to target organs as well as the migration of alloreactivity T cells. We observed that T cells from NFATc1/ΔS⁺ mice showed less infiltration and proliferation in the target organs, especially for the GI tract and mLN (Figure 22).

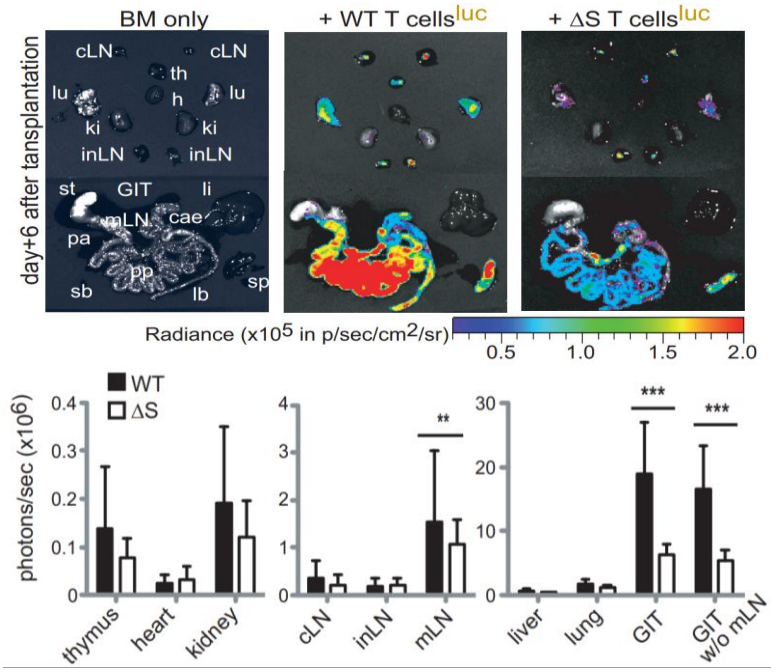

Figure 22: Less infiltration and proliferation of NFATc1/ΔS⁺ T cells in GvHD target organs.

Representative *ex vivo* BLI data from internal organs and quantification of allogenic luc⁺ WT⁺ versus NFATc1/ΔS⁺ T cells 6 d after allo-HCT. Data are compiled from at least two independent experiments with five mice per group per experiment (n = 10). Statistical analysis was performed by Two-way ANOVA; **, p < 0.01, ***, p < 0.001. [Figure 21 was performed by Musga Qureischi]

8.1.6 Transplanted NFATc1/ΔS$^+$ Tcon can reduce aGvHD

The suppressive properties of Treg are very important for the prevention or treatment of aGvHD. In our previous experiments, we had observed that the recipients who received NFATc1/ΔS$^+$ T cells developed less severe aGvHD, furthermore that NFATc1/ΔS$^+$ Tcon supported the expansion of Tregs. Moreover, TIGIT expression on NFATc1/ΔS$^+$ Tregs was significantly increased compared to WT$^+$ Tregs (Figure S4). Therefore, we wanted to investigate if naïve NFATc1/ΔS$^+$ T cells also can protect mice from aGvHD when Tregs are eliminated.

To deplete Tregs completely, we crossed WT and NFATc1/ΔS$^+$ donor mice with DEREG mice, which express a diphtheria toxin (DT) receptor-enhanced GFP fusion protein under the control of the Foxp3 gene locus [125]. Thus, Foxp3-expressing T cells can be depleted by treatment with DT. Therefore, transplanted donor T cells devoid of Tregs allowed us to study the effect of only Tcon. To this end, we checked whether Tregs can be completely depleted with DT. To do so, we treated WT mice with either 1 µg of DT or PBS at two continuous days by intraperitoneal injection (i.p. injection), then the frequency of Tregs was measured by flow cytometry from total splenocytes. As shown in Figure 23, the Treg population had almost disappeared compared to the PBS control group. Thus, 1 µg of DT can be used for the depletion of Tregs.

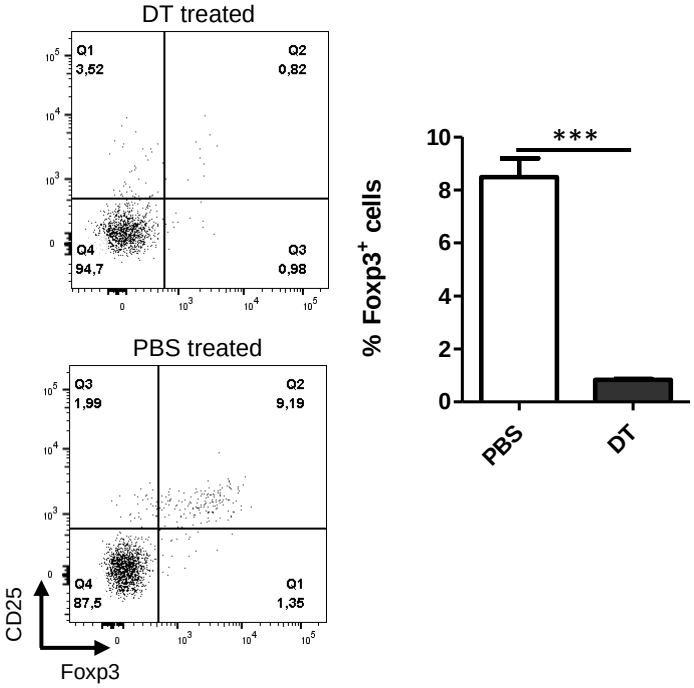

Figure 23: Treg depleted by DT treatment.

WT mice were treated with DT or PBS on day 1 and day 2. Splenocytes were obtained to check the frequency of Tregs by flow cytometry on day3. Statistical analysis was performed by Student's t test (*, $p < 0.05$; **, $p < 0.005$; ***, $p < 0.001$); n = 3.

Next, we applied DT to WT DEREG and NFATc1/ΔS$^+$ DEREG mice as mentioned above, the experiment set-up was described in 7.2.4. The results observed were consistent with Figure 22, i.e., naïve Tcon from NFATc1/ΔS$^+$ mice showed significantly reduced proliferation and less

target organ infiltration than WT$^+$ Tcon after transplantation in the major mismatch model (Figure 24 A).

In addition, we harvested mLN and spleen from recipients on day 6 after allo-HCT. Here, the donor pTreg cells were detected by GFP protein, encoded in the DEREG mice. The frequency of induced pTregs was very low in both transferred WT$^+$ and NFATc1/ΔS$^+$ Tcon recipients. However, the pTregs in transferred NFATc1/ΔS$^+$ Tcon recipients were still significantly enriched when compared to WT$^+$ Tcon (Figure 24 B). When checking the production of IL-2 in T cells, we observed not only the frequency of IL-2$^+$ Tcon to be increased, but also the IL-2 production per cell was enhanced (Figure 24 C). These data indicate that Tcon from NFATc1/ΔS$^+$ mice still supported their production of IL-2 *in vivo*, and that those elevated IL-2 was beneficial for the induction of pTreg.

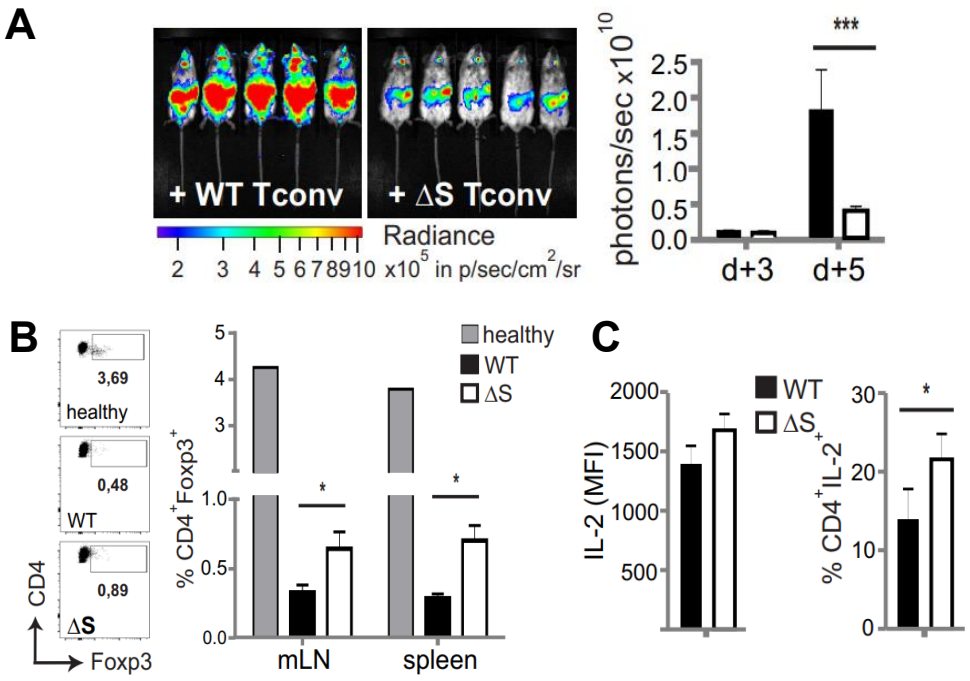

Figure 24: NFATc1/ΔS$^+$ Tcon cells produced more IL-2 and induced more pTregs.

(A) WT and NFATc1/ΔS$^+$ donors were treated with DT d1 and d2 before transplantation. 1,2 x 10^6 Tcon together with 5 x 10^6 BM cells were i.v. injected into irradiated BALB/c recipients, the proliferation of Tcon was measured on day 6 after allo-HCT by BLI. (B) CD4$^+$ T cells were isolated from the spleen and mLN to check the frequency of pTregs by flow cytometry. (C) CD4$^+$ T cells were stimulated with T/I for 5 h and IL-2 expression was measured intracellularly by flow cytometry. Values were displayed as mean ± SD. n = 5 per WT/ΔS group; n = 1 healthy DEREG, statistical analysis was performed by unpaired t-test (*, p ≤ 0.05; **, p ≤ 0.01; ***, p ≤ 0.001).

8.1.7 Th1 and Th17 cells from NFATc1/ΔS$^+$ mice ameliorate disease scores during passive EAE

We observed that NFATc1/ΔS$^+$ T cells express less IFN-γ in Th1-skewed cells, as well as less IL-17A in Th17-skewed cells. Since Th1 and Th17 cells play a very important role in mediating autoimmune diseases, especially for experimental autoimmune encephalomyelitis (EAE), we wondered whether these T cells from NFATc1/ΔS$^+$ mice could protect from EAE. We were also interested whether a possible protective effect would be gone upon blocking elevated IL-2 production by anti–mIL-2. For these purposes, the 2D2 mice were used in this experiment, which have a MOG_{35-55}-specific transgenic TCR. We isolated CD4$^+$ T cells from 2D2.WT and 2D2.NFATc1/ΔS$^+$ mice to differentiate into Th1 and Th17 cells *in vitro*, then transferred a mixture of Th1/Th17 cells into *Rag1*$^{-/-}$ mice. Anti–mIL2 was given during *in vitro* differentiation and later to such transplanted mice.

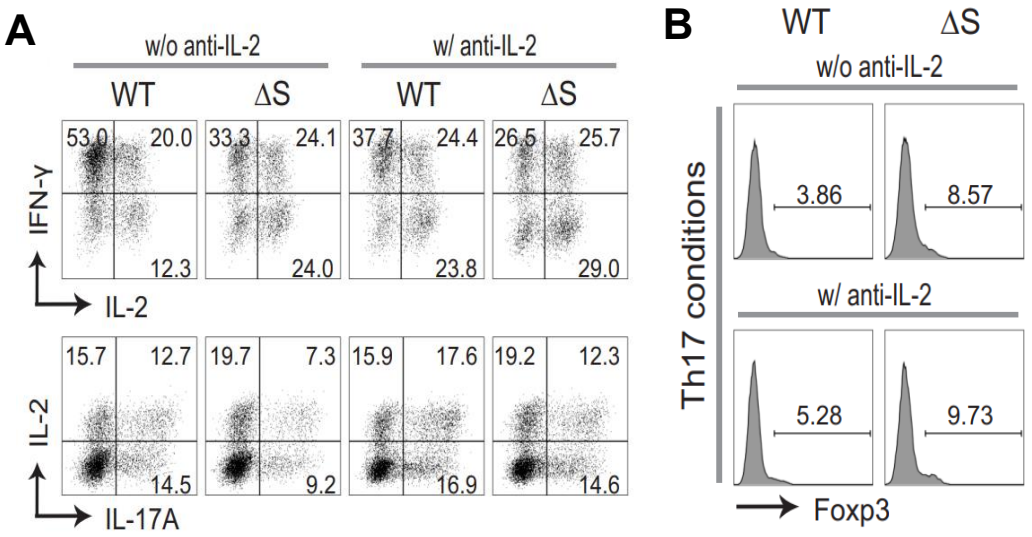

Figure 25: Th1 and Th17 differentiation *in vitro* with and without anti–mIL-2.

(A) Naïve CD4$^+$ T cells isolated from 2D2.WT and 2D2.NFATc1/ΔS$^+$ mice were skewed towards Th1 and Th17 differentiation *in vitro*, with (w/) and without (w/o) anti–mIL-2. On day 3, part of the cells was restimulated with T/I for 5 h, then the cells were measured for cytokine expression of IL-2, IFN-γ, and IL-17A by flow cytometry. Representative plots from flow cytometry and comparison of WT$^+$ versus NFATc1/ΔS$^+$ CD4$^+$ T cells. (B) Foxp3 expression of CD4$^+$ T cells undergoing Th17-differentiation was evaluated by flow cytometry.

Before transplantation, the quality of differentiation was assessed by flow cytometry. In normal differentiation conditions, the frequency of IL-2$^+$ T cells were much higher in the NFATc1/ΔS$^+$ Th1-skewed cells, and IFN-γ single-positive cells almost reduced half, although the frequency of IFN-γ$^+$ IL-2$^+$ T cells did not change in NFATc1/ΔS$^+$ Th1-skewed cells. However, in the presence of anti–mIL-2, the percentage of IL-2$^+$ cells and IFN-γ$^+$ cells in NFATc1/ΔS$^+$ Th1-skewed cells were similar to WT Th1-skewed cells (Figure 25 A). During Th17 differentiation,

the percentage of IL-17A$^+$ cells was reduced in NFATc1/ΔS$^+$ T cell in the absence of anti–mIL-2, while after being blocked with anti–mIL2, the percentage of IL-17A$^+$ cells among NFATc1/ΔS$^+$ T cells was similar to WT$^+$ T cells (Figure 25 A). Moreover, we also detected a small amount of Tregs to be induced (iTregs) in both WT and NFATc1/ΔS$^+$ Th17-skewed cells, but the percentage of iTregs was much higher in NFATc1/ΔS$^+$ T cells in the absence of anti–mIL-2.

The *in vitro* study of NFATc1/ΔS$^+$ CD4$^+$ T cells had revealed impaired effector functions of Th1 and Th17 cells, as IFN-γ and IL-17A secreted by Th1 and Th17 cells are considered as pro-inflammatory cytokines, also involved in several autoimmune diseases, including EAE. Thus, we hypothesized that reduced effector cytokine production by NFATc1/ΔS$^+$ CD4$^+$ T cells can protect from EAE disease. Therefore, we transplanted 5 x 10^6 cells with the mixture of Th1 and Th17 cells which were differentiated *in vitro* from 2D2.WT and 2D2. NFATc1/ΔS$^+$ mice into *Rag1*$^{-/-}$ mice. To level out the IL-2 effect, anti–mIL-2 was given during differentiation and later to such transplanted mice (Figure 12).

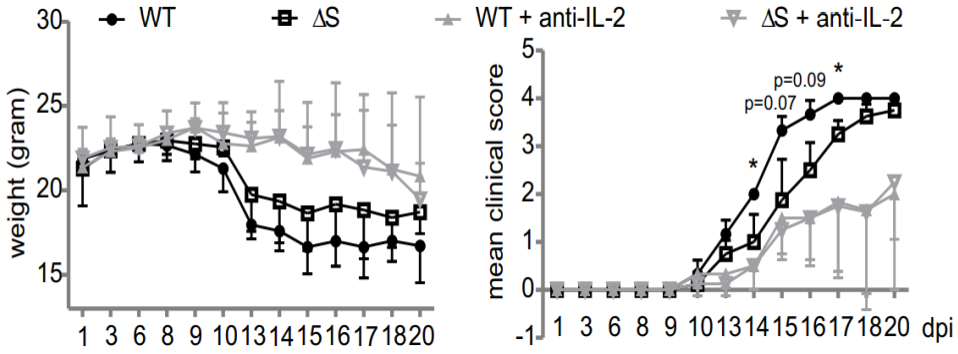

Figure 26: Clinical score and weight loss of mice receiving T cells from WT and NFATc1/ΔS$^+$ mice in a passive EAE model.

CD4$^+$ T cells from 2D2.WT and 2D2.NFATc1/ΔS$^+$ mice were isolated and differentiated into Th1 and Th17 cells with or without 10 µg/ml of anti–mIL-2 for 3 days *in vitro*, then transferred 5 x 10^6 cells with the mixture of Th1/Th17 cells into *Rag1*$^{-/-}$ mice, 200 µg of anti–mIL2 was given at day 3 and 6 after transplantation. (A) shows the weight of individual groups and (B) represented clinical scores of mice after passive EAE induction; statistical analysis was performed by Mann–Whitney U test; *, $p < 0.05$.

After transplantation, mice that received Th1 plus Th17 cells from 2D2.NFATc1/ΔS$^+$ mice showed less weight loss and reduced clinical score in comparison to WT-transplanted mice in the absence of anti–mIL-2 (Figure 26). Specifically, mice that received WT$^+$ and NFATc1/ΔS$^+$ T cells did not lose weight and had no symptoms in the first week. In the second week, all mice lost weight dramatically and also started to have symptoms. Still, clinical score differences between mice who received WT versus NFATc1/ΔS$^+$ T cells became significant in the second week (Figure 26). After being blocked with anti–mIL-2, the weight loss and clinical score were

equalized as the mice received T cells from WT and NFATc1/ΔS groups. However, the weight of these two groups was higher compared to the groups without anti–mIL-2, the clinical score was much lower in the groups with anti–mIL-2. This might be due to compensatory enhanced IL-2 expression upon external block with anti–mIL-2 (Figure 26 A) and the slightly elevated iTreg induction (Figure 26 B) and/or reduced T-cell proliferation in the presence of anti–mIL-2. Importantly though, 2D2.WT and 2D2.NFATc1/ΔS$^+$ T cells lost their functional difference in the presence of IL-2 blocking antibodies indicating that the surplus in IL-2 secretion is decisive in T cells which cannot SUMOylate NFATc1.

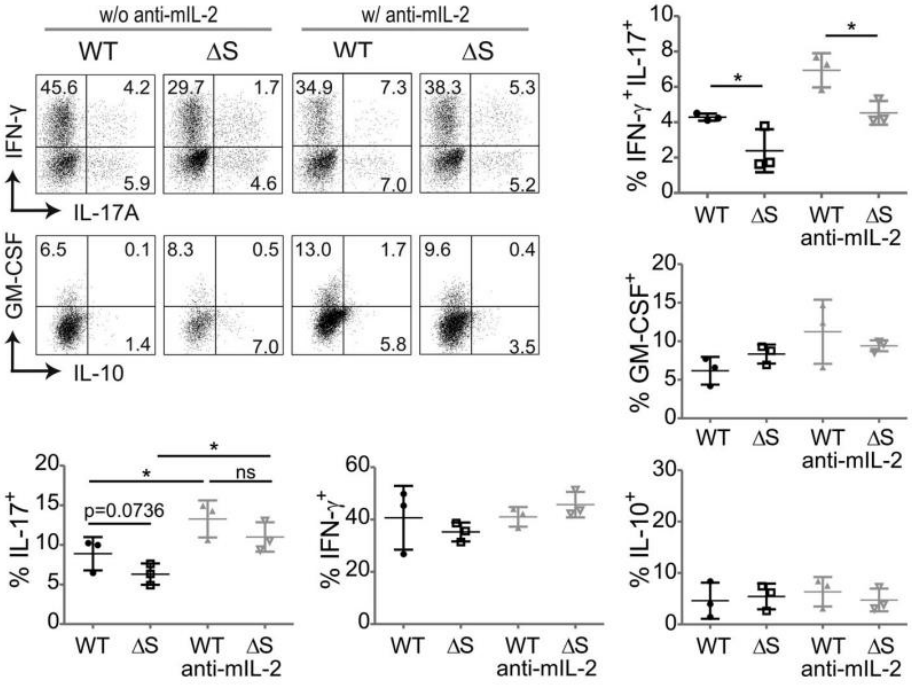

Figure 27: The infiltrating lymphocytes from the brain and spinal cord in EAE-induced mice.

Flow cytometric analysis of IFN-γ, IL-17A, GM-CSF, and IL-10 expression by infiltrated lymphocytes that were isolated from brain and spinal cord on day 20 after transplantation. Cells were restimulated with T/I for 5 h in the presence of Golgi-Stop and Golgi-Plug ex vivo before measuring. Statistical analysis was performed by Student's t-test; *, $p < 0.05$, n=3 each group.

To further investigate whether the weakened score is associated with the amounts of secreted cytokines and the composition of CNS tissue-infiltrating cells, we examined the cytokines' expression of infiltrating lymphocytes from the brain and spinal cord. As shown in Figure 27, the frequency of IL-17A$^+$ cells were significantly reduced in mice who received NFATc1/ΔS$^+$ T cells. IFN-γ$^+$ IL-17A$^+$ T cells were diminished as well in the absence of anti–mIL-2, whereas the difference in IFN-γ$^+$ T cells did not reach significance and IL-10$^+$ T cells, and GM-CSF$^+$ T cells remained unchanged. The drop in IL17A$^+$ and especially in pathogenic IFN-γ$^+$ IL-17A$^+$ T cells could explain the reason why mice that received NFATc1/ΔS$^+$ Th1 plus Th17 have less severe disease in comparison with WT-transplanted animals. Interestingly, anti–mIL-2, which not only

equalized, but diminished disease scores, elevated pro-inflammatory cytokine expression. In sum, however, the outcome of anti–mIL-2 treatments still suggested that the differences in 2D2.WT and 2D2.NFATc1/ΔS-transplanted mice are driven by enhanced IL-2 of NFATc1/ΔS$^+$, overall being causative for the differential behaviour.

8.1.8 Elevated IL-2 from NFATc1/ΔS$^+$ T cells up-regulates Blimp-1

To figure out whether less production of IFN-γ in NFATc1/ΔS$^+$ mice is regulated by NFATc1, we examined the binding ability between NFATc1 and the *Ifng* promoter by ChIP-qPCR assay. Thus, the Th1 and Th17-skewed cells were used for ChIP-qPCR analysis. No difference in the binding ability of NFATc1 to the *Il17a* promoter between WT NFATc1$^+$ and NFATc1/ΔS$^+$ Th17-skewed cells was observed. However, it bound less to the *Ifng* promoter in NFATc1/ΔS$^+$ Th1-skewed cells compared to WT NFATc1$^+$ Th1-skewed cells (Figure 28 A).

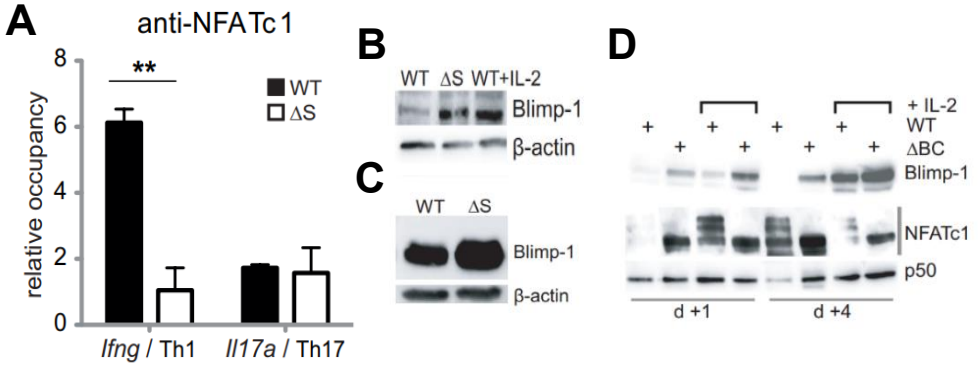

Figure 28: Deficiency of NFATc1 SUMOylation causes higher expression of Blimp-1.

(A) ChIP-qPCR assay performed from skewed Th1 and Th17 cells *in vitro* for 3 days from WT and NFATc1/ΔS$^+$ mice. Relative occupancy of NFATc1 at the *Ifng* promoter region (Th1 cells) or the *Il17a* promoter (Th17 cells) was calculated by the ΔΔCt method. Bars showed mean ± SD of two individual experiments. Two-way ANOVA followed by Bonferroni posttest; **, $p < 0.005$. (B) Western blot analysis of protein extracts from isolated CD3$^+$ T cells of WT and NFATc1/ΔSUMO$^+$ mice stimulated with ConA, WT cells in parallel with the addition of exogenous IL-2 ($n > 3$). (C) Western blot analysis of Blimp-1 expression in CD90.1$^+$ CD4$^+$ T cells, regained after transplantation of BM plus WT or NFATc1/ΔS$^+$ T cells on day 6 ($n = 3$). (D) Western blot analysis of Blimp-1 expression in CD4$^+$ T cells from WT and NFATc1/ΔBC$^+$ mice, stimulated for 1 or 4 d by ConA, with or without the addition of IL-2 ($n > 3$). [Figure 28 was done by Lena Dietz].

It has already been reported that IL-2 can induce Blimp-1 expression, in turn, Blimp-1 can inhibit IFN-γ and TNF-α expression as well as IL-2 in a thus negative feedback loop [139-141]. Therefore, we wanted to confirm whether the elevated IL-2 produced by NFATc1/ΔS$^+$ T cells increases Blimp-1 expression. For this purpose, western blots were performed with T cells either stimulated *ex vivo* or isolated from aGvHD mice. Indeed, stimulated CD3$^+$ T cells with ConA *in vitro* from NFATc1/ΔS$^+$ mice expressed a higher level of Blimp-1 compared to WT$^+$ T cells. Furthermore, WT$^+$ T cells can further enhance the expression of Blimp-1 in the presence

of exogenous IL-2 leading to an expression level of Blimp-1 similar to NFATc1/ΔS^+ T cells (Figure 28 B). Importantly, we sorted CD90.1$^+$ CD4$^+$ T cells from aGvHD mice after 6 d of transplantation and also performed western blots. Again, NFATc1/ΔS^+ T cells showed more Blimp-1 expression compared with WT$^+$ T cells (Figure 28 C).

So far we assumed that SUMOylation defines a major functional difference between the short isoforms and long isoforms. To directly compare short isoforms with long isoforms, the NFATc1/ΔBC^+ mice which only express short isoforms of NFATc1 was used again. As shown in Figure 28 D, CD4$^+$ T cells from NFATc1/ΔBC^+ mice expressed a significantly higher level of Blimp-1. In the presence of IL-2, the expression of Blimp-1 was even more enhanced. This indicates that T cells can express a higher amount of Blimp-1 in the absence of NFATc1 SUMOylation or the absence of NFATc1/B and especially NFATc1/C.

To evaluate whether Blimp-1 is needed to inhibit the expression of IFN-γ and IL-2 at later time points, we crossed *Prdm1*$^{fl/fl}$ mice to NFATc1/ΔBC^+ mice (*Nfatc1*^{deltaBC}.*Cd4cre*) to generate Blimp-1 deletion in T cells, as conventional *Prdm1*$^{-/-}$ die *in utero* [142, 143]. Afterwards, we tested the kinetics of IFN-γ and IL-2 expression of Th1-skewed cells at different time points. Therefore, we differentiated naïve CD4$^+$ T cells from WT, *Nfatc1*^{deltaSUMO}, *Nfatc1*^{deltaBC}.*Cd4cre* and *Nfatc1*^{deltaBC}.*Prdm1*$^{fl/fl}$.*Cd4cre* mice *in vitro* for 3 days. The flow cytometric analysis revealed a significant increase in the percentage of NFATc1/ΔS^+ IL-2$^+$ and NFATc1/ΔBC^+ IL-2$^+$ T cells compared to WT$^+$ T cells on d 2 and d 3. Moreover, without Blimp-1, the percentage of IL-2$^+$ cells was further enhanced. However, on day 5, the percentage of NFATc1/ΔS^+ or ΔBC^+ IL-2$^+$ cells was similar to WT, whereas in the absence of Blimp-1 the percentage of NFATc1/ΔBC^+ IL-2$^+$ T cells remained to be significantly higher (Figure 29 A).

On the other hand, the percentage of IFN-γ$^+$ cells was significantly reduced in NFATc1/ΔS^+ T cells on d 2 and d 3, as well as in NFATc1/ΔBC^+ T cells. However, the inhibition of IFN-γ was reverted in the absence of Blimp-1 on d 5 (Figure 29 A). To demonstrate whether the consequence of Blimp-1 deficiency was caused by elevated IL-2 secretion during the Th1 differentiation, we added anti–mIL-2 in parallel cultures. Indeed, after blocking with anti–mIL-2, all these effects were abolished (Figure 29 B).

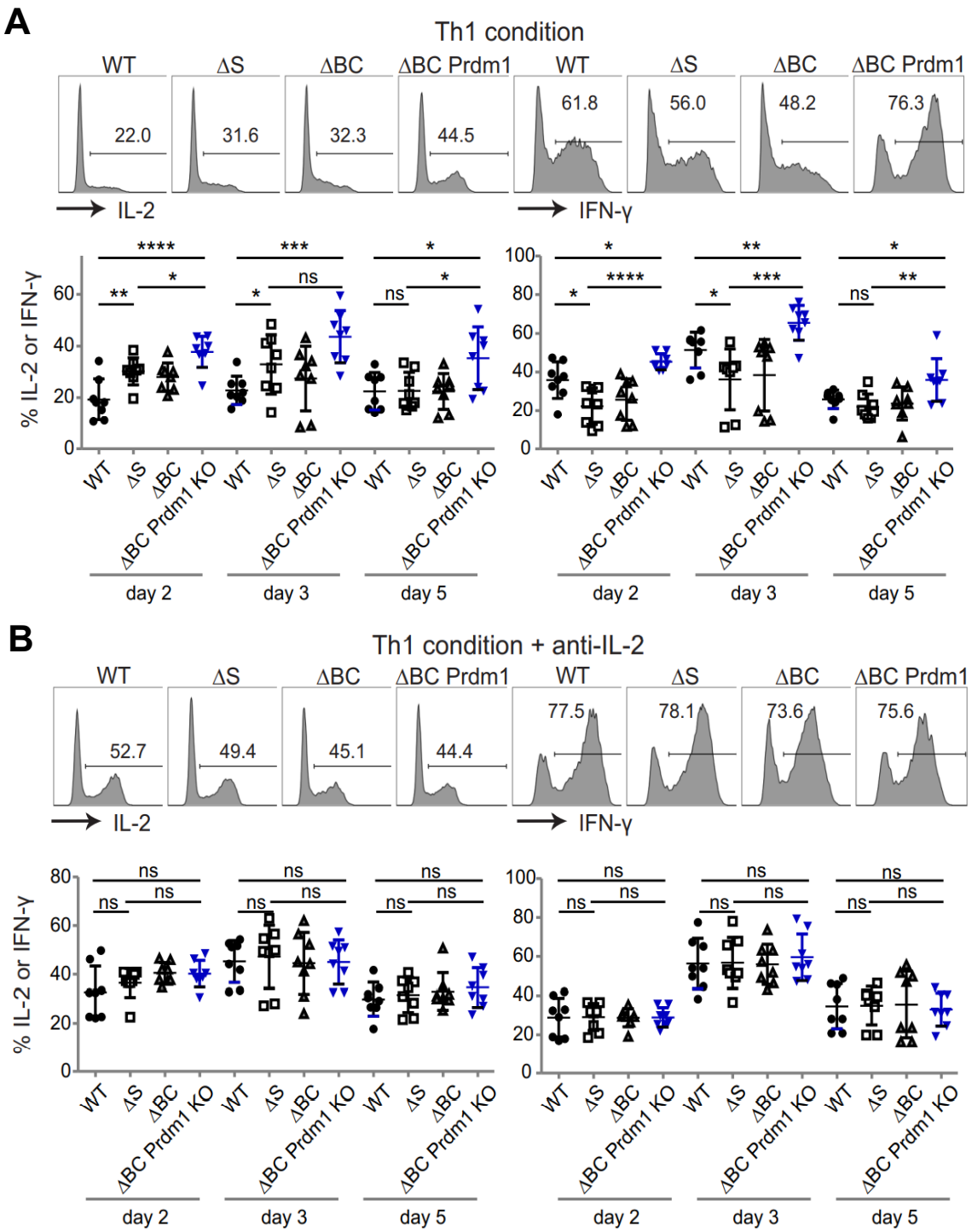

Figure 29: Blimp-1 inhibits the expression of IFN-γ and IL-2 at later time points of stimulation.

(A and B) Flow cytometric analysis of IL-2 and IFN-γ expression of Th1-skewed cells from WT, NFATc1/ΔS$^+$, NFATc1/ΔBC$^+$, and NFATc1/ΔBC$^+$ Blimp-1^{-} naïve CD4$^+$ T cells *in vitro*, without (w/o; A) or with (w/; B) anti—mIL-2 for 2, 3, and 5 days. Statistical analysis was performed by Student's t-test (comparing every two groups, n=11); *, $p < 0.05$; **, $p < 0.005$; ***, $p < 0.001$.

In summary, all these results illustrate that elevated IL-2 production by NFATc1/ΔS$^+$ T cells can enhance the induction of Blimp-1, in turn, Blimp-1 suppresses the production of IFN-γ as well as IL-2.

8.1.9 NFATc1/ΔS supports and Blimp-1 represses Bcl2A1 expression

Earlier during the course of this project, we had performed RNA sequencing of re-isolated CD90.1$^+$ CD4$^+$ T cells from WT and NFATc1/ΔS$^+$ mice during aGvHD. We found that the expression level of *Bcl2a1* was dramatically increased in NFATc1/ΔS$^+$ T cells. To validate on cells cultured *in vitro*, we performed qRT-PCR analysis of Th1-skewed cells from WT and NFATc1/ΔS$^+$ mice. We observed that T cells without the possibility of NFATc1 SUMOylation indeed can enhance the expression of *Bcl2a1* (Figure 30 A). Bcl2A1 belongs to the Bcl2 family, and functions as an anti-apoptotic member [144, 145]. In line, Chuvpilo *et al*. had reported that T cells over-expressing NFATc1/A showed less apoptosis during the stimulation with anti-CD3 *in vitro* when compared to the ones over-expressing NFATc1/C (or NFATc2) [146]. Therefore, we checked the frequency of live cells from WT and NFATc1/ΔS$^+$ mice during Th1 differentiation *in vitro* by co-staining Annexin-V and 7-AAD, where double-negative, i.e., Annexin-V$^-$ 7-AAD$^-$ cells resemble live cells. As shown in Figure 30 B, a potentially better survival of Th1-skewed NFATc1/ΔS$^+$ T cells was observed, although not reaching significance (Figure 30 B).

As RNAseq revealed *Bcl2a1* to be expressed differently in the two genotypes and since NFAT consensus site – resembling *Il2* Pubd (Figure 30 C) – could be detected in the *Bcl2a1* promoters, we tested whether NFAT can bind to the B*cl2a1* promoter by electromobility shift assays (EMSAs). As shown in Figure 30 C, not only the NFATc1-derived probe of the P1 promoter, but also the Bcl2A1-derived putative NFAT site was bound by proteins from stimulated EL-4 cells. Importantly, both anti-NFATc1 and anti-NFATc2 antibodies could 'super-shift' those bands, while the non-labelled NFAT site-containing P1 was able to compete. In addition, no bands could be detected with probes for NFAT site-mutated *Bcl2a1* oligos. This indicates that both NFATc1 and NFATc2 can bind to the *Bcl2a1* promoter.

Cimmino *et al.* have reported that Blimp1 can inhibit the induction of *Il2*, *Tnfsf2*, and *Ifng* [147]. We liked to test whether this can be applied to *Bcl2a1* as well, thereby resembling NFAT-transactivated and Blimp-1-repressed IL-2. For this purpose, firstly we measured the expression of Blimp-1 in Th1-skewed cells by qRT-PCR. It showed that the expression of Blimp-1 was significantly increased in NFATc1/ΔS$^+$ Th1-skewed cells (Figure 30 D). Secondly, we obtained CD4$^+$ T cells from spleen and mLN on day 4 after transplantation for aGVHD induction and checked the RNA levels of *Prdm1* and *Bcl2a1*. The RNA level of *Prdm1 ex vivo* was quite low compared to the one *in vitro*, as well as the level of *Bcl2a1*. However, the RNA

level of *Prdm1* and *Bcl2a1* was much higher in regained NFATc1/ΔS$^+$ CD90.1$^+$ CD4$^+$ T cells (Figure 30 E).

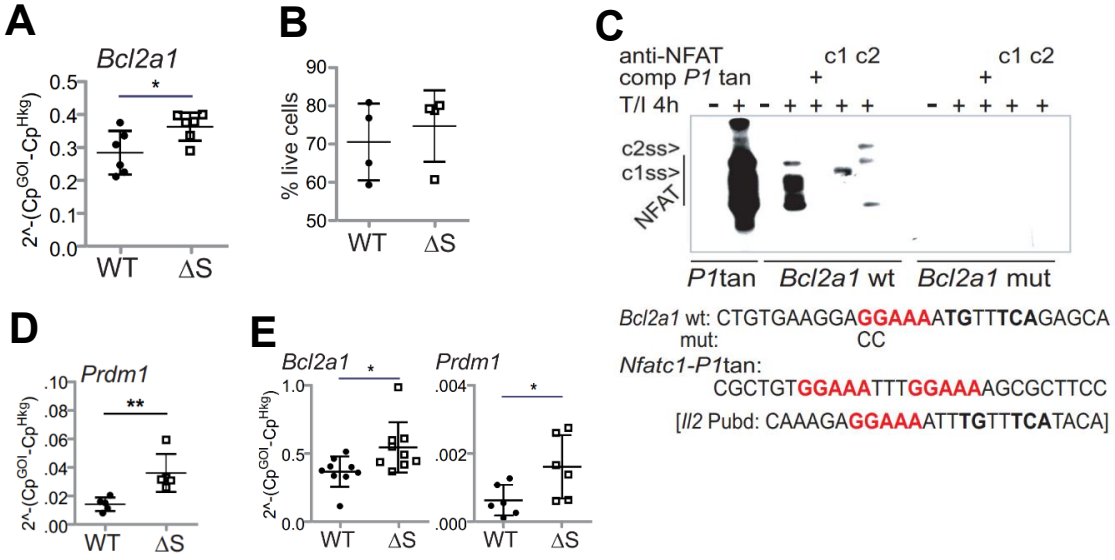

Figure 30: Bcl2A1 and Blimp-1 are enhanced in NFATc1/ΔS$^+$ mice.

(A) The RNA expression of *Bcl2a1* in Th1-skewed cells was measured by qRT-PCR. N = 6, statistical analysis was performed by Student's t-test; *, p < 0.05. (B) The frequency of live cells (7-AAD$^-$ Annexin$^-$) in Th1-skewed cells; n = 4. (C) EMSA with NFAT binding sites-containing probes from the *Nfatc1* promoter P1 (tandem site) and *Bcl2a1* promoters. Nuclear extracts were prepared from EL-4 cells, stimulated with T/I for 4 h. NFATc1 and NFATc2-specific antibodies supershifted the respective proteins (c1ss and c2ss). Consensus nucleotides for NFAT binding are indicated in red, for AP1 in bold only. (D) RNA expression of Blimp-1-encoding *Prdm1* in Th1-skewed cells was measured by qRT-PCR. n = 5, statistical analysis was performed by Student's t-test; **, p < 0.005. (E) RNA expression of *Bcl2a1* (n = 9) and *Prdm1* (n = 6) in CD4$^+$ T cells was measured by qRT-PCR, the cells were collected on day 4 of spleen and mLN of mice induced for aGvHD by transplantion with WT$^+$ versus NFATc1/ΔS$^+$ CD3$^+$ T cells. Statistical analysis was performed by Student's t-test *, p < 0.05.

Next, to confirm the negative regulation of the *Bcl2a1* gene by Blimp-1, 293T cells were transfected with a *Bcl2a1* promoter luciferase expression vector, comprising different length of the *Bcl2a1* promoter, and a Blimp-1 overexpression vector. We noticed that overexpression of Blimp-1 resulted in a strong reduction of *Bcl2a1*-driven luciferase activity, which was already effective at the very proximal 79 nucleotides (Figure 31 A). The *Bcl2a1* proximal promoter-regulated reporter construct contained three consensus Blimp-1 binding sites. Accordingly, we mutated the putative Blimp-1 response elements individually and in conjunction as shown in Figure 31 B. We found that upon mutating one Blimp-1 binding site (-50), the activity of *Bcl2a1*-driven luciferase was dramatically increased in spite of the presence of Blimp-1, while mutation of all three Blimp-1 sites almost completely abolished the suppressive ability of Blimp-1 (Figure 31 C). This means that Blimp-1 binds and represses *Bcl2a1* through response elements within the proximal *Bcl2a1* promoter.

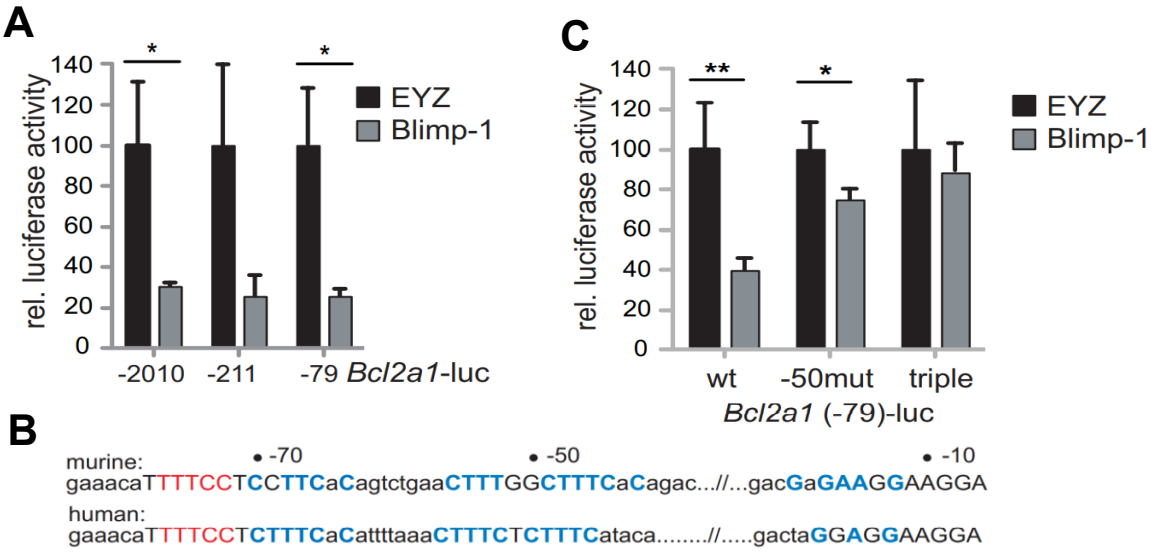

Figure 31: Blimp-1 represses the expression of Bcl2A1.

(A) The *Bcl2a1* promoter activity in response to Blimp-1 was evaluated after transfection with pEYZ/MCS or pEYZ/Blimp-1F along with the *Bcl2a1* promoter (length indicated)-driven luciferase reporter plasmids in 293T cells. After 36 h, luciferase activity was measured. Data are represented as the mean ± SE. Statistical analysis was performed by Student's t-test; *, $p < 0.05$. (B) The binding site for Blimp1 and NFAT on the proximal *Bcl2a1* promoter. The consensus nucleotides for Blimp-1 binding are in blue and for NFAT in red. (C) *Bcl2a1* minimal promoter activity in 293T depending on Blimp-1. pEYZ/MCS or pEYZ/Blimp-1F was transiently co-transfected with a luciferase reporter construct driven by an intact *Bcl2a1* promoter (WT), singly mutated for the −50 site (−50mut) or a variant in which all three Blimp sites had been erased (triple). After 36 h, luciferase activity was measured. Data are represented as the mean ± SE. Statistical analysis was performed by Student's t-test; *, $p < 0.05$; **, $p < 0.01$. [Figure 31 was performed by Subrahmanya D. Vallabhapurapu].

Overall, these results can be interpreted as such: NFATc1 binds and transactivates *Bcl2a1*, whereas Blimp-1 binds and represses its expression. This parallels the regulation of *Il2*. NFATc1, not modified by SUMO1 or devoid of the long isoforms, elevates the level of IL-2, which subsequently leads to enhanced STAT5 phosphorylation among other events causing enforced Blimp-1 expression. Blimp-1 in turn down-regulates the expression of Bcl2A1 and IL-2, thereby making the IL-2^{hi} Bcl2A1^{hi} period a transient event.

8.2 Part II

For translational reasons, we would like to investigate fine-tuned NFATc1 expression in humans. Since NFATc1 is highly expressed in human and mouse T-follicular cells [122, 123, 148], regulation in the germinal center response promises to be interesting. In mice with NFATc1-deficient T cells, the GC reaction was dramatically augmented by reduced T_{FR}. The reason for less T_{FR} is due to impaired upregulation of CXCR5 on T_{FR} cells in NFATc1-deficient mice [122]. We additionally demonstrated that both T_{FR} and T_{FH} cells were not only express especially robust NFATc1, but this predominantly as NFATc1/αA [123]. Since NFATc1 SUMOylation has strong effects on the effector function of Th1 and Th17 cells, we are also interested in the outcome of NFATC1 SUMOylation as well as long versus short isoform expression in human T cells including T_{FR} and T_{FH} cells. Of note, T_{FR} cells depend on IL-2 like other Tregs, but T_{FH} cells are inhibited by IL-2. Eventually, we hope to better understand the function of NFATc1 SUMOylation or the predominance of NFATc1/αA for the regulation of the GC reaction.

However, it is difficult to investigate the GC reaction in humans. Yet it is easier for us to get tonsil samples from surgery of patients with tonsillitis or hyperplasia. Tonsils are one kind of secondary lymphoid organ that contains all the cell types involved in adaptive immunity and all components for the GC response, the latter especially when they are resected upon recurrent infections. Thus, they allow us to rebuild the GC response *in vitro*. Up to now, many *in-vitro* culture systems rely on isolated B cells or slices of tissues to prepare explant culture. Unfortunately, these *in-vitro* culture systems either do not contain the whole tonsillar cell composition or cellular populations only can survive for 3-4 d. Therefore, we urgently need an optimized *in-vitro* culture system of tonsil organoids.

2D-cell cultures have been widely used since the early 1900s. However, they have many limitations as they only exist in two dimensions. For example, since 2D cultures cannot represent real cell environments, the cell morphology and functions might also be different [149, 150]. These disadvantages led to varying approaches for an establishment of three-dimensional (3D) cultures, which are more closely able to mimic conditions *in vivo*, something highly demanding. To be able to assess the regulation of and by human T-follicular cells, we also focused on the development of human tonsil organoid culture in 3D.

8.2.1 Optimizing the concentration of collagen gel

The concentration of collagen will cause a difference in stiffness, indirectly affecting the survival of cells. To find the best concentration of collagen gel for human tonsil cells in 3D culture, we checked total number of $CD19^+$ B cells after 6 d of culturing with different concentrations of collagen gel. As shown in Figure 32, the total number of $CD19^+$ B cells was increased by the

reduced concentration of collagen gel. These effects could be observed in both donors and were dose-dependent. When human tonsil cells cultured with 1 mg/ml of collagen gel, total number of $CD19^+$ B cells was dramatically increased over higher concentrations. If the concentration of collagen gel was reduced below 1 mg/ml, it became difficult to solidify. Therefore, in the following experiments, we chose 1 mg/ml of collagen gel as the best concentration for 3D culture.

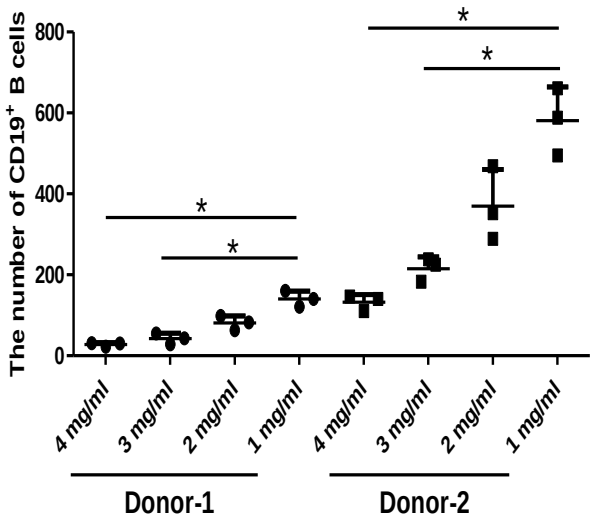

Figure 32: 1 mg/ml of collagen gel improves cell survival.

Total number of $CD19^+$ B cells was measured by flow cytometry; the cells were collected on day 6 after tonsil organoids cultured with different concentrations of collagen gel. Statistical analysis was performed by unpaired T test. *, $p < 0.05$.

8.2.2 The generation of hBAFF or/and hCD40L exogenously expressing cell lines

Many studies added feeder cell lines expressing BAFF and CD40L into the culture system to generate GC-B cells *in vitro* with both mouse and human naïve B cells [151-154]. The interaction between CD40L, normally on T_{FH} cells, and CD40 on B cells is important for receiving help *in vivo* and clonal expansion of GC-B cells *ex vivo* [155, 156]. BAFF, also named Blys, belongs to the TNF superfamily and was initially characterized as an important factor responsible for the survival and maturation of B cells [157-159]. BAFF can bind to several receptors, such as transmembrane activator and CAML interactor (TACI), BAFF receptor (BAFF-R), and B-cell maturation antigen (BCMA) [160, 161]. BCMA has been reported to enhance the function of B cells and promote the survival of long-lived plasma cells (LLPCs) in mouse BM [162]. However, the BAFF-R seems to be especially essential for the survival of mature B cells [161, 163]. Thus, we generated three cell lines: 293T cell line overexpressing hCD40L and hBAFF (named 293T-BAFF-CD40L), 293T cell lines overexpressing hBAFF or hCD40L (named 293T-BAFF and 293T-CD40L, respectively).

For the generation of 293T-CD40L, 293T-BAFF, and 293T-BAFF-CD40L cell lines, two pairs of primers, which included the restriction enzyme sites *Xball* and *Sall*, were designed to clone

hCD40L gene (786 bp) and hBAFF (858 bp) from human tonsillar RNA. Separation of the PCR products on agarose gels showed the correct size of the amplified DNA fragments (Figure S5). The sequence of the amplified hCD40L and hBAFF gene was confirmed by sequencing, data was not shown. A transfer plasmid was provided by Dr. Bin Cai from China, the plasmid map is given in Figure S6. The amplified BAFF and CD40L DNA fragments were inserted into the transfer plasmid by the usage of *XbaII* and *SalI* restriction enzymes to reconstruct two new plasmids, and the reconstructed plasmids were confirmed by restriction enzyme digestion. As shown in Figure 33 A, we picked four clones for hCD40L, all of them showed the correct fragment size after digestion (786 bp), while clones 2 and 4 in Figure 33 B showed the correct fragment size for the hBAFF gene.

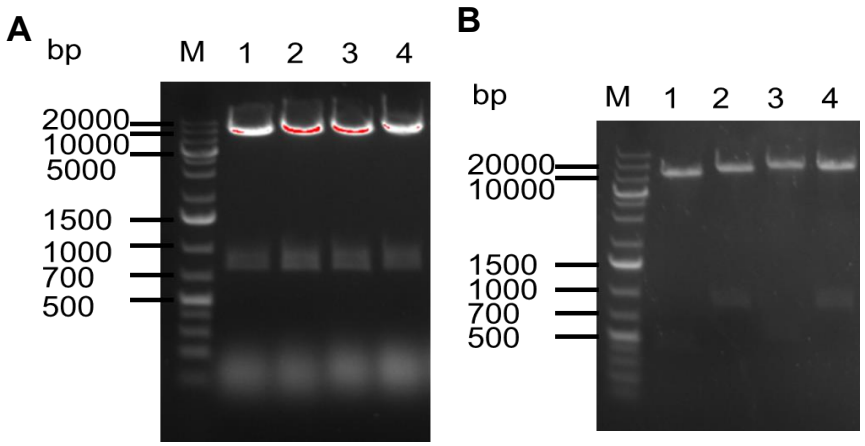

Figure 33: The enzyme validation of clones transformed with constructed hCD40L and hBAFF plasmids.

Gel electrophoresis of PCR product-encoding clones after digested with *XbaII* and *SalI* restriction enzymes for hCD40L plasmid (A) and hBAFF plasmid (B). M: 1kb DNA ladder.

We generated lentivirus particles expressing hBAFF and hCD40L according to the protocol, then infected 293T cells to generate cell lines, which exogenously expressed hCD40L and hBAFF separately. The overexpression of both molecules was confirmed by flow cytometry. As shown in Figure 34, the expression of hCD40L and hBAFF was quite low, wherefore we cultured these two cell lines in the presence of 1 µg/ml of puromycin to enrich the expression.

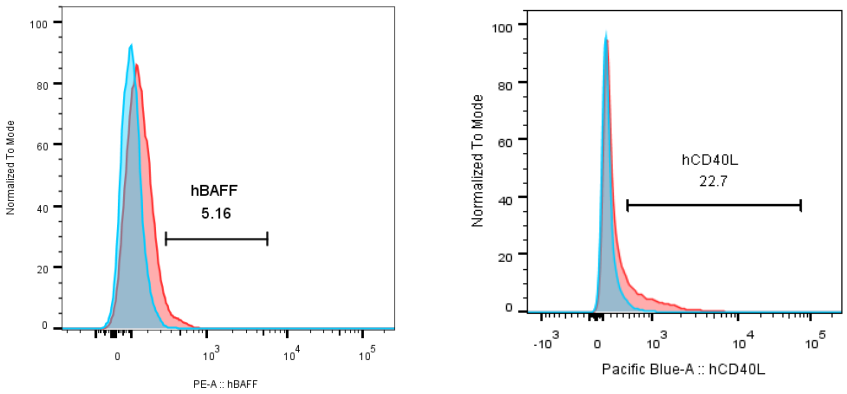

Figure 34: The expression of BAFF and CD40L on 293T cells.

Representative histograms of 293T-BAFF cell line (A) and 293T-CD40L cell line (B) were detected by flow cytometry, blue colour indicates negative control.

As shown in Figure 35 A, now more than 90% of cells were highly expressing CD40L and BAFF. For the generation of feeder cells, we used lentiviral particles containing hBAFF to super-infect 293T cells, and the cells were sorted by flow cytometry. In the end, we generated feeder cells that expressed both hBAFF and hCD40L (Figure 35 B).

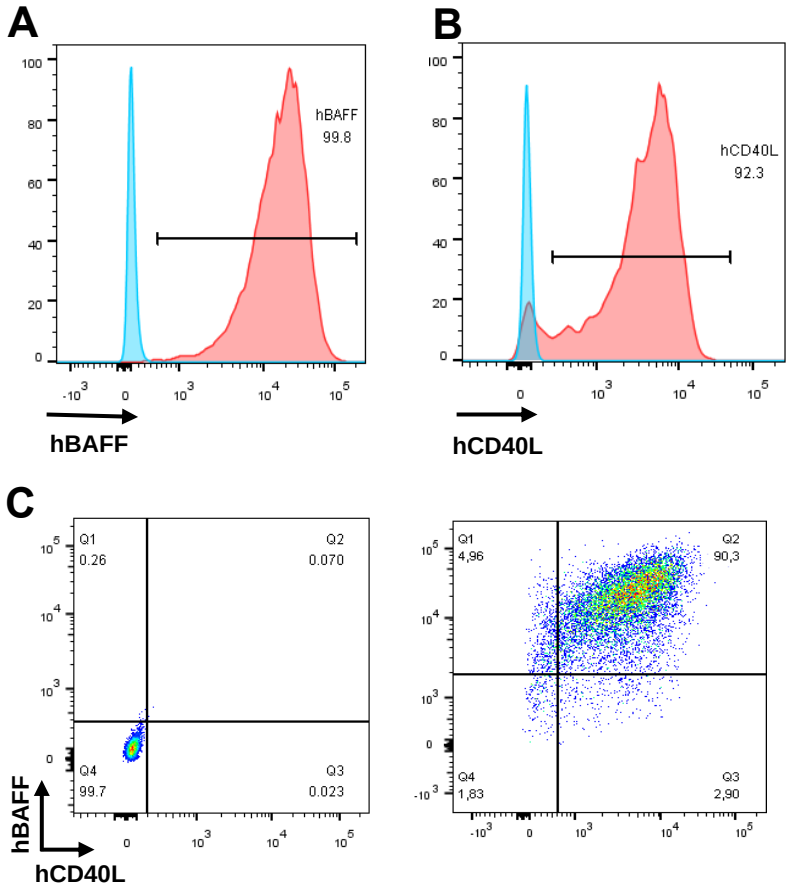

Figure 35: The generation of 293T-BAFF-CD40L, 293T-BAFF and 293T-CD40L cell lines.

(A+B) Representative histograms of 293T-BAFF cell line (A) and 293T-CD40L cell line (B) were detected by flow cytometry, blue colour indicates negative control (C) Representative flow cytometric plots for negative control and 293T-BAFF-CD40L cells line.

To investigate the best ratio of 293T-BAFF-CD40L cells (called feeder cells hereafter) for co-cultures with tonsil cells, we cultivated 4 x 10^4 tonsil cells together with different numbers of feeder cells for 6 days. Then the number of $CD19^+$ B cells was measured by flow cytometry determining the best ratio of feeder cells. As shown in Figure 36, the number of $CD19^+$ B cells was significantly increased with 10^4 feeder cells, while no improvement could be observed with less than 10^4 feeder cells. The number of $CD19^+$ B cells was further – although slightly – increased with 4 x 10^4 feeder cells. However, if co-cultured with more than 4 x 10^4 feeder cells, this ratio reduced $CD19^+$ B cell numbers below the outcome with 10^4 cells. These results indicated that co-culture with 4 x 10^4 feeder cells was the best condition for tonsil cells. Higher number of feeder cells might occupy too many spaces, resulting in inhibition of survival and proliferation of the $CD19^+$ B cells.

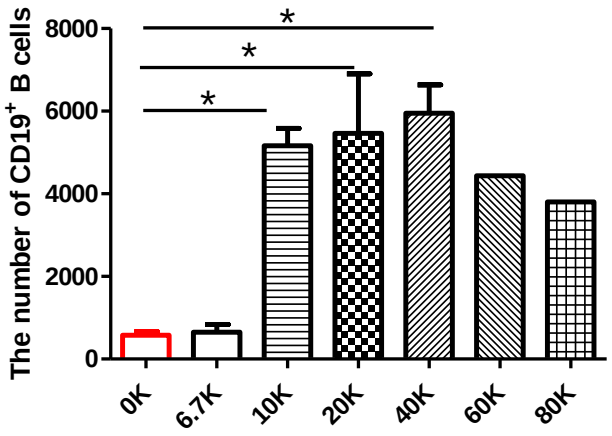

Figure 36: Certain amount of feeder cells promotes the growth of B cells.

Total number of $CD19^+$ B cells in human tonsil organoids was measured by flow cytometry, the tonsil cells were cultured with different numbers of feeder cells for 6 days. Statistical analysis was performed by Student's t-test. *, $p < 0.05$.

The expression of costimulatory molecules is tightly correlated with the function of APCs, which directly affect the stimulation of T cells. Therefore, the costimulatory molecules on B cells were analyzed by flow cytometry on tonsil organoids. We observed that the expression of CD86 and especially of CD80 was clearly enhanced on B cells which had been co-cultured with 293T-hCD40L or with feeder cells (Figure 37 A, B and C). Moreover, not only the percentage of CD80 and CD86 was heightened, but also the absolute numbers of $CD80^+$ B cells and $CD86^+$ B cells were increased (Figure 37 D and E).

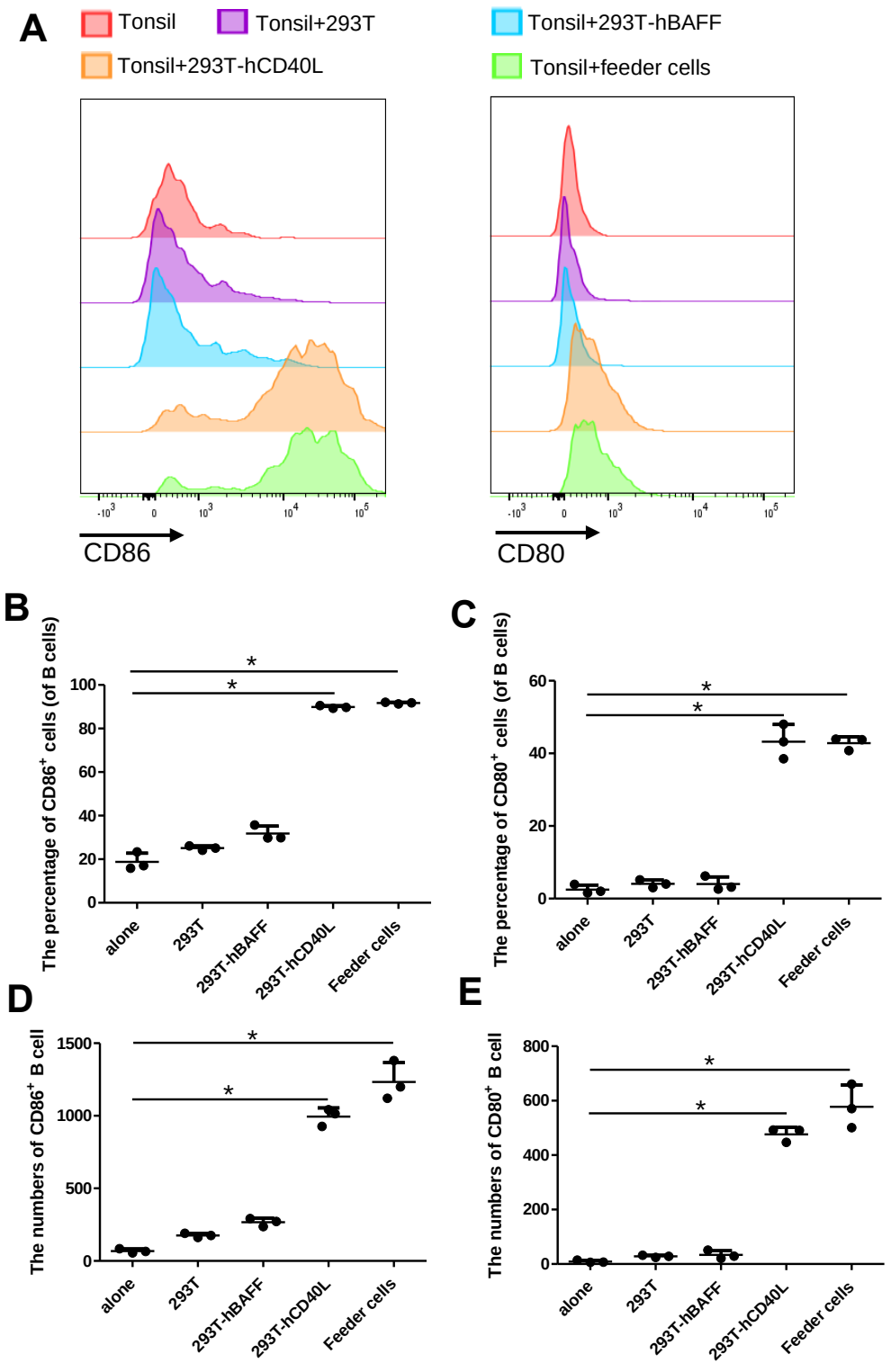

Figure 37: 293T-CD40L and feeder cells can upregulate the expression of CD80 and CD86 on B cells.

(A) Representative histograms showed surface expression of CD80 and CD86 on $CD19^+$ B cells in tonsil organoids, which were co-cultured with 293T, 293T-hBAFF, 293T-hCD40L and feeder cells for 6 days. (B+C) Summary of the percentage of $CD86^+$ (B) and $CD80^+$ B cells (C). (D+E) Summary of absolute numbers of $CD86^+$ B cells (D) and $CD80^+$ B cells (C). Values are displayed as means ± SD. n=3 in each group. Statistical analysis was performed by unpaired T test. *, $p < 0.05$.

CD40L and BAFF play a crucial role in the survival and differentiation on B cells. Thus, we wanted to monitor the number of different B-cell subsets in the human tonsil organoids to understand the effect and function of CD40L and BAFF signal pathways on B cells here. For this reason, we measured the total number of different B-cell subsets by flow cytometry after 6 days of tonsil organoid culture, including total $CD19^+$ B cells, naïve B cells, pre-GC-B cells, GC-B cells, plasmablasts, and memory cells. As shown in Figure 38 A, $CD19^+$ B cells were enriched in the tonsil organoids in the presence of 293T-BAFF cells, while the number of $CD19^+$ B cells was even enlarged in the presence of feeder cells or 293T-CD40L cells. These results were consistent with previous studies that BAFF and CD40L can promote the survival and proliferation of B cells [153, 164].

When we analyzed more deeply to check the number of specific B-cell subsets, we found that with 293T-CD40L cells, naïve B cells in the tonsil organoids were prone to differentiated into pre-GC-B and GC-B cells, in the end, enhancing the generation of plasmablasts (Figure 38 B, C, D and E). However, B cells seemed to be quiescent in the presence of 293T-BAFF, but 293T-BAFF cells also supported the survival of memory cells (Figure 38 B and F). The feeder cells had a similar effect on B cells as the 293T-CD40L cells by provoking differentiation towards pre-GC-B and GC-B cells. The number of plasmablasts was also higher with feeder cells, but less than the ones with 293T-CD40L cells (Figure 38 E).

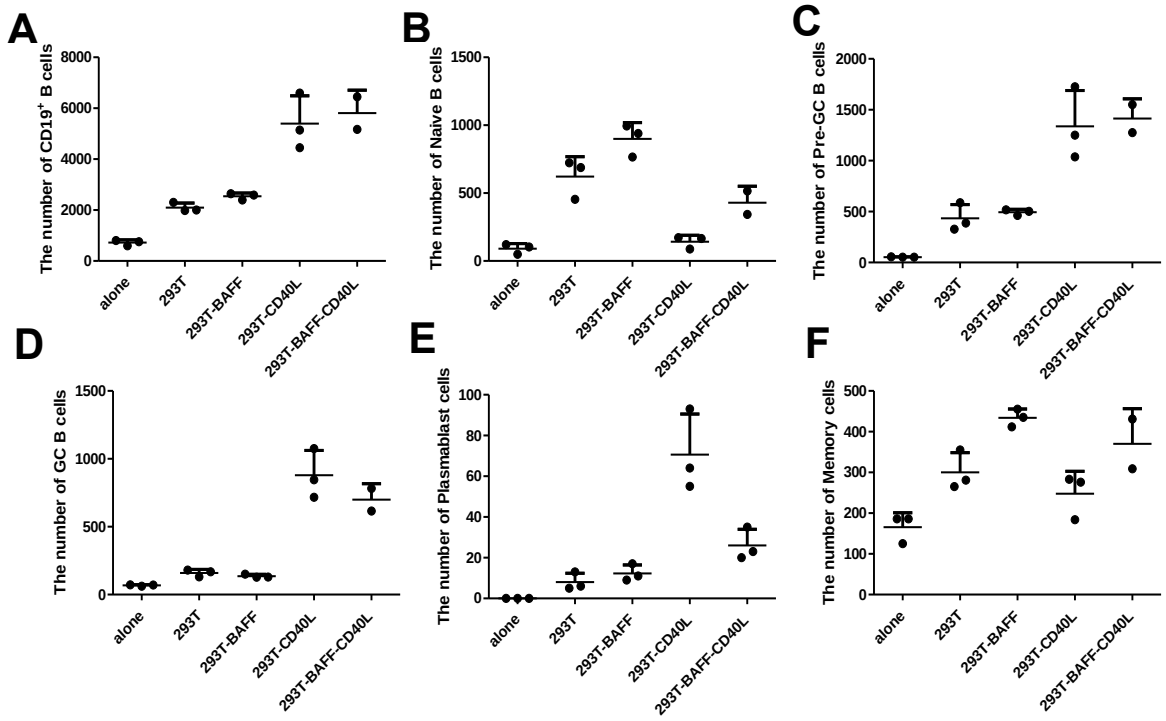

Figure 38: The co-culture with feeder cells enhanced the differentiation of plasmablasts.

(A-F) The total number of $CD19^+$ B cells (A), naïve B cells (B), pre-GC-B cells (C), GC-B cells (D), plasmablasts (E) and memory B cells (F) in tonsil organoids were detected by flow cytometry; tonsil cells were measured on day 6 after being cultured in the absence of presence of 293T, 293T-hBAFF, 293T-hCD40L or feeder cells.

8.2.3 Optimizing cytokine additions for 3D tonsil organoids

Also cytokines are extremely important for the proliferation and differentiation of B cells. IL-4 has been used for promoting the proliferation and differentiation in the presence of CD40 stimulatory signal pathway *in vitro* [165]. IL-7 is known to be one of the T-cell survival cytokines and it can even induce low-level proliferation of naïve T cell [166, 167]. Although there are also other cytokines, which are important for B-cell differentiation, basically, we would like to add cytokines as less as possible to the culture system to avoid an overriding of the *in vitro* GC response. Therefore, we only tried different concentrations of IL-4 and IL-7 during the tonsil organoids culture. The effects of cytokines were determined by checking different T-cell subsets and B-cell subsets.

As shown in Figure 39, the overall number of $CD19^+$ B cells was significantly higher in the tonsil organoids upon the addition of IL-4, when compared to no extra cytokines. This notion extended to supported numbers of naïve B cells, GC-B cells and memory cells. Moreover, with the lowest concentration of IL-4 at 1 µg/ml, it already led to an almost saturated effect. The IL-4 effect on the number of naïve B cells was consistent with the study of Wagner *et al.* [168]. They claimed IL-4 can prevent naïve B cells from apoptosis when B cells lack activation, due to the fact that resting naïve B cells express higher amount of the IL-4 receptor α chain.

However, no effect of IL-7 on B cells could be detected. Thus, the effect of cytokines in combination was similar to the culture with IL-4 alone.

In addition to B-cell subsets, we also detected the total number of different T-cell subsets in tonsil organoids after 6 days of culturing. Vella *et al*. have reported that IL-4 also can prevent T cells from apoptosis [169]. Unfortunately, the effect of IL-4 on the survival of T cells was almost invisible, in both $CD3^+$ T cells, $CD4^+$ T cells and $CD8^+$ T cells (Figure 40 A, B and C). However, the number of all T-cell subsets which were detected in this experiment was significantly increased in the presence of IL-7 (Figure 40). Seo *et al*. have demonstrated that IL-7 is essential for the development of T_{FH} cells in mouse [170]. Here, we observed that the number of human T_{FH} cells was also enhanced by IL-7, particularly, the number of T_{FH} cells expressing CD40L were augmented (Figure 40 E and F). Surprisingly, the T-cell subsets seemed to be slightly reduced under the combination with higher concentration of IL-4 and IL-7 (Figure 40). These results indicate that 1 µg/ml of IL-4 and 1 µg/ml of IL-7 is the best condition for culturing tonsil organoids *in vitro*.

In summary, our 3D-*in-vitro* culture system for tonsil organoids shows that the numbers of B cells and memory cells were significantly increased in the presence of feeder cells, IL-4 and IL-7. All in all, this indicates that our 3D-culture system could be used as a promising platform to study human germinal center reactions.

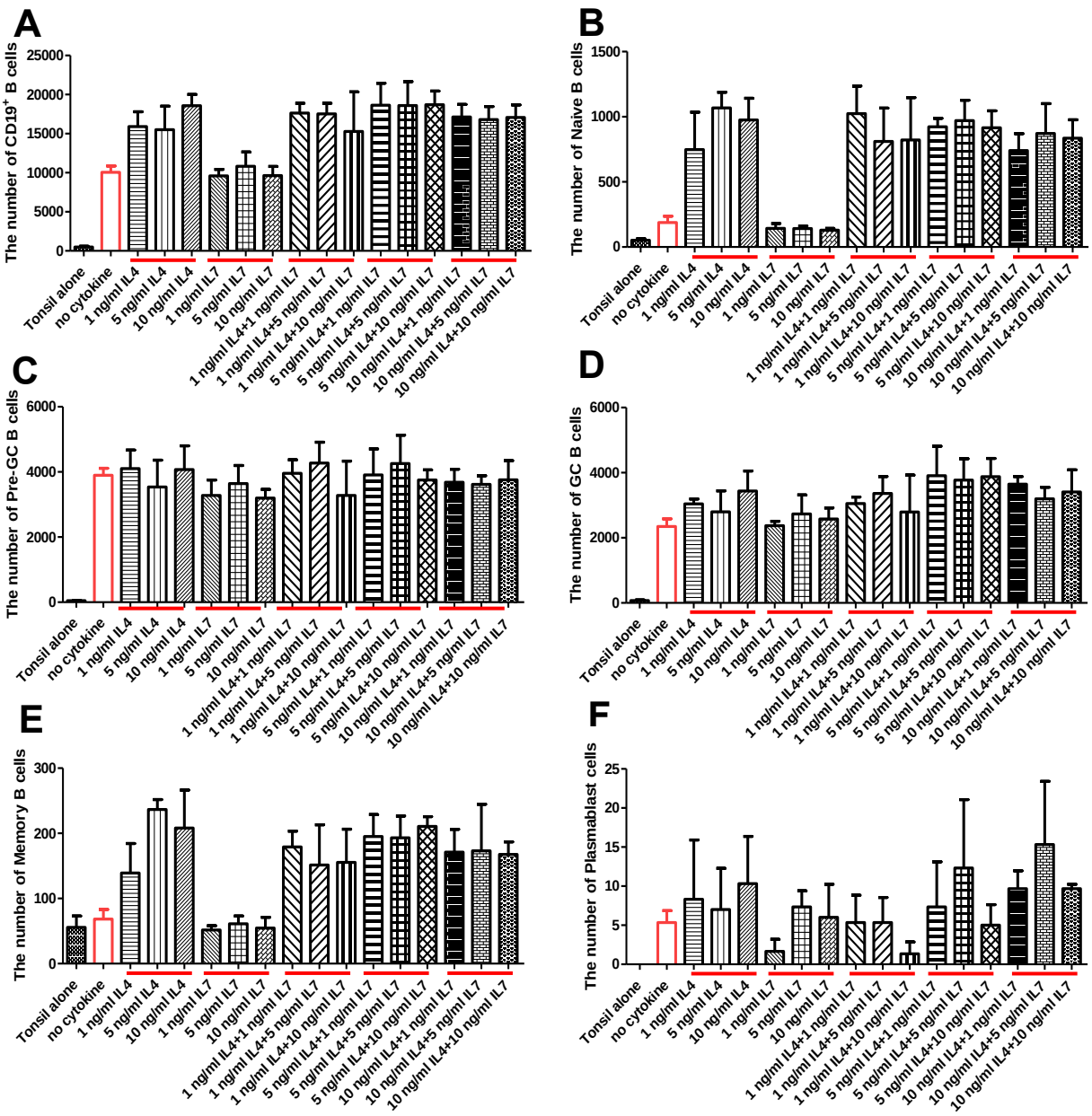

Figure 39: IL-4 can increase the proliferation and survival of B cells in the presence of feeder cells.

(A-F) The total number of CD19$^+$ B cells (A), naïve B cells (B), pre-GC-B cells (C), GC-B cells (D), memory B cells (E) and plasmablasts (F) in tonsil organoids was detected by flow cytometry, tonsil cells were culture with feeder cells in all conditions except for tonsil alone and were measured on day 6.

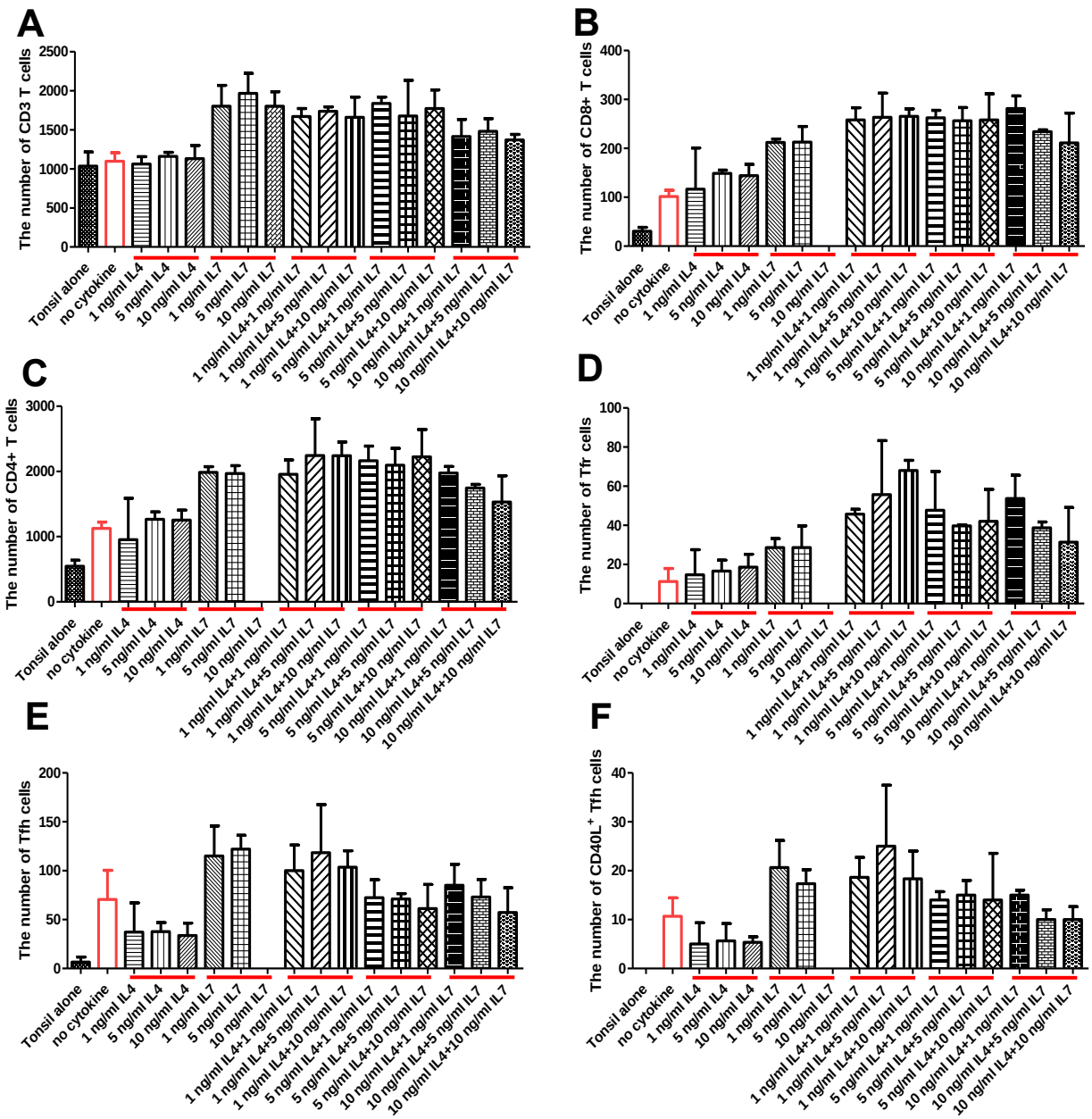

Figure 40: IL-7 helps to keep different subsets of T cells.

(A-F) The total number of $CD3^+$ T cells (A), $CD8^+$ T cells (B), $CD4^+$ T cells (C), T_{FR} cells (D), T_{FH} cells (E) and $CD40L^+$ T_{FH} cells (F) in tonsil organoids were detected by flow cytometry; tonsil cells were cultured with feeder cells in all conditions except for tonsil alone and were measured on day 6.

8.2.4 Responding to real antigens in tonsil organoids

Next, we investigated whether tonsil organoids could respond to real antigens and induce a germinal center reaction. We stimulated tonsil organoids with a CMV-peptide pool or peptides from Covid-19 spike protein (called SP peptides hereafter)**.** For the normal germinal center reaction, T cells are activated by DCs, and then T cells move to the T-B board in order to contact B cells. Afterwards, B cells will receive costimulatory signals and cytokines from T cells and further undergo proliferation and differentiation. To mimic the nature of a germinal center

reaction, in which B cells get into close contact with T cells, we decided to exclude feeder cells in the following experiments. We tested the CMV-peptide pool or Covid-19 SP peptides on two different donors and kept the same tonsil cell numbers as before (4 x 10^4 cells/well). We determined different B-cell subsets after stimulation by flow cytometry. As shown in Figure 41, too less cells could be detected for almost all subsets of B cells, especially GC-B cells and plasmablasts. When we observed the organoids under the microscope, this also revealed that the density of cells was quite low without feeder cells. There was no difference in each subset of B cells in the presence of antigens due to the lack of cells and cell communications. Thus, we needed to increase the density of tonsil cells in each organoid.

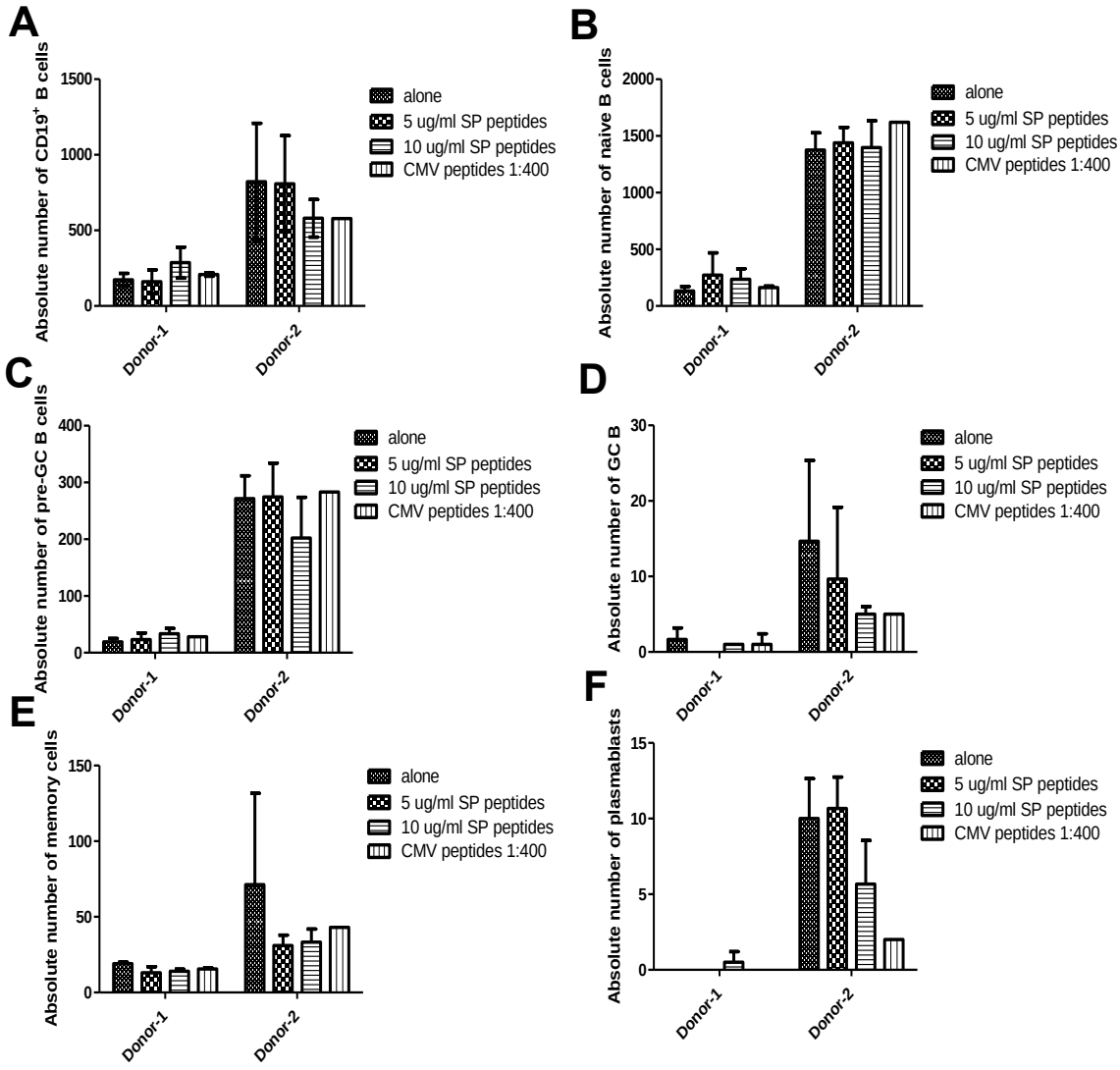

Figure 41: The density of tonsil cells in the organoid was not sufficient in the absence of feeder cells.

(A-F) The total number of CD19$^+$ B cells (A), naïve B cells (B), pre-GC-B cells (C), GC-B cells (D), memory B cells (E) and plasmablasts (F) in tonsil organoids was detected by flow cytometry, tonsil cells were culture with or without antigens (5 µg/ml SP peptides, 10 µg/ml SP peptides or CMV peptides 1:400) and cells were measured on day 6.

To improve the density of tonsil cells in 3D organoids, we increased the cell concentration and repeated the same experiments with two different donors. Again, there were almost no changes to be observed in all the subsets of B cells with the concentration of 1 x 10^5 cells (Figure 42). However, the absolute number of $CD19^+$ B cells and naïve B cells showed a tendency to accumulate, and pre-GC B and memory cells are significantly increased in the presence of 10 µg/ml SP peptides with the concentration of 2 x 10^5 cells. Moreover, the memory cells were also enhanced in the presence of CMV peptides. Interestingly, we also checked another donor, who showed different results (Figure 43). Specifically, the memory cells were not increased, but the plasmablasts were augemented in the presence of 5 µg/ml SP peptides in the second donor. A germinal center reaction was not induced by CMV peptides.

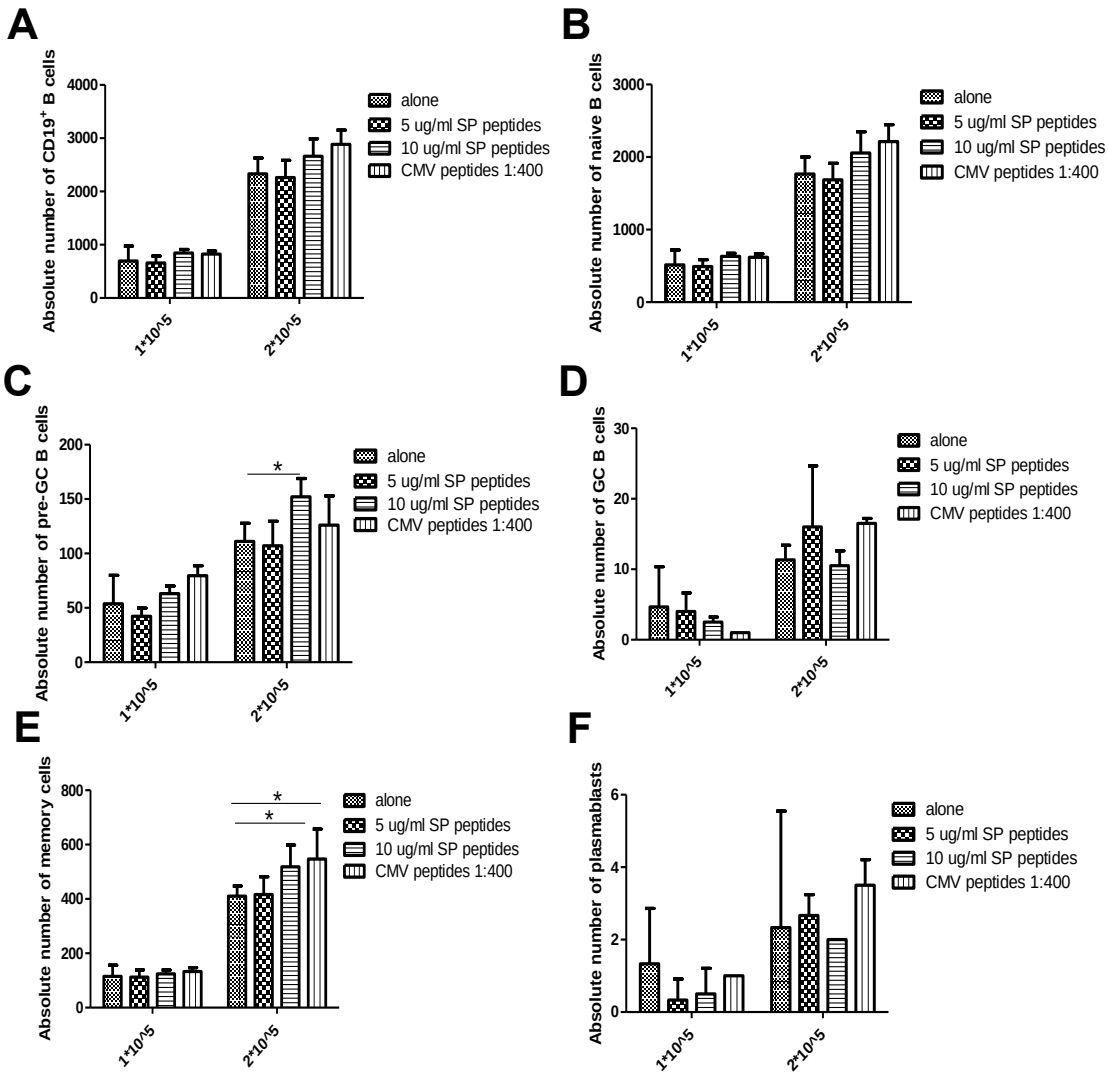

Figure 42: SP peptides or CMV peptides could increase memory cells in 3D culture.

(A-F) The total number of $CD19^+$ B cells (A), naïve B cells (B), pre-GC-B cells (C), GC-B cells (D), memory B cells (E) and plasmablasts (F) in tonsil organoids was detected by flow cytometry, tonsil cells were culture with or without antigens (5 µg/ml SP peptides, 10 µg/ml SP peptides or CMV peptides 1:400) in different cell numbers and the cells were measured on day 6. Values are displayed as means ± SD. Statistical analysis was performed by unpaired T test (one-tail), *, $p < 0.05$.

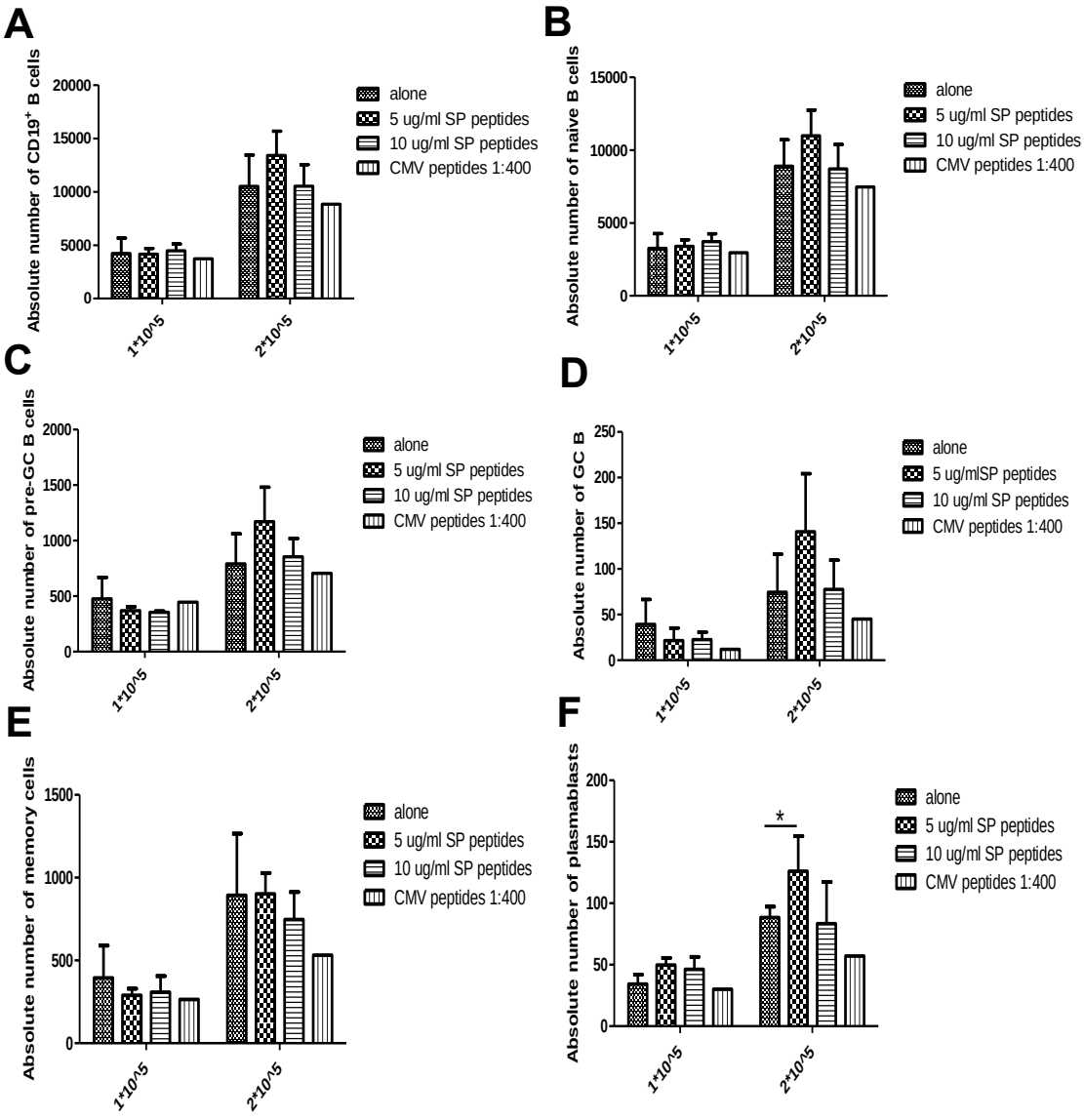

Figure 43: SP peptides could increase plasmablasts in another donor in 3D culture.

(A-F) The total number of CD19$^+$ B cells (A), naïve B cells (B), pre-GC-B cells (C), GC-B cells (D), memory B cells (E) and plasmablasts (F) in tonsil organoids was detected by flow cytometry, tonsil cells were cultured with or without antigens (5 µg/ml SP peptides, 10 µg/ml SP peptides or CMV peptides 1:400) in different cell numbers and the cells were measured on day 6. Values are displayed as means ± SD. Statistical analysis was performed by unpaired T test (one-tail), *, $p < 0.05$.

We also wondered whether tonsil organoids cultured in 3D were indeed better compared to 2D. For this reason, we directly compared tonsil organoids cultured in 3D collagen gel to 2D. As shown in Figure 44, we could see that all subsets of B cells were significantly higher in 2D culture. Since 3D organoids had no advantages over 2D cultures, we also wanted to know whether the results from 3D organoids would hold true for 2D cultures. To figure out this question, we stimulated tonsil cells with the same antigens in 2D culture from the same donors that we did for 3D culture. As shown in Figure 45 and Figure 46, we could see the same tendency as showed for 3D organoids, i.e., memory B cells were significantly enhanced by SP

peptides in the first donor tonsil cells, and plasmablasts were significantly enlarged in the second donor. All in all, the well-established 3D-culture system, could be reproduced with similar results in 2D cultures. Although the total numbers were much less than that in 2D culture. Still, it indicates that this *in vitro* culture system has its limitation, while being usable for studies of the human germinal center reaction.

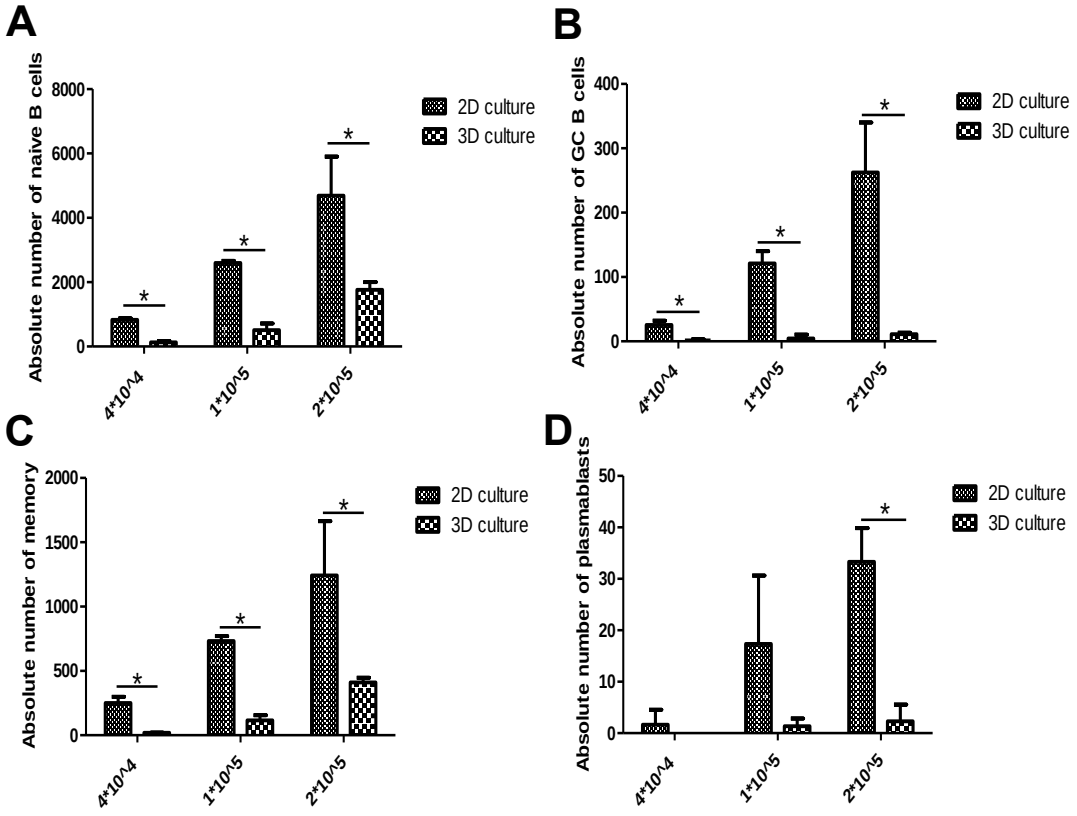

Figure 44: Tonsil organoids survived better without collagen gel.

(A-D) The total number of naïve B cells (A), GC-B cells (B), memory B cells (C) and plasmablasts (D) in tonsil organoids was detected by flow cytometry, tonsil cells were cultured with different cell numbers with (3D) or without collagen gel (2D) and the cells were measured on day 6. Values are displayed as means ± SD. Statistical analysis was performed by unpaired T test (one-tail), *, $p < 0.05$.

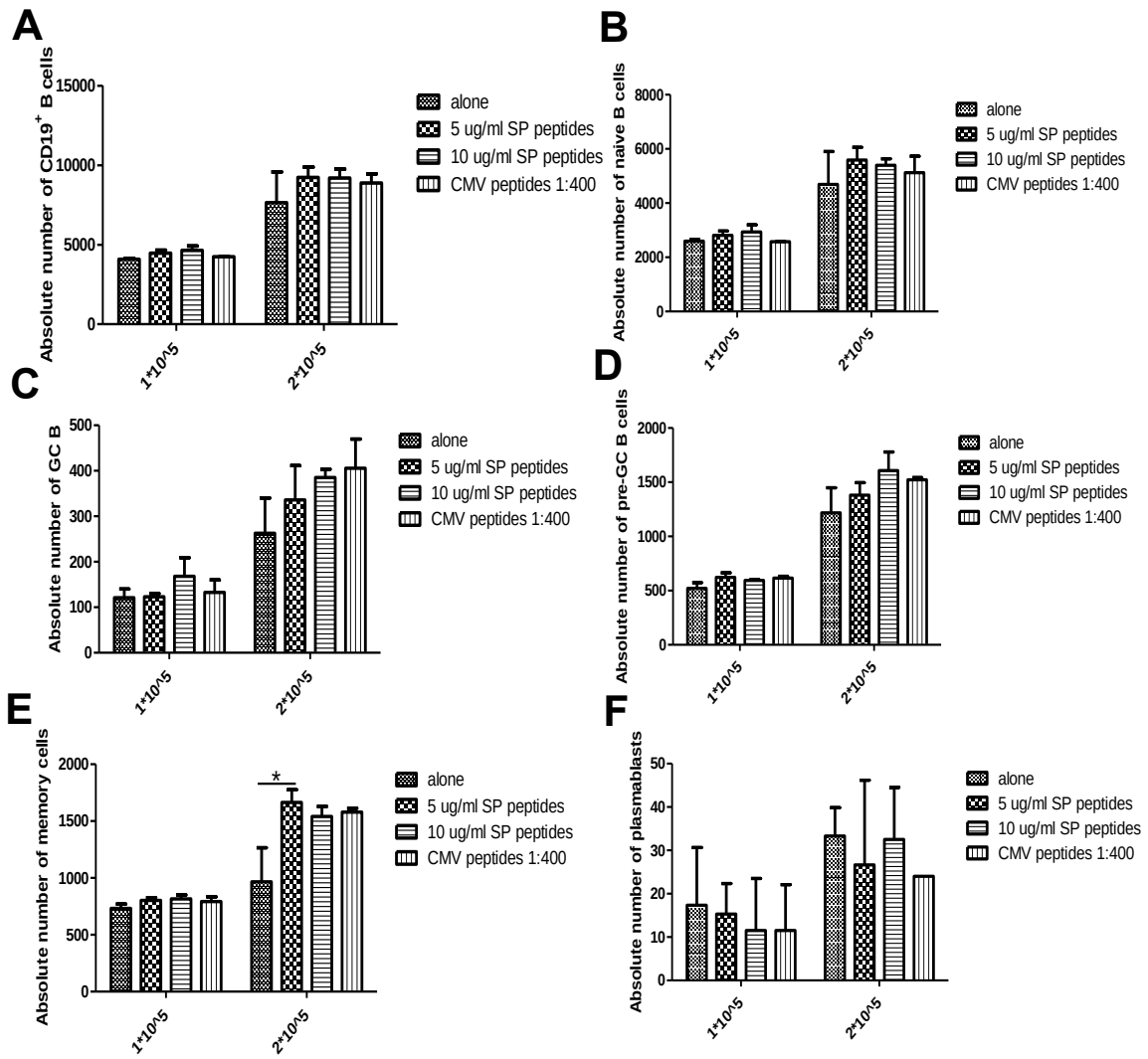

Figure 45: SP peptides could increase memory cells in 2D culture.

(A-F) The total number of CD19$^+$ B cells (A), naïve B cells (B), pre-GC-B cells (C), GC-B cells (D), memory B cells (E) and plasmablasts (F) in tonsil organoids was detected by flow cytometry, tonsil cells were cultured with or without antigens (5 µg/ml SP peptides, 10 µg/ml SP peptides or CMV peptides 1:400) in different cell numbers in the absence of collagen gel and the cells were measured on day 6. Values are displayed as means ± SD. Statistical analysis was performed by unpaired T test (one-tail), *, $p < 0.05$.

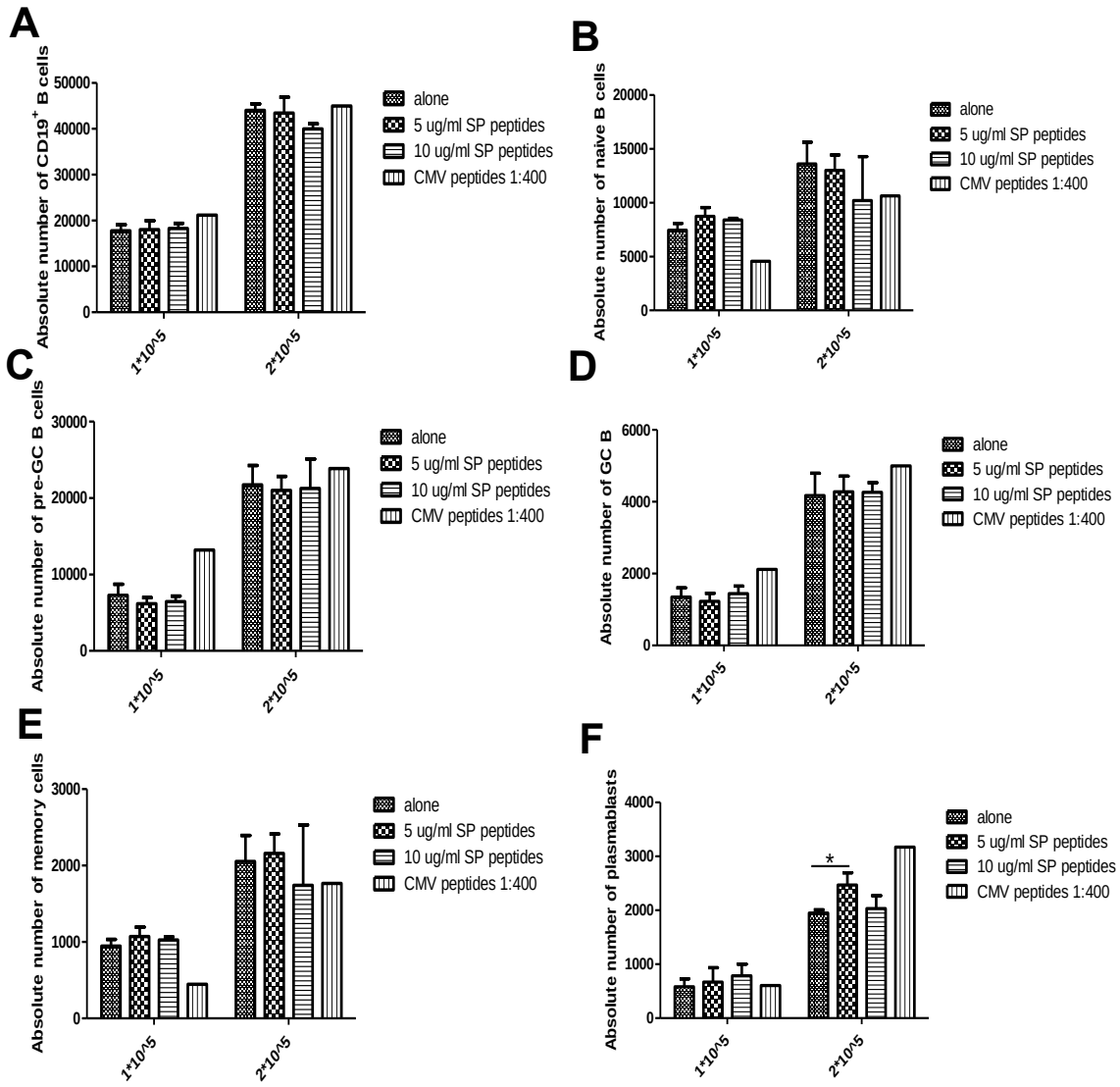

Figure 46: SP peptides could increase plasmablasts in another donor in 2D culture.

(A-F) The total number of CD19$^+$ B cells (A), naïve B cells (B), pre-GC B cells (C), GC-B cells (D), memory B cells (E) and plasmablasts (F) in tonsil organoids was detected by flow cytometry, tonsil cells were culture with or without antigens (5 µg/ml SP peptides, 10 µg/ml SP peptides or CMV peptides 1:400) in different cell numbers in the absence of collagen gel and the cells were measured on day 6. Values are displayed as means ± SD. Statistical analysis was performed by unpaired T test (one-tail), *, $p < 0.05$.

9 Discussion

9.1 Part I

Nuclear factor of activated T cell (NFAT) transcription factors play a central role in inducible gene transcription during the immune response [171-173]. NFATs were initially described as binding to the *Il2* promoter in activated T cells [117]. NFATc1 and NFATc2 are highly expressed in peripheral T cells and regulate their effector function. Different from other NFATs – as far as known, NFATc1 is transcribed by two distinctively different promoters: the inducible P1 and the constitutive P2, which encode the N-terminal peptides α and β, respectively. Together with the usage of alternative splicing and poly-A sites, it leads to different isoforms and regarding their C-terminus designated as short isoforms A and long isoforms B and C [93-95]. The function and structure of the short isoform NFATc1/αA are quite different from the other isoforms of NFATc1. For example, NFATc1/αA is expressed dominantly in effector T cells, and its synthesis is controlled by positive autoregulation and does not affect the expression of activation-induced cell death (AICD) in primary murine T cells, while the long isoform NFATc1/C – usually NFATc1/βC - behaves similarly to NFATc2 [96, 146]. The short isoform NFATc1/A lacks the long C-terminal peptide with two SUMOylation sites. In our previous study, we had found that NFATc1 has three SUMOylation sites, two SUMOylation sites specially located at lysine 702 and 914 in the C-terminus of long isoform C, and one common SUMOylation site at lysine 349 in the short isoform NFATc1/A. The SUMOylation site in the short isoform is an extremely weak SUMOylation site by itself, but depends on prior SUMOylation within the C-terminus [130]. At least *in vitro*, we could not reveal any functional difference in separated point mutation experiments. Therefore, the other SUMOylation sites at lysines 702 and 914 specific for the long isoform C are the most important sites for NFATc1/C SUMOylation, and mutation in either of those SUMOylation sites significantly reduced the overall SUMOylation pattern. Furthermore, transfections of SUMO-deficient or SUMO-NFATc1 fusion proteins revealed that SUMOylation of NFATc1/C inhibits the IL-2 expression [130].

In the present study, we went deeply to investigate the function of SUMOylation sites in the C-terminus of the long isoforms *in vivo*. For this purpose, we generated a transgenic mouse by point mutating the two SUMOylation sites K702 and K914 to arginines (K702R and K914R), and then examined the role of NFATc1 SUMOylation in T cell-mediated immune responses *in vivo*. Our flow cytometric data of stimulated T cells *in vitro* confirmed previous results that without SUMOylation in the C-terminal NFATc1 IL-2 expression is upregulated. Apart from more IL-2 expression, it also showed that T cells produce fewer IFN-γ, which was confirmed by differentiated Th1 and Th17 cells *in vitro*. Furthermore, under Th17 differentiation condition, T cells from NFATc1/ΔS^{+} mice produced more IL-2 but less IL-17A. Subsequently, we also found that elevated IL-2 can lead to a significant increase in the number of Tregs. Due to fewer

effector cytokines expression and higher number of Tregs in the NFATc1/ΔS$^+$ mice, SUMO-deficient NFATc1 might protect mice from autoimmune diseases and alloreactivity diseases. To tackle and finally confirm this hypothesis, we tested NFATc1/ΔS in two different disease models, namely EAE and aGvHD. In both independent mouse models, mice that received T cells from NFATc1/ΔS$^+$ mice had less severe disease.

IL-2 was initially described as a T-cell growth factor, which included the finding of IL-2 as a potent growth regulator of T cells *in vitro* [171-174]. Later on, people found that IL-2 can influence effector T-cell differentiation, which can determine different fates of CD4$^+$ T cells after activation by APCs. IL-2 can induce many transcription factors, such as Eomesodermin (Eomes) [175], T-bet (Tbx21) [176], and Blimp-1 [177] while suppressing BCL6 [178]. Moreover, IL-2 also can affect cytokine expression, such as the expression of IL-17A due to IL-2-mediated activation of STAT5, which attenuates IL-17A production by competing with STAT3 to directly bind at the *Il17a* promoter [132]. IL-2 is also thought to inhibit the formation of GC by directly suppressing the differentiation of T_{FH} cells via upregulating Blimp-1 expression, which is the repressor of Bcl6, a key transcription factor of T_{FH} cells [179, 180]. Thus, IL-2 can promote Th1 and Th2 differentiation [176, 181, 182], but inhibits the differentiation of Th17 cells [132, 183] and T_{FH} cells [180, 184]. Accordingly, in this study, T cells from NFATc1/ΔS$^+$ mice expressed higher amounts of IL-2 compared to the ones from WT mice but produced lesser IL-17A under Th17-skewed conditions. Confirming an IL-2-dependent mechanism, once blocked with anti–mIL-2 antibodies, the expression of IL-17A was recovered to the same level as in WT$^+$ T cells. Th17 cells have been characterized as one of the major pathogenic Th-cell populations for the development of many autoimmune diseases, especially for multiple sclerosis and in the EAE model. Duhen *et al.* reported that Th17 cells expressing GM-CSF and/or IFN-γ are highly enriched in MOG-specific T cells in the CNS and can induce disease independently of Th1 cells [185]. In previous studies, we challenged NFATc1/ΔS$^+$ mice by the induction of EAE with MOG, EAE-diseased NFATc1/ΔS$^+$ mice were less severely sick in comparison with EAE-diseased WT mice. To investigate the functional difference of WT and NFATc1/ΔS$^+$ Th1 and Th17 in an isolated manner, we applied a passive EAE mice model by transferring Th1 plus Th17-skewed cells *in vitro* from 2D2.WT and 2D2.NFATc1/ΔS$^+$ mice to *Rag1*$^{-/-}$ mice. Again, NFATc1/ΔS$^+$ T cells-transplanted mice caused fewer symptoms of EAE. Furthermore, the frequency of pathogenic Th1/17 cells, which co-expressed IFN-γ and IL-17A, was significantly reduced in the CNS of NFATc1/ΔS-transplanted mice.

In contrast to IL-2, which was elevated in mice with NFATc1/ΔS$^+$ T cells, IFN-γ was significantly reduced in Th1-skewed cells *in vitro*. This was also proven by T cells regained from induced aGvHD and passive EAE mouse models. As it has been already published [139], IFN-γ can

be repressed by Blimp-1, which itself is induced by STAT factors including STAT5, activated by IL-2. However, Blimp-1 in turn suppresses not only IFN-γ, but also IL-2 [139, 141, 186-188]. To investigate whether the reduced expression of IFN-γ was indirectly caused by elevated IL-2 in NFATc1/ΔS$^+$ mice, we measured Blimp-1 expression from both mRNA and protein level in NFATc1/ΔS$^+$ CD4$^+$ T cells regained from aGvHD-challenged mice. The results from western blot and qRT-PCR both showed higher amounts of Blimp1 in NFATc1/ΔS$^+$ CD4$^+$ T cells at both mRNA and protein levels. Moreover, we also monitored the kinetics of the expression of IFN-γ by flow cytometry in stimulated NFATc1/ΔS$^+$ and NFATc1/ΔBC$^+$ Th1-skewed cells, as well as the Th1-skewed cells from NFATc1/ΔBC$^+$ mice in the absence of *Prdm-1*. Theoretically, in *Prdm-1* knock-out mice, T cells should express higher amounts of IFN-γ and IL-2. We also have observed such results. Furthermore, once we blocked the elevated IL-2 with anti-mIL-2, these effects of reduced IL-2 and IFN-γ over time were lost. In line, Wang *et al.* reported that Th1 differentiation can be suppressed by Blimp-1 overexpression [189].

From RNA-sequencing data of CD4$^+$ CD90.1$^+$ T cells regained from aGvHD-induced mice, we noticed one gene of *Bcl2a1*, expressed in three genes (a, b, d) and the pseudogene c due to gene duplication in the mouse, which harbor two consensus NFAT sites within their promoters, to be significantly upregulated in NFATc1/ΔS$^+$ T cells. Our analysis of the expression of *Bcl2a1* by qRT-PCR in both Th1-skewed cells and the cells regained from aGvHD-induced mice also demonstrated the same result. Bcl2A1 is a prosurvival member of the Bcl2 family. To investigate whether Bcl2A1 can affect the survival of T cells, we applied the apoptosis staining on Th1-skewed cells. We found that enhanced Bcl2A1 alone did not affect cellular survival significantly, which is also consistent with other studies [190, 191].

We observed a higher percentage of iTregs to be induced from NFATc1/ΔS$^+$ T cells *in vitro* in the presence of TGF-β compared to the one from WT$^+$ T cells due to the elevated IL-2 produced by T cells. This result was confirmed by challenging the T cells from *in vivo*. For example, when we induced EAE in mice with MOG_{35-55} peptide, we could detect an increased population of Tregs in EAE-diseased NFATc1/ΔS$^+$ mice. Furthermore, transplanting Tcon only to provoke aGvHD, an amplified iTregs population could be detected upon NFATc1/ΔS$^+$ T-cell transfer. Thus, both iTregs and tTreg frequencies were supported by the surplus of IL-2, either by enhanced induction and / or by augmented maintenance and proliferation. To test the functional capacity of those Tregs, we applied a suppression assay *in vitro* and the suppressive ability to Tcon of NFATc1/ΔS$^+$ Tregs was similar to that of WT$^+$ Tregs. Moreover, NFATc1/ΔS$^+$ mice developed normally without any symptoms of autoimmune diseases, even-aged mice did not show any signs of inflammation. Ding *et al.* group had published that Tregs reduced many suppressor molecules when Ubc9, the only known SUMO-conjugating enzyme, is deficient specifically in Tregs. Without Ubc9 in Tregs and all SUMOylation processes blocked in Tregs,

mice indeed succumb with severe autoimmune disease [192]. Since multiple transcription factors cooperate with Foxp3 to establish or stabilize the Treg transcriptional program [193-195], the authors found that more than 30% NFAT-targeted genes were disturbed upon *Ubc9* deletion, indicating a major role of NFAT SUMOylation in Tregs. One difference to our model is that we exclusively prevented NFATc1 from SUMOylation. In agreement, we had found before that Tregs do not depend on a particular NFAT family member, but function well with reduced NFAT expression [196, 197]. Even more important might be the fact that in Ubc9-deficient Tregs IRF4-controlled genes had the most significant defect due to *Ubc9* depletion as around 67% of IRF4-dependent genes were downregulated. Therefore, IRF-4 could be considered the most important SUMO target in Tregs [198]. This also could indicate why the suppressive function of Tregs had not been worse in our NFATc1/ΔS$^+$ mice.

As said, in our previous studies, we have found that deletion of one or two NFAT proteins did not change the function of tTregs, pTregs, and iTregs [126, 199, 200]. Nevertheless, the homeostasis and function of Tregs depend on continuous TCR signaling, especially for effector Tregs. Upon TCR stimulation, driving several signaling cascades, NF-κB, NFAT, and IRF4 up-regulate Treg cells' signature molecules, such as CTLA-4, CD103, GITR, and TIGIT [201]. TIGIT is a co-inhibitory molecule that can inhibit T-cell responses by binding its ligand CD155 on DCs and thereby repressing IL-12 production while inducing the production of IL-10 [202]. In addition, TIGIT also directly inhibits the activation and proliferation of T cells [203-205]. Joller *et al.* characterized that TIGIT$^+$ Treg cells are an activated Treg subset with a high expression of Treg signature genes, specifically suppressing pro-inflammatory Th1 and Th17 cells, but not Th2 cell responses [206]. This notion supports our observation of enhanced expression of TIGIT on NFATc1/ΔS$^+$ Tregs and subsequent superior suppressiveness during criss-cross GvHD experiments, as well as amelioration of EAE.

All these data together lead us to consider whether SUMOylation on NFATc1 might be a new target for therapeutic intervention. And the outcome might resemble the treatment with low-dose IL-2, or monoclonal antibodies to IL-2 complex [207]. Tregs typically express high levels of the trimeric IL-2Rαβγ, whereas the dimeric IL-2Rβγ is expressed mostly on activated CD8$^+$ T cells and NK cells. The low-dose IL-2 therapy preferentially activates Tregs because of the constitutively high expression of IL-2Rα, whereas, mIL-2:anti–mIL-2 antibody JES6-1 complex blocks the IL-2/IL-2Rβ and IL-2/IL-2Rγ interactions, inducing a special activation of IL-2Rα^{hi} cells, i.e., preferentially expanded Treg cells [208]. Such therapeutic approaches aim to increase the number of Tregs while minimizing the generation of effector cells and other cells population to treat autoimmune diseases. Blocking the SUMOylation of NFATc1 or deletion of the long isoform of NFATc1 would have the same effect without any complexing of IL-2. This is an attractive idea for settings when T cells are transplanted anyhow like during allo-HCT,

giving the opportunity to manipulate T cells before transfer. That this is possible by CRISPR/Cas9 has been demonstrated by us for murine T cells at least [209], while for human studies we depend on elaborated *in* vitro cultures.

9.2 Part II

The GC is the place where B cells undergo rapid proliferation, affinity-based selection, and class switching, eventually differentiating into long-lived plasma cells and memory B cells. GC models have been established and widely used to study the differentiation of B cells in mice *in vitro* [151, 171, 174]. However, the establishment of human germinal center responses *in vitro* is a major challenge. Here, we aimed to set up an *in-vitro* culture system with primary human tonsil cells to mimic the GC response *in vivo*. Tonsils are easily accessible secondary lymphoid tissues in humans and contain all the cell subsets involved in adaptive immunity, especially those cell subsets absent from peripheral blood. We chose to focus on 3D culture instead of traditional 2D culture techniques to reflect the complex nature of the GC. Without Bcl2 expression and highly Fas-positive, GC-B cells are prone to apoptosis when cultured alone *in vitro* [172], which indicates that GC-B cells require a multicellular culture system to rescue their survival *in vitro*. For this purpose, a 3D-culture system is a suitable way to achieve it. Such systems have already been extensively explored for many organoid cultures derived from different human tissues [173, 175, 176]. Moreover, cells have different morphology in a 3D matrix compared to cultures in 2D [177]. We chose collagen I as the matrix to establish 3D tonsil organoids, as the collagen I is the most abundant natural material used for the fabrication of scaffolds for culturing different cell types. Furthermore, collagen scaffolds can promote the adhesion, proliferation, and differentiation of many types of cells [210]. With the matrix surrounding the cells, it inhibits the movement of cells and the diffusion of chemicals and nutrition to an extent closer to the environment *in vivo* [178, 181, 182]. Kuczek *et al*. reported that the density of the collagen matrix influences the surrounded T-cell response, especially for proliferation [183]. We observed a similar effect as the survival of T cells was better with a lower concentration of collagen gel, the best condition for tonsil organoid culture being cultures with 1 mg/ml of collagen gel.

In this study, to achieve the expansion and further differentiation of GC-B cells, we tried to co-culture tonsillar lymphocytes along with generated feeder cells which overexpressed hCD40L and hBAFF. The interaction between CD40 on B cells and CD40L on T cells can activate several downstream signaling pathways, such as PI3K, MAPK, PLCγ and NF-κB [180, 184], and provides survival signals to human GC-B cells [211]. BAFF is important for the regulation of selection, differentiation [186], and the survival of B cells [187, 188, 212]. Therefore, we introduced BAFF and hCD40L into the culture system. The ratio between feeder cells and tonsil cells might influence the growth of B cells. For this reason, we checked the percentage of B cells in total tonsil cells after co-cultured with different numbers of feeder cells, and we observed that it can increase the frequency of B cells co-cultured with feeder cells. However, once the number of feeder cells was more than 4 x 10^4 cells it inhibited the survival of B cells, which might be due to the limited space. In summary, the number of live B cells was

significantly increased once co-cultured with feeder cells, as well as co-cultured with 293T-BAFF cells. Therefore, our culture system provides an economic and efficient way to proliferate human B cells without adding commercial BAFF cytokine.

Adequate expression of costimulatory molecules has been closely associated with the function of APCs [190, 191]. Constitutive expression of MHC II and costimulatory molecules on GC-B cells enables them to act as potent APCs to activate $CD4^+$ T cells. In this study, after co-culture with feeder cells, B cells significantly increased the expression of co-stimulatory molecules, CD80 and CD86, even co-cultured with 293T-BAFF cells also slightly enhanced the expression of CD86 on B cells. These results were consistent with previous reports, which claimed that CD80 and CD86 can be induced via the interaction between BAFF and BCMA through NF-κB and JNK signaling pathways [198]. The GC-B cell can express B cell maturation Ag (BCMA) and BAFF-R, both molecules can bind to BAFF, whereas BAFF-provided survival effect on B cells is most likely achieved through an interaction with the BAFF-R [158, 193]. Then, the enhanced CD86 expression leads to a stronger stimulatory signal to T cells via interaction with CD28, resulting in the survival and proliferation of T cells [194, 195]. It was demonstrated by our results that the percentage of different T-cell subsets was increased upon co-culture with feeder cells. Robinson *et al.* found that BAFF plays a more important role in the survival of quiescent cells and mainly affects the accumulation of memory-like B cells during *in vitro* cultures with mouse naïve B cells, while CD40L together with IL-4 is more prone to generate GC-B cells *in vitro* [153], which is also consistent with our results on human B cells: when tonsils were co-culture with 293T-CD40L or feeder cells, we could detect more plasmablasts, however, when co-cultured only with 293T-hBAFF cells, we enhanced the generation of memory cells.

The exogenous cytokines added to the culture system play a distinct role on activated B cells, such as influencing the proliferation, survival, and differentiation of B cells. Co-cultured with feeder cells can significantly increase the proliferation of B cells, and it even enhanced the proliferation in the presence of IL-4. Meanwhile, we also observed that only stimulated with feeder cells, the number of plasmablasts was significantly increased. Interestingly, Ding *et al*. reported that B cells stimulated only with CD40L showed no induction of Blimp-1, stimulated with only IL-21 upregulated IRF4 moderately and weakly induced Blimp-1 by activation of STAT3. But stimulation with IL-21 and CD40L can synergistically induce massive Blimp-1 expression, leading to the differentiation of plasma cells [200]. As IL-21 is predominately produced by T_{FH} cells, with that in mind, we believed that the T_{FH} cells in our culture system contribute to the increased number of plasmablasts when co-cultured with feeder cells.

IL-7 is a crucial T-cell survival factor, and it exhibits anti-apoptotic function on human $CD4^+$ effector and memory T cells by enhancing the expression of Bcl-xL, Bcl2, and Mcl-1

through the JAK/STAT signaling pathway [166, 201]. Furthermore, IL-7 also supports a low level of proliferation of naive T-cell [167, 202]. Therefore, we also added IL-7 cytokine in our culture system to extend the survival of T cells. Indeed, we found the survival of different T-cell subsets to be significantly increased in the presence of IL-7. Interestingly, others demonstrated that IL-4 also can increase the survival of T cells by upregulating the expression of Bcl2 in both mice and humans [169, 203], but we did not see the effect on the survival of T cells in our culture system.

Here, we provided an *in-vitro* culture system for tonsil organoids in the presence of cytokines. In this culture system, we mimicked germinal center responses by adding feeder cells, which provided constant costimulatory signals to B cells. However, the optimal scenario would be that the B cells receive the costimulatory signals provided by T_{FH} cells, which originally existed in the tonsils. While BAFF-expressing cells might be necessary to replace the missing stroma cells, at least CD40L could be provided by T_{FH} cells to ensure the proper interaction between T_{FH} and GC-B cells. What we can do is to stimulate with immunogens instead of complete feeder cells. For example, we can expose T and B cells to different vaccines and thus produce high-affinity antibodies within several days. We also can use this platform to evaluate the efficacy of novel adjuvants. Therefore, this culture system provides a fully human system that allows us to test vaccines and adjuvants to find the best way to trigger broadly neutralizing antibodies and, consequently, to offer an *in-vitro* culture system for a better understanding of the germinal center responses in humans.

In the end, we also checked the response of our 3D-tonsil organoids culture system to real antigens, during which we used CMV peptides and binding peptides of Covid-19 spike protein as models. We found that the same antigens in organoids of two different donors provoked different responses. Specifically, it favoured the generation of memory cells in the first donor, while more plasmablasts were generated in the second donor. The regulation of memory and plasmablast differentiation from GC-B cells or pre-GC-B cells is different. *In vitro* studies indicated that IL-4 can increase the differentiation of plasma cells in a dose-dependent manner [213]. Furthermore, CD40L/IL-4-activated mouse B cells obtained a transcription program which is much closer to plasma cells [214]. Our human tonsil organoids co-cultured with 293T-CD40L or feeder cells also elicited these consistent results. Shinnakasu *et al*. reported that pre-GC-B cells with BCRs of relatively low affinity that receive weak help from T cells were prone to become memory cells [215]. Taylor *et al*. also found that naïve B cells with low-affinity BCRs are more prone to become memory B cells in transfer experiment [216].

We also compared 3D tonsil organoids with 2D culture. Unfortunately and opposite from expectation, it turned out that the 2D culture was actually much better. It could be due to less efficient cell-cell interaction in our 3D cultures than that in the 2D cultures. However, although

the quantity in gain of all lymphocyte subsets was much less in 3D organoids compared to the 2D culture in the presence of antigens, their quality was similar as that in the 2D culture, i.e., the 3D organoids still could reflect the same. In the current system, hBAFF was revealed crucial for the survival of B cells but was excluded here due to the avoidance of feeder cells. In the future, we could add some recombinant hBAFF to see whether it would improve the overall germinal center response to real antigens in 3D organoids. Despite the seemingly superiority of 2D over 3D here, it is worthy to stress that the 3D culture is considered as very important to mimic *in vivo* situations, especially for tumour cells. For instance, many tumour cell lines change the morphology and gene expression in 2D compared to 3D culture [217-220]. Furthermore, the 3D organoids experience gradient hypoxia and nutrients while they are homogenous in 2D culture [221]. Since the metabolism as well as phenotypic changes in 3D culture, the sensitivity to drugs of 3D organoids also showed more similarity to that of *in vivo* [219]. It might be, however, that primary cells derived from tonsils spontaneously form 3D-resembling aggregates that for this particular purpose a forced 3D by a scaffold with collagen is not necessary. Nevertheless, when it comes to *in-vitro* cultures with GC-derived lymphoma, we will expand on our experience with 3D organoids.

The T cells in NFATc1/ΔS^+ mice enlarged the expression of IL-2, behaving similarly with those in NFATc1/ΔBC^+ mice which only expressed NFATc1 short isoforms. Elevated IL-2 promotes the proliferation of Tregs but also affects follicular T cells including T_{FH} and T_{FR} cells. As we know, IL-2 inhibits the differentiation of T_{FH} cells. In extension, Botta *et al.* demonstrated that a high concentration of IL-2 at the peak of the infection even inhibits T_{FR} development by induction of high Blimp-1 expression on Tregs, thus preventing Bcl6 induction [222]. Recently, $CD25^-$ T_{FR} cells were discovered in both humans and mice [223, 224]. In mice, the gradual loss of CD25 was a marker for the differentiation of T_{FR} cells. They downregulate CD25 expression, limit Foxp3, but enhance the expression of Bcl6 and other T_{FH} cell-related genes, and eventually become T_{FH}–like mature T_{FR} cells [224]. The majority of T_{FR} cells located in the follicle and close to the T-B border express CD25, while T_{FR} cells that migrate deep into the GC lose CD25 expression. However, in humans, $CD25^-$ T_{FR} cells located in GC seem to be very rare [225]. Our previous data have already demonstrated that T_{FH} and T_{FR} cells highly express NFATc1 and that this is due to P1-induced dominance of NFATc1/αA [125, 126]. Of note, we additionally revealed that overexpression of NFATc1/αA in murine Tregs provokes an enhanced homing of T_{FR} cells to the GC itself as well as a better control of the GC response [123]. Lastly, we used CRISPR/Cas 9 technology to generate NFATc1/ΔBC^+ human primary T cells, mimicking murine transgenic *Nfatc1*^{deltaBC}.*Cd4cre* and hopefully again resembling the mutations at the two SUMOylation sites of NFATc1 in exon 10 in human T cells. Although the relevant data are not presented in this thesis, we have gathered preliminary results as we found in mice recently. We believe that our tonsil organoid culture system can provide a

promising platform to understand the function of SUMOylation of NFATc1 and / or the functional differences of its isoforms on T_{FH} and T_{FR} cells during the GC response.

10 List of abbreviations

ADCC	Antibody-dependent cellular cytotoxicity
aGvHD	Acute GvHD
AID	Activation-induced deaminase
allo-HSCT	Allogeneic hematopoietic stem cell transplantation
AMP	Adenosine monophosphate
Aos-1	Activator of SUMO1
APC	Antigen-presenting cell
BAFF	B cell-activating factor
BBB	Blood-brain barrier
Bcl2	B-cell lymphoma 2
Bcl-xL	B-cell lymphoma-extra large
BCR	B-cell receptor
BM	Bone marrow
Ca^{2+}	Calcium ions
CDC	Complement-mediated cytotoxicity
cGvHD	Chronic GvHD
ChIP	Chromatin immunoprecipitation
CNS	Central nervous system
ConA	Concanavalin A
CR2	Complement receptor 2
CSR	Class switch recombination
CTL	Cytotoxic T lymphocyte
d	day
DAG	Diacylglycerol
DAMP	Danger-associated molecular pattern
DAXX	Death-domain-associated protein
DC	Dendritic cell
DZ	Dark zone
EAE	Experimental autoimmune encephalomyelitis
EBV	Epstein–Barr virus
EMSA	Electromobility shift assay
Eomes	Eomesodermin
ER	Endoplasmic reticulum
FACS	Flow cytometric cell sorting
FDC	Follicular dendritic cell

g	gram
GC	Germinal center
GI	Gastrointestinal tract
GvHD	Graft-versus-host disease
GvL	Graft-versus-leukemia
h	hour
HCT	Hematopoietic stem cell transplantation
HDAC	Histone deacetylases
HLA	Human leukocyte antigens
I	Ionomycin
IFN-γ	Interferon-γ
IgG2a	Immunoglobulin G2a
IL-12	Interleukin-12
IP_3	Inositol-1,4,5-trisphosphate
IP_3R	IP_3 receptor
ITAM	Immunoreceptor tyrosine-based activation motif
L	liter
LPS	Lipopolysaccharide
LZ	Light zone
M	Molar, mol per liter
MAIT	Mucosa-associated invariant T
MBP	Myelin basic protein
MHC	Major histocompatibility complex
MHC	Major histocompatibility complex
min	Minutes
MMP-3	Matrix metalloproteinase-3
MOG	Myelin oligodendrocyte glycoprotein
MRI	Magnetic resonance imaging
MS	Multiple sclerosis
NES	Nuclear export signal
NFAT	Nuclear factor of activated T-cells
NHR	NFAT-homology region
NK	Natural killer cell
NLR	NOD-like receptor
NLS	Nuclear localization signal
PAMP	Pathogen-associated molecular pattern
PIP_2	Phosphatidylinositol-4,5-bisphosphate

PLCγ1	Phospholipase C-γ1
PLP	Proteolipid protein
PP	Peyer's patches
PPMS	Primary progressive multiple sclerosis
PRMS	Progressive relapsing multiple sclerosis
PT	Pertussis toxin
RA	Rheumatoid arthritis
RHR	Rel-homology region
rpm	rounds per minute
RRMS	Relapsing-remitting multiple sclerosis
s	second
SDF-1	Stromal cell-derived factor-1
SENP	Sentrin/SUMO-specific protease
SHM	Somatic hypermutation
SLE	Systemic lupus erythematosus
SLO	Secondary lymphoid organ
SPMS	Secondary-progressive multiple sclerosis
STAT1	Signal transducer and activator of transcription 1
STAT4	Signal transducer and activator of transcription 4
SUMO	Small Ubiquitin-like Modifier
T	12-O-Tetradecanoylphorbol-13-acetate (TPA)
TAD-N	N-terminal transactivation domain
TCR	T-cell receptor
TF	Transcriptional factor
T_{FH}	Follicular T helper cell
Th	T helper
TJ	Tight junction
TLR	Toll-like receptor
TNF	Tumour-necrosis factor
TNF-α	Tumor necrosis factor-α
Treg	Regulatory T cell
Uba2	Ubiquitin-like modifier activating enzyme 2
Ubc9	Ubiquitin-conjugating enzyme 9
VLA	Very late activation antigen
α	alpha
β	beta
γδ	gamma-delta

°C	degrees Celsius

11 Bibliography

1. Nicholson, L.B., *The immune system.* Essays in biochemistry, 2016. **60**(3): p. 275-301.
2. Germain, R.N., *T-cell development and the CD4–CD8 lineage decision.* Nature Reviews Immunology, 2002. **2**(5): p. 309-322.
3. Kuhns, M.S., M.M. Davis, and K.C. Garcia, *Deconstructing the form and function of the TCR/CD3 complex.* Immunity, 2006. **24**(2): p. 133-9.
4. Birnbaum, M.E., et al., *Molecular architecture of the αβ T cell receptor–CD3 complex.* 2014. **111**(49): p. 17576-17581.
5. Willcox, C.R., F. Mohammed, and B.E. Willcox, *The distinct MHC-unrestricted immunobiology of innate-like and adaptive-like human γδ T cell subsets-Nature's CAR-T cells.* Immunol Rev, 2020. **298**(1): p. 25-46.
6. Brandes, M., K. Willimann, and B. Moser, *Professional Antigen-Presentation Function by Human γδ T Cells.* 2005. **309**(5732): p. 264-268.
7. Hwang, J.-R., et al., *Recent insights of T cell receptor-mediated signaling pathways for T cell activation and development.* Experimental & Molecular Medicine, 2020. **52**(5): p. 750-761.
8. Tai, Y., et al., *Molecular Mechanisms of T Cells Activation by Dendritic Cells in Autoimmune Diseases.* 2018. **9**(642).
9. Zhang, X., et al., *Follicular helper T cells: new insights into mechanisms of autoimmune diseases.* Ochsner J, 2013. **13**(1): p. 131-9.
10. Murphy, K.M. and S.L. Reiner, *The lineage decisions of helper T cells.* Nat Rev Immunol, 2002. **2**(12): p. 933-44.
11. Wing, K. and S. Sakaguchi, *Regulatory T cells exert checks and balances on self tolerance and autoimmunity.* Nat Immunol, 2010. **11**(1): p. 7-13.
12. Thieu, V.T., et al., *Signal transducer and activator of transcription 4 is required for the transcription factor T-bet to promote T helper 1 cell-fate determination.* Immunity, 2008. **29**(5): p. 679-90.
13. Hsieh, C.S., et al., *Development of TH1 CD4+ T cells through IL-12 produced by Listeria-induced macrophages.* Science, 1993. **260**(5107): p. 547-9.
14. Siebenkotten, G., et al., *The murine IgG1/IgE class switch program.* Eur J Immunol, 1992. **22**(7): p. 1827-34.
15. Olatunde, A.C., J.S. Hale, and T.J. Lamb, *Cytokine-skewed Tfh cells: functional consequences for B cell help.* Trends in Immunology, 2021. **42**(6): p. 536-550.
16. Kondělková, K., et al., *Regulatory T cells (TREG) and their roles in immune system with respect to immunopathological disorders.* Acta Medica (Hradec Kralove), 2010. **53**(2): p. 73-7.

17. Romano, M., et al., *Past, Present, and Future of Regulatory T Cell Therapy in Transplantation and Autoimmunity.* 2019. **10**(43).
18. Nurieva, R.I. and Y. Chung, *Understanding the development and function of T follicular helper cells.* Cell Mol Immunol, 2010. **7**(3): p. 190-7.
19. Kurosaki, T., H. Shinohara, and Y. Baba, *B cell signaling and fate decision.* Annu Rev Immunol, 2010. **28**: p. 21-55.
20. Yang, J. and M. Reth, *Receptor Dissociation and B-Cell Activation.* Curr Top Microbiol Immunol, 2016. **393**: p. 27-43.
21. Hoogeboom, R. and P. Tolar, *Molecular Mechanisms of B Cell Antigen Gathering and Endocytosis.* Curr Top Microbiol Immunol, 2016. **393**: p. 45-63.
22. Carroll, M.C. and D.E. Isenman, *Regulation of humoral immunity by complement.* Immunity, 2012. **37**(2): p. 199-207.
23. Suthers, A.N. and S. Sarantopoulos, *TLR7/TLR9- and B Cell Receptor-Signaling Crosstalk: Promotion of Potentially Dangerous B Cells.* Front Immunol, 2017. **8**: p. 775.
24. Stebegg, M., et al., *Regulation of the Germinal Center Response.* 2018. **9**(2469).
25. Batista, F.D. and N.E. Harwood, *The who, how and where of antigen presentation to B cells.* Nature Reviews Immunology, 2009. **9**(1): p. 15-27.
26. Okada, T., et al., *Antigen-Engaged B Cells Undergo Chemotaxis toward the T Zone and Form Motile Conjugates with Helper T Cells.* PLOS Biology, 2005. **3**(6): p. e150.
27. Chan, T.D., et al., *Antigen Affinity Controls Rapid T-Dependent Antibody Production by Driving the Expansion Rather than the Differentiation or Extrafollicular Migration of Early Plasmablasts.* 2009. **183**(5): p. 3139-3149.
28. Coffey, F., B. Alabyev, and T. Manser, *Initial Clonal Expansion of Germinal Center B Cells Takes Place at the Perimeter of Follicles.* Immunity, 2009. **30**(4): p. 599-609.
29. MacLennan, I.C.M., et al., *Extrafollicular antibody responses.* 2003. **194**(1): p. 8-18.
30. Linterman, M. and D. Hill, *Can follicular helper T cells be targeted to improve vaccine efficacy?* F1000Research, 2016. **5**.
31. Hauser, A.E., et al., *Definition of Germinal-Center B Cell Migration In Vivo Reveals Predominant Intrazonal Circulation Patterns.* Immunity, 2007. **26**(5): p. 655-667.
32. Mesin, L., J. Ersching, and Gabriel D. Victora, *Germinal Center B Cell Dynamics.* Immunity, 2016. **45**(3): p. 471-482.
33. MacLennan, I.C.M., *Germinal Centers.* Annual Review of Immunology, 1994. **12**(1): p. 117-139.
34. Liu, D., et al., *T–B-cell entanglement and ICOSL-driven feed-forward regulation of germinal centre reaction.* Nature, 2015. **517**(7533): p. 214-218.
35. Linterman, M.A., et al., *IL-21 acts directly on B cells to regulate Bcl-6 expression and germinal center responses.* J Exp Med, 2010. **207**(2): p. 353-63.

36. Good, K.L., V.L. Bryant, and S.G. Tangye, *Kinetics of human B cell behavior and amplification of proliferative responses following stimulation with IL-21.* J Immunol, 2006. **177**(8): p. 5236-47.
37. Dufort, F.J., et al., *Cutting edge: IL-4-mediated protection of primary B lymphocytes from apoptosis via Stat6-dependent regulation of glycolytic metabolism.* J Immunol, 2007. **179**(8): p. 4953-7.
38. Wurster, A.L., et al., *Interleukin-4-mediated protection of primary B cells from apoptosis through Stat6-dependent up-regulation of Bcl-xL.* J Biol Chem, 2002. **277**(30): p. 27169-75.
39. Morawetz, R.A., et al., *Interleukin (IL)-4-independent immunoglobulin class switch to immunoglobulin (Ig)E in the mouse.* The Journal of experimental medicine, 1996. **184**(5): p. 1651-1661.
40. Zhang, F., et al., *BAFF upregulates CD28/B7 and CD40/CD154 expression and promotes mouse T and B cell interaction in vitro via BAFF receptor.* Acta Pharmacologica Sinica, 2016. **37**(8): p. 1101-1109.
41. Smulski, C.R. and H. Eibel, *BAFF and BAFF-Receptor in B Cell Selection and Survival.* 2018. **9**(2285).
42. Klingebiel, T., et al., *Results and factors influencing outcome after fully haploidentical hematopoietic stem cell transplantation in children with very high-risk acute lymphoblastic leukemia: impact of center size: an analysis on behalf of the Acute Leukemia and Pediatric Disease Working Parties of the European Blood and Marrow Transplant group.* Blood, 2010. **115**(17): p. 3437-46.
43. Copelan, E.A., *Hematopoietic Stem-Cell Transplantation.* 2006. **354**(17): p. 1813-1826.
44. Zulu, S. and M. Kenyon, *Principles of Conditioning Therapy and Cell Infusion*, in *The European Blood and Marrow Transplantation Textbook for Nurses*. 2018, Springer: Cham (CH). p. 89-96.
45. Ottinger, H.D., et al., *Hematopoietic stem cell transplantation: contrasting the outcome of transplantations from HLA-identical siblings, partially HLA-mismatched related donors, and HLA-matched unrelated donors.* Blood, 2003. **102**(3): p. 1131-7.
46. Peled, A., et al., *The chemokine SDF-1 stimulates integrin-mediated arrest of CD34(+) cells on vascular endothelium under shear flow.* J Clin Invest, 1999. **104**(9): p. 1199-211.
47. Kollet, O., et al., *Rapid and efficient homing of human CD34(+)CD38(-/low)CXCR4(+) stem and progenitor cells to the bone marrow and spleen of NOD/SCID and NOD/SCID/B2m(null) mice.* Blood, 2001. **97**(10): p. 3283-91.
48. Mehta, R.S. and K. Rezvani, *Immune reconstitution post allogeneic transplant and the impact of immune recovery on the risk of infection.* Virulence, 2016. **7**(8): p. 901-916.

49. Dekker, L., et al., *Reconstitution of T Cell Subsets Following Allogeneic Hematopoietic Cell Transplantation.* 2020. **12**(7): p. 1974.
50. Velardi, E., J.J. Tsai, and M.R.M. van den Brink, *T cell regeneration after immunological injury.* Nature Reviews Immunology, 2021. **21**(5): p. 277-291.
51. Toubai, T., Y. Sun, and P. Reddy, *GVHD pathophysiology: is acute different from chronic?* Best Practice & Research Clinical Haematology, 2008. **21**(2): p. 101-117.
52. Ferrara, J.L.M., et al., *Graft-versus-host disease.* Lancet (London, England), 2009. **373**(9674): p. 1550-1561.
53. Jamil, M.O. and S. Mineishi, *State-of-the-art acute and chronic GVHD treatment.* Int J Hematol, 2015. **101**(5): p. 452-66.
54. MacMillan, M.L., et al., *A refined risk score for acute graft-versus-host disease that predicts response to initial therapy, survival, and transplant-related mortality.* Biology of blood and marrow transplantation : journal of the American Society for Blood and Marrow Transplantation, 2015. **21**(4): p. 761-767.
55. Gale, R.P., et al., *Risk factors for acute graft-versus-host disease.* Br J Haematol, 1987. **67**(4): p. 397-406.
56. Gratwohl, A., et al., *Gender and Graft-versus-Host Disease after Hematopoietic Stem Cell Transplantation.* Biol Blood Marrow Transplant, 2016. **22**(6): p. 1145-1146.
57. Magenau, J. and P. Reddy, *Next generation treatment of acute graft-versus-host disease.* Leukemia, 2014. **28**(12): p. 2283-2291.
58. Devetten, M.P. and J.M. Vose, *Graft-versus-host disease: how to translate new insights into new therapeutic strategies.* Biol Blood Marrow Transplant, 2004. **10**(12): p. 815-25.
59. Cho, J.H. and P.K. Gregersen, *Genomics and the Multifactorial Nature of Human Autoimmune Disease.* 2011. **365**(17): p. 1612-1623.
60. Agmon-Levin, N., Z. Lian, and Y. Shoenfeld, *Explosion of autoimmune diseases and the mosaic of old and novel factors.* Cell Mol Immunol, 2011. **8**(3): p. 189-92.
61. Olsson, T., L.F. Barcellos, and L. Alfredsson, *Interactions between genetic, lifestyle and environmental risk factors for multiple sclerosis.* Nat Rev Neurol, 2017. **13**(1): p. 25-36.
62. Lublin, F.D. and S.C. Reingold, *Defining the clinical course of multiple sclerosis: results of an international survey. National Multiple Sclerosis Society (USA) Advisory Committee on Clinical Trials of New Agents in Multiple Sclerosis.* Neurology, 1996. **46**(4): p. 907-11.
63. Dendrou, C.A., L. Fugger, and M.A. Friese, *Immunopathology of multiple sclerosis.* Nature Reviews Immunology, 2015. **15**(9): p. 545-558.
64. Vanderlugt, C.J. and S.D. Miller, *Epitope spreading.* Current opinion in immunology, 1996. **8**(6): p. 831-836.

65. Glass, C.K., et al., *Mechanisms underlying inflammation in neurodegeneration.* Cell, 2010. **140**(6): p. 918-34.
66. Grigoriadis, N. and V. van Pesch, *A basic overview of multiple sclerosis immunopathology.* Eur J Neurol, 2015. **22 Suppl 2**: p. 3-13.
67. Mitsdoerffer, M. and A. Peters, *Tertiary Lymphoid Organs in Central Nervous System Autoimmunity.* 2016. **7**(451).
68. Luo, C., et al., *The role of microglia in multiple sclerosis.* Neuropsychiatric disease and treatment, 2017. **13**: p. 1661-1667.
69. Mayo, L., et al., *Regulation of astrocyte activation by glycolipids drives chronic CNS inflammation.* Nat Med, 2014. **20**(10): p. 1147-56.
70. van den Hoogen, W.J., J.D. Laman, and B.A. 't Hart, *Modulation of Multiple Sclerosis and Its Animal Model Experimental Autoimmune Encephalomyelitis by Food and Gut Microbiota.* 2017. **8**(1081).
71. Gustavsson, C., et al., *Vascular cellular adhesion molecule-1 (VCAM-1) expression in mice retinal vessels is affected by both hyperglycemia and hyperlipidemia.* PLoS One, 2010. **5**(9): p. e12699.
72. Marchetti, L. and B. Engelhardt, *Immune cell trafficking across the blood-brain barrier in the absence and presence of neuroinflammation* 2020. **2**(1): p. H1-H18.
73. Sonar, S.A., et al., *IFN-γ promotes transendothelial migration of CD4(+) T cells across the blood-brain barrier.* Immunol Cell Biol, 2017. **95**(9): p. 843-853.
74. Ottum, P.A., et al., *Opposing Roles of Interferon-Gamma on Cells of the Central Nervous System in Autoimmune Neuroinflammation.* 2015. **6**(539).
75. Park, H., et al., *A distinct lineage of CD4 T cells regulates tissue inflammation by producing interleukin 17.* Nat Immunol, 2005. **6**(11): p. 1133-41.
76. Yong, V.W., et al., *Metalloproteinases in biology and pathology of the nervous system.* Nat Rev Neurosci, 2001. **2**(7): p. 502-11.
77. Kang, Z., et al., *Astrocyte-restricted ablation of interleukin-17-induced Act1-mediated signaling ameliorates autoimmune encephalomyelitis.* Immunity, 2010. **32**(3): p. 414-25.
78. Codarri, L., et al., *RORγt drives production of the cytokine GM-CSF in helper T cells, which is essential for the effector phase of autoimmune neuroinflammation.* Nat Immunol, 2011. **12**(6): p. 560-7.
79. Naves, R., et al., *The interdependent, overlapping, and differential roles of type I and II IFNs in the pathogenesis of experimental autoimmune encephalomyelitis.* J Immunol, 2013. **191**(6): p. 2967-77.
80. Platten, M., et al., *Treatment of autoimmune neuroinflammation with a synthetic tryptophan metabolite.* 2005. **310**(5749): p. 850-855.

81. Arellano, G., et al., *Stage-Specific Role of Interferon-Gamma in Experimental Autoimmune Encephalomyelitis and Multiple Sclerosis.* 2015. **6**.
82. Losy, J. and A. Niezgoda, *IL-18 in patients with multiple sclerosis.* Acta Neurol Scand, 2001. **104**(3): p. 171-3.
83. Willing, A., et al., *CD8 $^{+}$ MAIT cells infiltrate into the CNS and alterations in their blood frequencies correlate with IL-18 serum levels in multiple sclerosis.* Eur J Immunol, 2014. **44**(10): p. 3119-28.
84. Kimura, K., et al., *Disrupted balance of T cells under natalizumab treatment in multiple sclerosis.* Neurol Neuroimmunol Neuroinflamm, 2016. **3**(2): p. e210.
85. Sospedra, M. and R. Martin, *Immunology of multiple sclerosis.* Annu Rev Immunol, 2005. **23**: p. 683-747.
86. Raddassi, K., et al., *Increased frequencies of myelin oligodendrocyte glycoprotein/MHC class II-binding CD4 cells in patients with multiple sclerosis.* J Immunol, 2011. **187**(2): p. 1039-46.
87. Hofstetter, H.H., C.L. Shive, and T.G. Forsthuber, *Pertussis Toxin Modulates the Immune Response to Neuroantigens Injected in Incomplete Freund's Adjuvant: Induction of Th1 Cells and Experimental Autoimmune Encephalomyelitis in the Presence of High Frequencies of Th2 Cells.* 2002. **169**(1): p. 117-125.
88. Bettelli, E., et al., *Myelin oligodendrocyte glycoprotein-specific T cell receptor transgenic mice develop spontaneous autoimmune optic neuritis.* J Exp Med, 2003. **197**(9): p. 1073-81.
89. Hermann-Kleiter, N. and G. Baier, *NFAT pulls the strings during CD4+ T helper cell effector functions.* Blood, 2010. **115**(15): p. 2989-97.
90. Macian, F., *NFAT proteins: key regulators of T-cell development and function.* Nat Rev Immunol, 2005. **5**(6): p. 472-84.
91. Lee, N., D. Kim, and W.-U. Kim, *Role of NFAT5 in the Immune System and Pathogenesis of Autoimmune Diseases.* 2019. **10**(270).
92. Mognol, G.P., et al., *Cell cycle and apoptosis regulation by NFAT transcription factors: new roles for an old player.* Cell Death Dis, 2016. **7**(4): p. e2199.
93. Sherman, M.A., et al., *NF-ATc Isoforms Are Differentially Expressed and Regulated in Murine T and Mast Cells.* The Journal of Immunology, 1999. **162**(5): p. 2820.
94. Park, J., A. Takeuchi, and S. Sharma, *Characterization of a new isoform of the NFAT (nuclear factor of activated T cells) gene family member NFATc.* J Biol Chem, 1996. **271**(34): p. 20914-21.
95. Chuvpilo, S., et al., *Alternative polyadenylation events contribute to the induction of NF-ATc in effector T cells.* Immunity, 1999. **10**(2): p. 261-9.

96. Chuvpilo, S., et al., *Autoregulation of NFATc1/A Expression Facilitates Effector T Cells to Escape from Rapid Apoptosis.* Immunity, 2002. **16**(6): p. 881-895.
97. Nayak, A., et al., *Sumoylation of the transcription factor NFATc1 leads to its subnuclear relocalization and interleukin-2 repression by histone deacetylase.* J Biol Chem, 2009. **284**(16): p. 10935-46.
98. Terui, Y., et al., *Dual Role of Sumoylation in the Nuclear Localization and Transcriptional Activation of NFAT1*.* Journal of Biological Chemistry, 2004. **279**(27): p. 28257-28265.
99. Vihma, H. and T. Timmusk, *Sumoylation regulates the transcriptional activity of different human NFAT isoforms in neurons.* Neuroscience Letters, 2017. **653**: p. 302-307.
100. Serfling, E., et al., *NFATc1 autoregulation: a crucial step for cell-fate determination.* Trends Immunol, 2006. **27**(10): p. 461-9.
101. Hay, R.T., *SUMO: a history of modification.* Mol Cell, 2005. **18**(1): p. 1-12.
102. Melchior, F., *SUMO--nonclassical ubiquitin.* Annu Rev Cell Dev Biol, 2000. **16**: p. 591-626.
103. Gill, G., *SUMO and ubiquitin in the nucleus: different functions, similar mechanisms?* Genes Dev, 2004. **18**(17): p. 2046-59.
104. Lyst, M.J. and I. Stancheva, *A role for SUMO modification in transcriptional repression and activation.* Biochem Soc Trans, 2007. **35**(Pt 6): p. 1389-92.
105. Saitoh, H. and J. Hinchey, *Functional heterogeneity of small ubiquitin-related protein modifiers SUMO-1 versus SUMO-2/3.* J Biol Chem, 2000. **275**(9): p. 6252-8.
106. Wei, W., et al., *A stress-dependent SUMO4 sumoylation of its substrate proteins.* Biochemical and Biophysical Research Communications, 2008. **375**(3): p. 454-459.
107. Hickey, C.M., N.R. Wilson, and M. Hochstrasser, *Function and regulation of SUMO proteases.* Nature Reviews Molecular Cell Biology, 2012. **13**(12): p. 755-766.
108. Nayak, A. and S. Müller, *SUMO-specific proteases/isopeptidases: SENPs and beyond.* Genome Biol, 2014. **15**(7): p. 422.
109. Olsen, S.K., et al., *Active site remodelling accompanies thioester bond formation in the SUMO E1.* Nature, 2010. **463**(7283): p. 906-912.
110. Flotho, A. and F. Melchior, *Sumoylation: a regulatory protein modification in health and disease.* Annu Rev Biochem, 2013. **82**: p. 357-85.
111. Rodriguez, M.S., C. Dargemont, and R.T. Hay, *SUMO-1 Conjugation in Vivo Requires Both a Consensus Modification Motif and Nuclear Targeting*.* Journal of Biological Chemistry, 2001. **276**(16): p. 12654-12659.
112. Sarge, K.D. and O.K. Park-Sarge, *Sumoylation and human disease pathogenesis.* Trends Biochem Sci, 2009. **34**(4): p. 200-5.

113. Wilkinson, K.A. and J.M. Henley, *Mechanisms, regulation and consequences of protein SUMOylation.* Biochem J, 2010. **428**(2): p. 133-45.
114. Yang, S.H. and A.D. Sharrocks, *SUMO promotes HDAC-mediated transcriptional repression.* Mol Cell, 2004. **13**(4): p. 611-7.
115. Kuo, H.Y., et al., *SUMO modification negatively modulates the transcriptional activity of CREB-binding protein via the recruitment of Daxx.* Proc Natl Acad Sci U S A, 2005. **102**(47): p. 16973-8.
116. Geiss-Friedlander, R. and F. Melchior, *Concepts in sumoylation: a decade on.* Nature Reviews Molecular Cell Biology, 2007. **8**(12): p. 947-956.
117. de la Pompa, J.L., et al., *Role of the NF-ATc transcription factor in morphogenesis of cardiac valves and septum.* Nature, 1998. **392**(6672): p. 182-186.
118. Crabtree, G.R. and E.N. Olson, *NFAT signaling: choreographing the social lives of cells.* Cell, 2002. **109 Suppl**: p. S67-79.
119. Gaud, G., R. Lesourne, and P.E. Love, *Regulatory mechanisms in T cell receptor signalling.* Nat Rev Immunol, 2018. **18**(8): p. 485-497.
120. Muro, R., H. Takayanagi, and T. Nitta, *T cell receptor signaling for γδT cell development.* Inflammation and Regeneration, 2019. **39**(1): p. 6.
121. Bhattacharyya, N.D. and C.G. Feng, *Regulation of T Helper Cell Fate by TCR Signal Strength.* 2020. **11**(624).
122. Vaeth, M., et al., *Follicular regulatory T cells control humoral autoimmunity via NFAT2-regulated CXCR5 expression.* J Exp Med, 2014. **211**(3): p. 545-61.
123. Koenig, A., et al., *NFATc1/αA and Blimp-1 Support the Follicular and Effector Phenotype of Tregs.* Front Immunol, 2021. **12**: p. 791100.
124. Mombaerts, P., et al., *RAG-1-deficient mice have no mature B and T lymphocytes.* Cell, 1992. **68**(5): p. 869-877.
125. Lahl, K., et al., *Selective depletion of Foxp3+ regulatory T cells induces a scurfy-like disease.* J Exp Med, 2007. **204**(1): p. 57-63.
126. Dietz, L., et al., *NFAT1 deficit and NFAT2 deficit attenuate EAE via different mechanisms.* Eur J Immunol, 2015. **45**(5): p. 1377-89.
127. Livak, K.J. and T.D. Schmittgen, *Analysis of relative gene expression data using real-time quantitative PCR and the 2(-Delta Delta C(T)) Method.* Methods, 2001. **25**(4): p. 402-8.
128. Winer, J., et al., *Development and validation of real-time quantitative reverse transcriptase-polymerase chain reaction for monitoring gene expression in cardiac myocytes in vitro.* Anal Biochem, 1999. **270**(1): p. 41-9.

129. Rao, X., et al., *An improvement of the 2ˆ(-delta delta CT) method for quantitative real-time polymerase chain reaction data analysis.* Biostatistics, bioinformatics and biomathematics, 2013. **3**(3): p. 71-85.
130. Nayak, A., et al., *Sumoylation of the Transcription Factor NFATc1 Leads to Its Subnuclear Relocalization and Interleukin-2 Repression by Histone Deacetylase *.* Journal of Biological Chemistry, 2009. **284**(16): p. 10935-10946.
131. Laurence, A., et al., *Interleukin-2 Signaling via STAT5 Constrains T Helper 17 Cell Generation.* Immunity, 2007. **26**(3): p. 371-381.
132. Laurence, A., et al., *Interleukin-2 signaling via STAT5 constrains T helper 17 cell generation.* Immunity, 2007. **26**(3): p. 371-81.
133. Liu, Y., et al., *Heat-stable antigen is a costimulatory molecule for CD4 T cell growth.* The Journal of experimental medicine, 1992. **175**(2): p. 437-445.
134. Enk, A.H. and S.I. Katz, *Heat-stable antigen is an important costimulatory molecule on epidermal Langerhans' cells.* J Immunol, 1994. **152**(7): p. 3264-70.
135. Liu, Y., et al., *Distinct costimulatory molecules are required for the induction of effector and memory cytotoxic T lymphocytes.* The Journal of experimental medicine, 1997. **185**(2): p. 251-262.
136. Bai, X.F., et al., *The heat-stable antigen determines pathogenicity of self-reactive T cells in experimental autoimmune encephalomyelitis.* The Journal of clinical investigation, 2000. **105**(9): p. 1227-1232.
137. Tang, Q., et al., *Cutting edge: CD28 controls peripheral homeostasis of CD4+CD25+ regulatory T cells.* J Immunol, 2003. **171**(7): p. 3348-52.
138. de la Rosa, M., et al., *Interleukin-2 is essential for $CD4^+CD25^+$ regulatory T cell function.* European Journal of Immunology, 2004. **34**(9): p. 2480-2488.
139. Cimmino, L., et al., *Blimp-1 Attenuates Th1 Differentiation by Repression of ifng, tbx21, and bcl6 Gene Expression.* 2008. **181**(4): p. 2338-2347.
140. Gong, D. and T.R. Malek, *Cytokine-dependent Blimp-1 expression in activated T cells inhibits IL-2 production.* J Immunol, 2007. **178**(1): p. 242-52.
141. Martins, G.A., et al., *Blimp-1 directly represses Il2 and the Il2 activator Fos, attenuating T cell proliferation and survival.* The Journal of experimental medicine, 2008. **205**(9): p. 1959-1965.
142. Ohinata, Y., et al., *Blimp1 is a critical determinant of the germ cell lineage in mice.* Nature, 2005. **436**(7048): p. 207-13.
143. Vincent, S.p.D., et al., *The zinc finger transcriptional repressor Blimp1/Prdm1 is dispensable for early axis formation but is required for specification of primordial germ cells in the mouse.* Development, 2005. **132**(6): p. 1315-1325.

144. Vogler, M., *BCL2A1: the underdog in the BCL2 family.* Cell Death & Differentiation, 2012. **19**(1): p. 67-74.
145. Jenal, M., et al., *The anti-apoptotic gene BCL2A1 is a novel transcriptional target of PU.1.* Leukemia, 2010. **24**(5): p. 1073-1076.
146. Chuvpilo, S., et al., *Autoregulation of NFATc1/A expression facilitates effector T cells to escape from rapid apoptosis.* Immunity, 2002. **16**(6): p. 881-95.
147. Cimmino, L., et al., *Blimp-1 attenuates Th1 differentiation by repression of ifng, tbx21, and bcl6 gene expression.* J Immunol, 2008. **181**(4): p. 2338-47.
148. Rasheed, A.U., et al., *Follicular B helper T cell activity is confined to CXCR5(hi)ICOS(hi) CD4 T cells and is independent of CD57 expression.* Eur J Immunol, 2006. **36**(7): p. 1892-903.
149. Kenny, P.A., et al., *The morphologies of breast cancer cell lines in three-dimensional assays correlate with their profiles of gene expression.* Molecular Oncology, 2007. **1**(1): p. 84-96.
150. Zhou, Y., et al., *3D culture increases pluripotent gene expression in mesenchymal stem cells through relaxation of cytoskeleton tension.* Journal of Cellular and Molecular Medicine, 2017. **21**(6): p. 1073-1084.
151. Nojima, T., et al., *In-vitro derived germinal centre B cells differentially generate memory B or plasma cells in vivo.* Nature Communications, 2011. **2**(1): p. 465.
152. Haniuda, K., T. Nojima, and D. Kitamura, *In Vitro-Induced Germinal Center B Cell Culture System.* Methods Mol Biol, 2017. **1623**: p. 125-133.
153. Robinson, M.J., et al., *BAFF, IL-4 and IL-21 separably program germinal center-like phenotype acquisition, BCL6 expression, proliferation and survival of CD40L-activated B cells in vitro.* Immunology & Cell Biology, 2019. **97**(9): p. 826-839.
154. Zhang, Y., et al., *Efficient generation of antigen-specific CTLs by the BAFFactivated human B Lymphocytes as APCs: A novel approach for immunotherapy.* Oncotarget, 2016. **7**.
155. von Bergwelt-Baildon, M.S., et al., *Human primary and memory cytotoxic T lymphocyte responses are efficiently induced by means of CD40-activated B cells as antigen-presenting cells: potential for clinical application.* Blood, 2002. **99**(9): p. 3319-25.
156. von Bergwelt-Baildon, M., et al., *CD40-activated B cells express full lymph node homing triad and induce T-cell chemotaxis: potential as cellular adjuvants.* Blood, 2006. **107**(7): p. 2786-9.
157. Batten, M., et al., *BAFF mediates survival of peripheral immature B lymphocytes.* The Journal of experimental medicine, 2000. **192**(10): p. 1453-1466.
158. Thompson, J.S., et al., *BAFF-R, a Newly Identified TNF Receptor That Specifically Interacts with BAFF.* 2001. **293**(5537): p. 2108-2111.

159. Pieper, K., B. Grimbacher, and H. Eibel, *B-cell biology and development.* J Allergy Clin Immunol, 2013. **131**(4): p. 959-71.
160. Mackay, F., et al., *BAFF AND APRIL: a tutorial on B cell survival.* Annu Rev Immunol, 2003. **21**: p. 231-64.
161. Goenka, R., et al., *New roles for the BLyS/BAFF family in antigen-experienced B cell niches.* Cytokine & growth factor reviews, 2014. **25**(2): p. 107-113.
162. Mackay, F. and P. Schneider, *Cracking the BAFF code.* Nat Rev Immunol, 2009. **9**(7): p. 491-502.
163. Schiemann, B., et al., *An essential role for BAFF in the normal development of B cells through a BCMA-independent pathway.* Science, 2001. **293**(5537): p. 2111-4.
164. Jacque, E., et al., *BAFF activation of the ERK5 MAP kinase pathway regulates B cell survival.* The Journal of experimental medicine, 2015. **212**(6): p. 883-892.
165. Banchereau, J. and F. Rousset, *Functions of interleukin-4 on human B lymphocytes.* Immunologic Research, 1991. **10**(3): p. 423-427.
166. Chetoui, N., et al., *Interleukin-7 promotes the survival of human CD4$^+$ effector/memory T cells by up-regulating Bcl-2 proteins and activating the JAK/STAT signalling pathway.* Immunology, 2010. **130**(3): p. 418-426.
167. Tan, J.T., et al., *IL-7 is critical for homeostatic proliferation and survival of naive T cells.* 2001. **98**(15): p. 8732-8737.
168. Wagner, E.F., et al., *Novel Diversity in IL-4-Mediated Responses in Resting Human Naive B Cells Versus Germinal Center/Memory B Cells.* 2000. **165**(10): p. 5573-5579.
169. Vella, A., et al., *Interleukin 4 (IL-4) or IL-7 prevents the death of resting T cells: stat6 is probably not required for the effect of IL-4.* The Journal of experimental medicine, 1997. **186**(2): p. 325-330.
170. Seo, Y.B., et al., *Crucial roles of interleukin-7 in the development of T follicular helper cells and in the induction of humoral immunity.* J Virol, 2014. **88**(16): p. 8998-9009.
171. Kitabatake, M., et al., *JNK Regulatory Molecule G5PR Induces IgG Autoantibody-Producing Plasmablasts from Peritoneal B1a Cells.* Journal of immunology (Baltimore, Md. : 1950), 2015. **194**.
172. Zhang, J., et al., *Maintenance of Germinal Center B Cells by Caspase-9 through Promotion of Apoptosis and Inhibition of Necroptosis.* 2020. **205**(1): p. 113-120.
173. Guan, Y., et al., *A human multi-lineage hepatic organoid model for liver fibrosis.* Nature Communications, 2021. **12**(1): p. 6138.
174. Finney, J. and G. Kelsoe, *Continuous Culture of Mouse Primary B Lymphocytes by Forced Expression of Bach2.* 2021: p. ji2100172.
175. Salahudeen, A.A., et al., *Progenitor identification and SARS-CoV-2 infection in human distal lung organoids.* Nature, 2020. **588**(7839): p. 670-675.

176. Lawlor, K.T., et al., *Cellular extrusion bioprinting improves kidney organoid reproducibility and conformation.* Nature Materials, 2021. **20**(2): p. 260-271.
177. Hakkinen, K.M., et al., *Direct comparisons of the morphology, migration, cell adhesions, and actin cytoskeleton of fibroblasts in four different three-dimensional extracellular matrices.* Tissue engineering. Part A, 2011. **17**(5-6): p. 713-724.
178. Mak, M., R.D. Kamm, and M.H.J.P.c.b. Zaman, *Impact of dimensionality and network disruption on microrheology of cancer cells in 3D environments.* 2014. **10**(11): p. e1003959.
179. Ballesteros-Tato, A., et al., *Interleukin-2 Inhibits Germinal Center Formation by Limiting T Follicular Helper Cell Differentiation.* Immunity, 2012. **36**(5): p. 847-856.
180. Elgueta, R., et al., *Molecular mechanism and function of CD40/CD40L engagement in the immune system.* 2009. **229**(1): p. 152-172.
181. Nelson, C.M. and M.J. Bissell. *Modeling dynamic reciprocity: engineering three-dimensional culture models of breast architecture, function, and neoplastic transformation*. in *Seminars in cancer biology*. 2005. Elsevier.
182. Zietarska, M., et al., *Molecular description of a 3D in vitro model for the study of epithelial ovarian cancer (EOC).* 2007. **46**(10): p. 872-885.
183. Kuczek, D.E., et al., *Collagen density regulates the activity of tumor-infiltrating T cells.* Journal for ImmunoTherapy of Cancer, 2019. **7**(1): p. 68.
184. Sun, S.-C., *The non-canonical NF-κB pathway in immunity and inflammation.* Nature Reviews Immunology, 2017. **17**(9): p. 545-558.
185. Duhen, R., et al., *Cutting edge: the pathogenicity of IFN-γ-producing Th17 cells is independent of T-bet.* Journal of immunology (Baltimore, Md. : 1950), 2013. **190**(9): p. 4478-4482.
186. Treml, J.F., et al., *The BLyS family: toward a molecular understanding of B cell homeostasis.* Cell Biochem Biophys, 2009. **53**(1): p. 1-16.
187. Do, R.K., et al., *Attenuation of apoptosis underlies B lymphocyte stimulator enhancement of humoral immune response.* J Exp Med, 2000. **192**(7): p. 953-64.
188. Jacque, E., et al., *BAFF activation of the ERK5 MAP kinase pathway regulates B cell survival.* Journal of Experimental Medicine, 2015. **212**(6): p. 883-892.
189. Wang, A.Y.L., et al., *Blimp-1 prolongs allograft survival without regimen via influencing T cell development in favor of regulatory T cells while suppressing Th1.* Molecular Immunology, 2018. **99**: p. 53-65.
190. Croft, M. and C. Dubey, *Accessory molecule and costimulation requirements for CD4 T cell response.* Crit Rev Immunol, 1997. **17**(1): p. 89-118.
191. Bluestone, J.A., *New perspectives of CD28-B7-mediated T cell costimulation.* Immunity, 1995. **2**(6): p. 555-9.

192. Ding, X., et al., *Protein SUMOylation Is Required for Regulatory T Cell Expansion and Function.* Cell Reports, 2016. **16**(4): p. 1055-1066.
193. Yan, M., et al., *Identification of a novel receptor for B lymphocyte stimulator that is mutated in a mouse strain with severe B cell deficiency.* Current Biology, 2001. **11**(19): p. 1547-1552.
194. Thiel, M., et al., *Efficiency of T-cell costimulation by CD80 and CD86 cross-linking correlates with calcium entry.* Immunology, 2010. **129**(1): p. 28-40.
195. Broeren, C.P.M., et al., *Costimulation Light: Activation of CD4$^+$ T Cells with CD80 or CD86 Rather Than Anti-CD28 Leads to a Th2 Cytokine Profile.* 2000. **165**(12): p. 6908-6914.
196. Vaeth, M., et al., *Dependence on nuclear factor of activated T-cells (NFAT) levels discriminates conventional T cells from Foxp3+ regulatory T cells.* Proc Natl Acad Sci U S A, 2012. **109**(40): p. 16258-63.
197. Vaeth, M., et al., *Selective NFAT targeting in T cells ameliorates GvHD while maintaining antitumor activity.* Proc Natl Acad Sci U S A, 2015. **112**(4): p. 1125-30.
198. Yang, M., et al., *B Cell Maturation Antigen, the Receptor for a Proliferation-Inducing Ligand and B Cell-Activating Factor of the TNF Family, Induces Antigen Presentation in B Cells.* 2005. **175**(5): p. 2814-2824.
199. Saito, M., et al., *A signaling pathway mediating downregulation of BCL6 in germinal center B cells is blocked by BCL6 gene alterations in B cell lymphoma.* 2007. **12**(3): p. 280-292.
200. Ding, B.B., et al., *IL-21 and CD40L synergistically promote plasma cell differentiation through upregulation of Blimp-1 in human B cells.* Journal of immunology (Baltimore, Md. : 1950), 2013. **190**(4): p. 1827-1836.
201. Wojciechowski, S., et al., *Bim/Bcl-2 balance is critical for maintaining naive and memory T cell homeostasis.* 2007. **204**(7): p. 1665-1675.
202. Fry, T.J. and C.L.J.T.J.o.I. Mackall, *The many faces of IL-7: from lymphopoiesis to peripheral T cell maintenance.* 2005. **174**(11): p. 6571-6576.
203. Li, Z., L. Chen, and Z. Qin, *Paradoxical roles of IL-4 in tumor immunity.* Cell Mol Immunol, 2009. **6**(6): p. 415-22.
204. Levin, S.D., et al., *Vstm3 is a member of the CD28 family and an important modulator of T-cell function.* Eur J Immunol, 2011. **41**(4): p. 902-15.
205. Lozano, E., et al., *The TIGIT/CD226 axis regulates human T cell function.* J Immunol, 2012. **188**(8): p. 3869-75.
206. Joller, N., et al., *Treg cells expressing the coinhibitory molecule TIGIT selectively inhibit proinflammatory Th1 and Th17 cell responses.* Immunity, 2014. **40**(4): p. 569-581.

207. Abbas, A.K., et al., *Revisiting IL-2: Biology and therapeutic prospects.* 2018. **3**(25): p. eaat1482.
208. Spangler, J.B., et al., *Antibodies to Interleukin-2 Elicit Selective T Cell Subset Potentiation through Distinct Conformational Mechanisms.* Immunity, 2015. **42**(5): p. 815-25.
209. Majumder, S., et al., *Rapid and Efficient Gene Editing for Direct Transplantation of Naive Murine Cas9+ T Cells.* 2021. **12**.
210. Somaiah, C., et al., *Collagen Promotes Higher Adhesion, Survival and Proliferation of Mesenchymal Stem Cells.* PloS one, 2015. **10**(12): p. e0145068-e0145068.
211. Liu, Y.J., et al., *Mechanism of antigen-driven selection in germinal centres.* Nature, 1989. **342**(6252): p. 929-931.
212. Ke, Z., et al., *hsBAFF promotes proliferation and survival in cultured B lymphocytes via calcium signaling activation of mTOR pathway.* Cytokine, 2013. **62**(2): p. 310-21.
213. Hasbold, J., et al., *Evidence from the generation of immunoglobulin G–secreting cells that stochastic mechanisms regulate lymphocyte differentiation.* Nature Immunology, 2004. **5**(1): p. 55-63.
214. Shi, W., et al., *Transcriptional profiling of mouse B cell terminal differentiation defines a signature for antibody-secreting plasma cells.* Nature Immunology, 2015. **16**(6): p. 663-673.
215. Shinnakasu, R., et al., *Regulated selection of germinal-center cells into the memory B cell compartment.* Nature Immunology, 2016. **17**(7): p. 861-869.
216. Taylor, J.J., et al., *Humoral immunity. Apoptosis and antigen affinity limit effector cell differentiation of a single naïve B cell.* Science (New York, N.Y.), 2015. **347**(6223): p. 784-787.
217. Yoshida, T., et al., *Impact of spheroid culture on molecular and functional characteristics of bladder cancer cell lines.* Oncol Lett, 2019. **18**(5): p. 4923-4929.
218. Rocha, S., et al., *3D Cellular Architecture Affects MicroRNA and Protein Cargo of Extracellular Vesicles.* 2019. **6**(4): p. 1800948.
219. Jacobi, N., et al., *Organotypic three-dimensional cancer cell cultures mirror drug responses in vivo: lessons learned from the inhibition of EGFR signaling.* Oncotarget, 2017. **8**(64): p. 107423-107440.
220. Luca, A.C., et al., *Impact of the 3D microenvironment on phenotype, gene expression, and EGFR inhibition of colorectal cancer cell lines.* PLoS One, 2013. **8**(3): p. e59689.
221. Darrigues, E., et al., *3D cultures for modeling nanomaterial-based photothermal therapy.* Nanoscale Horizons, 2020. **5**(3): p. 400-430.

222. Botta, D., et al., *Dynamic regulation of T follicular regulatory cell responses by interleukin 2 during influenza infection.* Nature Immunology, 2017. **18**(11): p. 1249-1260.
223. Ritvo, P.G., et al., *T(fr) cells lack IL-2Rα but express decoy IL-1R2 and IL-1Ra and suppress the IL-1-dependent activation of T(fh) cells.* Sci Immunol, 2017. **2**(15).
224. Wing, J.B., et al., *A distinct subpopulation of CD25(-) T-follicular regulatory cells localizes in the germinal centers.* Proc Natl Acad Sci U S A, 2017. **114**(31): p. E6400-e6409.
225. Sayin, I., et al., *Spatial distribution and function of T follicular regulatory cells in human lymph nodes.* Journal of Experimental Medicine, 2018. **215**(6): p. 1531-1542.

12 Annex

12.1 Supplementary information

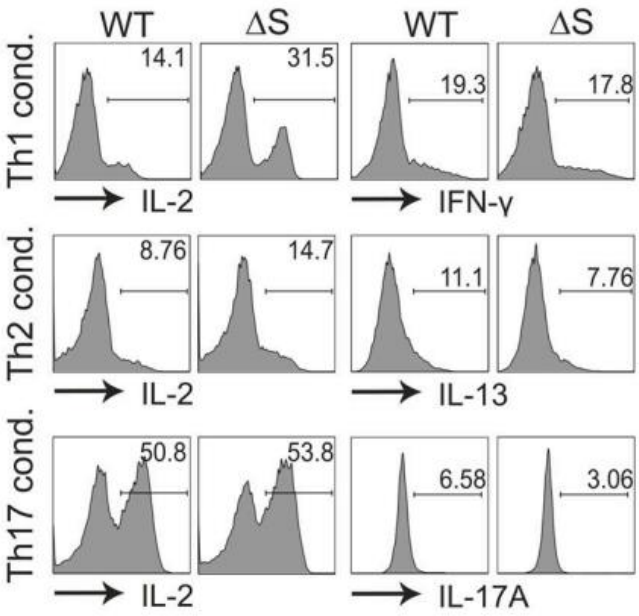

Figure S1: Representative flow cytometry plots of cytokines produced by Th1, Th2 and Th17-skewed cells.

Before NSG analyses, naive $CD4^+$ T cells from WT and NFATc1/ΔS^+ mice were skewed towards Th1, Th2, and Th17. Cells were restimulated with T/I, and the expression of IL-2, IL-4, IFN-γ, and IL-17A was confirmed on day 2.5.

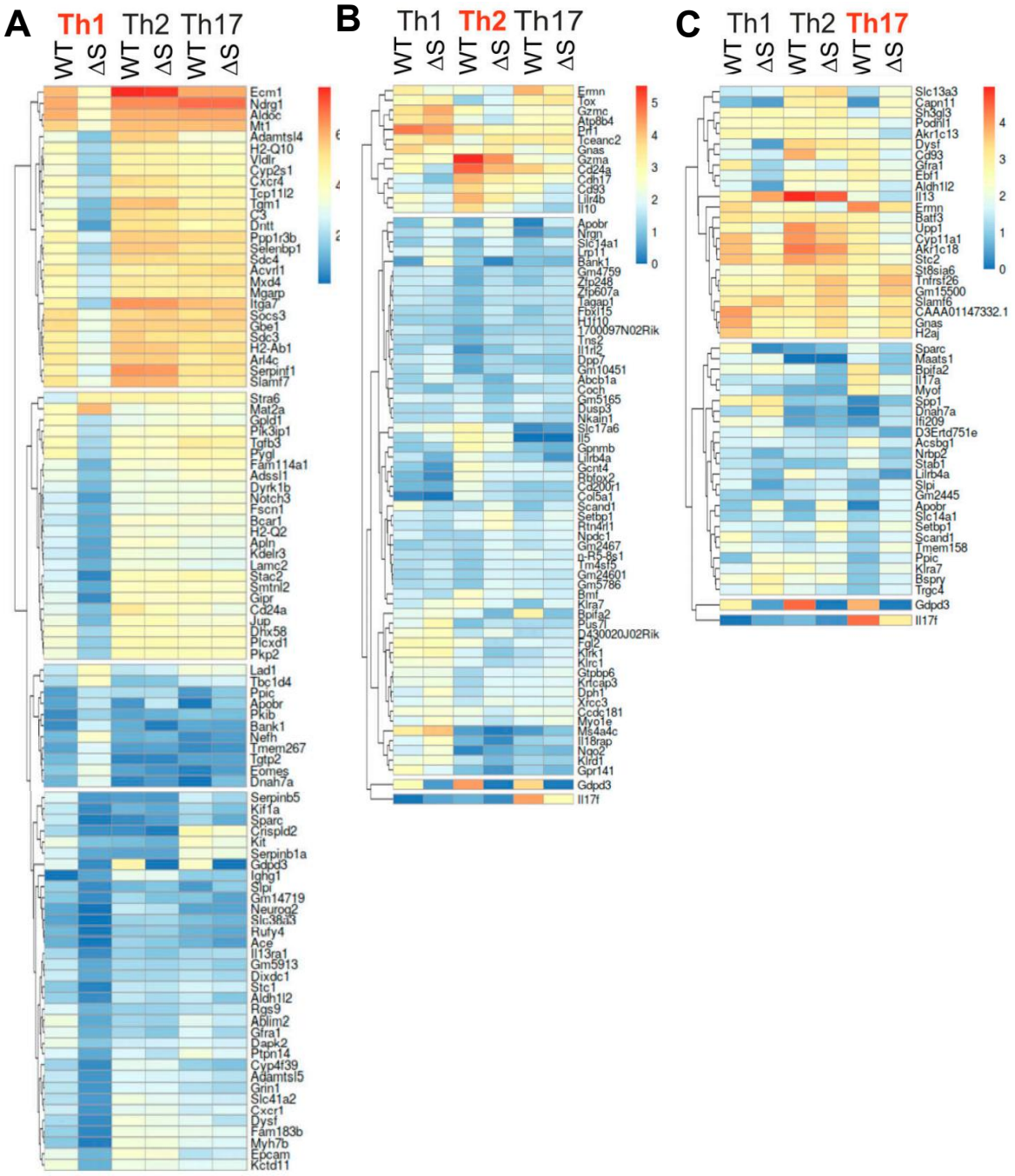

Figure S2: The heat maps of differentially expressed genes of Th1, Th2, and Th17-skewed cells between WT and NFATc1/ΔS.

(A, B, and C) Heat maps calculated according to the comparison of the differently expressed genes for Th1 (A), Th2 (B), or Th17-skewed cells (C) from WT and NFATc1/ΔS (P = 0.02, log fold-change 1.2).

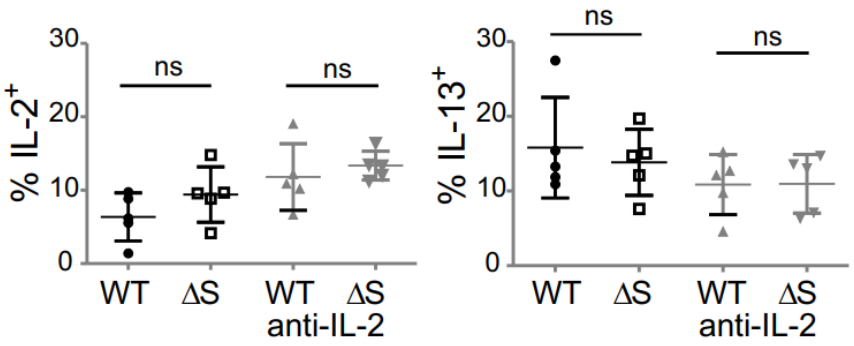

Figure S3: The percentage of IL-2⁺ and IL-13⁺ T cells among Th2-skewed cells was measured by flow cytometry.

Naïve CD4⁺ T cells from WT and NFATc1/ΔS⁺ mice were differentiated under Th2 differentiating conditions with or without anti–mIL-2, and cells were restimulated with T/I for 5 h on day 3 for the expression of IL-2 and IL-13; n = 5. Statistical analysis was performed by Student's t-test (*, p < 0.05); mean ± SD.

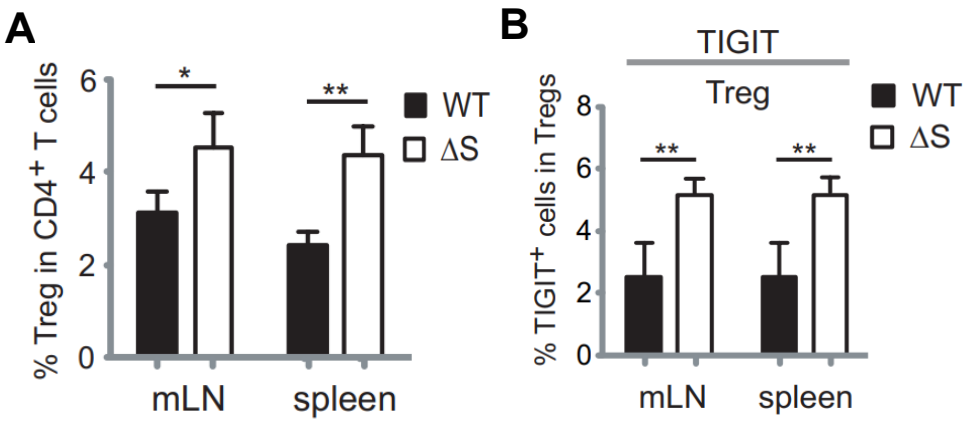

Figure S4: NFATc1/ΔS⁺ Tregs expanded more during acute GvHD exhibiting an activated TIGIT⁺ phenotype.

(A) The percentage of CD25⁺ Foxp3⁺ T cells in CD4⁺ CD90.1⁺ T cells was measured by flow cytometry in spleen and mLNs of aGvHD induced mice on day 6. Statistical analysis was performed by Student's t-test; *, p < 0.05; **, p < 0.01. (B) The percentage of TIGIT expression on CD4⁺ CD90.1⁺ Foxp3⁺ Tregs was measured by flow cytometry in spleen and mLNs of aGvHD-induced mice on day 6. Statistical analysis was performed by Student's t-test; **, p < 0.01. [Figure S4 was performed by Lena Dietz].

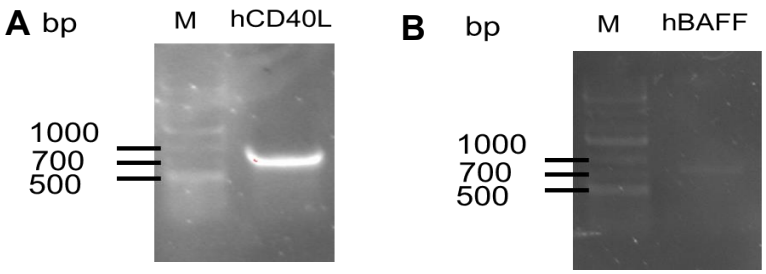

Figure S5: The amplified DNA fragments of hCD40L and hBAFF were confirmed by gel electrophoresis.

Gel electrophoresis of hCD40L (A) and hBAFF PCR products (B). M: 1kb DNA ladder.

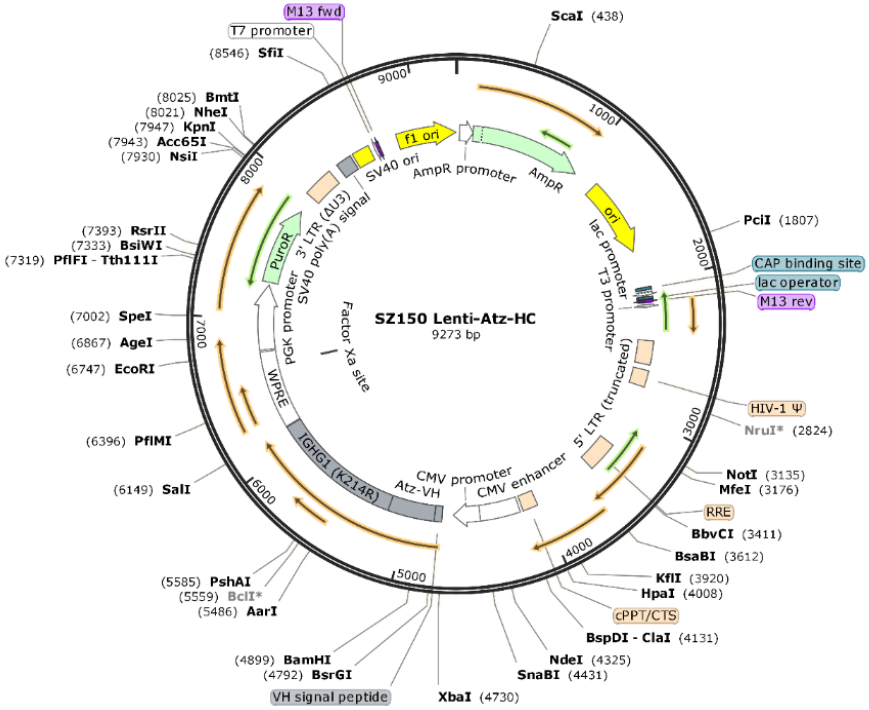

Figure S6: The plasmid map of the transfer plasmid for the lentiviral system.

Restriction sites *Xball* and *Sall* were used to insert the gene into this plasmid.